
# SEARCH FOR A HEAVY BOSON IN DIPHOTON AND MULTILEPTON FINAL STATES AT THE LARGE HADRON COLLIDER IN pp AT $\sqrt{s} = 13$ TeV

**Abdualazem Fadol Mohammed**
amohammed@aims.ac.tz

**Supervised by: Prof Bruce Mellado**
Bruce.Mellado@wits.ac.za
**Co-Supervisored by: Dr Xifeng Ruan**
Xifeng.Ruan@cern.ch

A Dissertation submitted to the Faculty of Science, University of the Witwatersrand, Johannesburg, in fulfilment of the requirements for the degree of Master of Science.

Johannesburg, 2018

## Declaration

I, the undersigned, hereby declare that the work contained in this dissertation is my original work, and that any work done by others or by myself previously has been acknowledged and referenced according to the requirement of the Faculty of Science of the University of the Witwatersrand.

This dissertation has produced two papers and one conference proceedings, which they are listed bellow:

- Search for Higgs boson pair production in the final state of $\gamma\gamma WW^*(\rightarrow \ell\nu jj)$ using 36.1 fb$^{-1}$ of pp collision data recorded at $\sqrt{s}$= 13 TeV with the ATLAS detector. ATL-COM-PHYS-2017-1006; **Contribution**: Cutflow cross-check, modelling the signal and the background shape (in form of the spurious signal study).
- Search for a heavy boson in $WW\gamma\gamma$ channel at the Large Hadron Collider in pp at $\sqrt{s}$ = 13 TeV and integrated luminosity of 36.5 fb$^{-1}$ with the ATLAS detector. Proceedings, Workshop on High Energy Particle Physics. Published in J.Phys.Conf.Ser. 889 (2017) no.1, 012001; **Contribution**: The analysis and the text.
- Multi-lepton signatures of additional scalar bosons beyond the Standard Model at the LHC. ArXiv:1711.07874; **Contribution**: Monte Carlo simulation of the direct production of the heavy boson, di-lepton final states analyses and the comparison of the di-lepton invariant mass spectrum with the ATLAS and CMS data at $\sqrt{s}$ = 8 TeV. In addition, the kinematics distribution of the tri-lepton final states and the text.

Abdualazem Fadol Mohammed

31 May 2018 in Johannesburg

# Abstract

A search for the resonant and non-resonant Higgs pair production is presented based on events containing $WW$ bosons with the semi-leptonic decay from one Higgs boson and $\gamma\gamma$ from the other Higgs boson. This search is performed by a proton–proton collision data recorded by the ATLAS detector at the Large Hadron Collider with an integrated luminosity of 36.1 fb$^{-1}$ at $\sqrt{s} = 13$ TeV. The observed and expected upper limits of the non-resonant Higgs pair production ($pp \to hh$) at 95% confidence-level on the cross-section are 7.6 pb and 5.3 pb, respectively. While by assuming a narrow-width the observed and expected upper limit for the resonant Higgs pair production at 95% confidence-level on its cross-section times the branching fraction (($pp \to X$) $\times$ Br($X \to hh$)) are as follow: a range between 37.5 pb to 6.1 pb are observed and 16.9 pb to 4.4 pb are expected for the resonant mass between 260 GeV to 500 GeV. In addition, a study of multilepton signatures arising from two new scalar bosons $H$ and $S$ at the Large Hadron Collider is carried out. These two new bosons are an extension of the Standard Model and they interact with the Higgs boson. We consider two production modes for $H$, one being gluon fusion and the other being in association with top quarks. The $H \to Sh$ decay mode is considered, where leptonic final states are studied. The nature of the $S$ boson is considered in two separate contexts. Firstly, in a simplified model, it is considered to have Higgs-like couplings. Secondly, we consider a heavy neutrino model and its interactions with the $Z, W^{\pm}$ and $S$ bosons. In Refs. [1, 2] an excess in di-lepton plus jets and missing transverse energy is predicted. The available data form the ATLAS and CMS experiments displays this excess. Assuming a simplified model where all the signal comes from $H \to Sh$, with $m_H = 270$ GeV and $m_S = 150$ GeV, the significance of the excess is 3.2 standard deviations. This result is combined with other excesses predicted by the model, yielding $\beta_g^2 = 1.38 \pm 0.22$, or $6.3\sigma$, where $\beta_g$ is the strength of the Yukawa coupling of $H$ to top quarks. A number of regions of the phase-space is suggested to the experiments for further exploration.

*To my beloved Mom*

*And*

*To the soul of my Dad*

# Acknowledgements

I would like to offer my sincere gratitude to my dissertation supervisor Prof Bruce Mellado. Thank you for guiding, advising and supporting me through the completion of this research. Thanks are also due to Dr Xifeng Ruan for his continuous monitoring, the useful discussion on statistics and technical support. I would like to extend my tributes to Dr Mukesh Kumar for his patient response to my questions and criticism. Thanks to the senior member of the Higher Energy Physics (HEP) group of the University of the Witwatersrand, especially, Prof Alan Cornell and Dr Deepak Kar. Most of the Standard Model chapter inspired by Prof Cornell's lecture notes on the Standard Model for the honour students. Thanks to my colleagues in the HEP group for creating such collaborative environment.

I would also like to acknowledge the funding support from the African Institute for Mathematical Sciences in Tanzania and the research office of the University of the Witwatersrand. This research wouldn't have come to light without their financial support. Thanks to iThemba LABS for supporting my trip to CERN, starting from the plane ticket and ending upon the subsistence and accommodation for the whole period. Surely the journey to CERN was having a great impact on my research and my experience for the time to come.

I must express my heartfelt gratitude to my family for encouraging and supporting me during the entire period. Big thanks to my mom for the funny words that she used to push me when I get tired. My beloved sister, brothers, nieces and nephews thank you all for the exceptional support and the distraction. For those who, by any means, offered me help and I did not mention their names, thank you all for any assistance you have provided me.

# Contents

# List of Figures

# List of Tables

# Nomenclature

**Acronyms**

| | |
|---|---|
| $th$ | Higgs production in association with $t$ |
| $Vh$ | Higgs production in association with $W^{\pm}/Z$ |
| ATLAS | A Toroidal LHC Apparatus |
| BEH | Brout-Englert-Higgs Mechanism |
| BR | Branching ratio |
| BSM | Beyond the SM |
| CL | Confidence-level |
| CMS | Compact Muon Solenoid |
| CP | Charge conjugation and parity |
| DSCB | Double-sided crystal ball |
| EW | Electroweak interaction |
| EWSB | Electroweak symmetry breaking |
| ggF | gluon–gluon fusion to produce $H$ |
| ggh | gluon–gluon fusion to produce $h$ |
| HNM | Heavy neutrino model |
| ID | Inner Detector |
| IP | Interaction point |
| LAr | Liquid Argon Calorimeter |
| LH | Left-handed fermions |
| LHC | The Large Hadron Collider |
| LINAC | Linear accelerator |
| LO | Leading order |
| MC | Monte Carlo |
| MH | Madala hypothesis |
| NLO | Next to leading order |
| NNLO | Next to Next leading order |
| OS | Opposit sing leptons |
| PDF | Probability density function |
| PS | Paraton shower |
| PSB | Proton synchrotron booster |
| RH | Right-handed fermions |
| Run-I | The LHC data taking period from year 2009 to 2012 |
| Run-II | The LHC data taking period from year 2015 2017 |
| SCT | Silicon microstrip tracker |
| SF | Same-flavour leptons |

| | |
|---|---|
| SM | Standard Model |
| SPS | Super proton synchrotron |
| SS | Same sing leptons |
| TileCal | Tile Hadronic Calorimeter |
| TRT | Transition radiation tracker |
| VBF | Vector boson fusion |
| vev | Vacuum expectation value |

**Symbols**

| | |
|---|---|
| $\beta_g$ | The strength of the Yukawa coupling of $H$ to top quarks |
| $\eta$ | Pseudorapidity |
| $\gamma$ | Photon |
| $\hbar$ | Plank constant |
| $\mathcal{L}$ | Lagrangian density |
| $\mathscr{L}$ | Likelihood function |
| $\mu$ | Muon |
| $\nu_\mu$ | Muon neutrino |
| $\nu_\tau$ | Tau neutrino |
| $\nu_e$ | Electron neutrino |
| $\Phi$ | General field |
| $\phi$ | Scalar complex field |
| $\tau$ | Tau lepton |
| **c** | Charm quark |
| $b$ | Bottom quark |
| $c$ | Speed of light in vacuum |
| $d$ | Down quark |
| $e$ | Electron |
| $E_{\mathrm{T}}^{\mathrm{miss}}$ | The missing energy transverse |
| $g$ | Gluon |
| $H$ | Heavy boson, heavier than $h$ |
| $h$ | Standard Model Higgs boson |
| $L$ | Lagrangian |
| $N_i$ | Heavy neutrinos unlike the SM neutrino $\nu$ |
| $p_{\mathrm{T}}$ | The transverse momentum of a particle |
| $S$ | Higgs-like scalar boson |
| $s$ | Strange quark |
| $t$ | Top quark |
| $u$ | Up quark |
| $W^{\pm}$ | $W$-boson |
| $Z^0$ | $Z$-boson |

# 1 Introduction

The discovery of the Standard Model (SM) Higgs boson ($h$) [3, 4] in 2012 was announced by the ATLAS and CMS [5, 6] experiments; in which its spin, charge and parity (CP) have been extensively studied. There is a great excitement as to what new physics may arise, from the theoretical side with the discovery of the scalar Higgs boson the particle spectrum of the SM is complete. This opened a wide range of research area to investigate whether the discovered Higgs boson is unique in its nature or just one of the spectrum of the SM Higgs boson. This comes from the fact that the neutrino oscillation experiments showed that the neutrinos possess tiny masses. However, the theory of the SM, which we look at in chapter 2, reports that neutrinos are massless particles. Many theories have been introduced in the so-called beyond the Standard Model of particle physics (BSM), such as the 2HDM [7]. These theories are an extension of the SM, where additional massive Higgs bosons appear, as explained in chapter 3.

From the experimental point of view, to reveal the mystery of the SM and BSM an upgrade of the Large Hadron Collider (LHC) and its associated experiments has been scheduled. The first run of the LHC (Run-I), in which the SM Higgs boson was observed, had a centre-of-mass energy of 8 TeV of pp collision. Now in the second data taking period (Run-II) the total energy of the collider beams reached 13 TeV and the luminosity increased almost twice of the first run. This upgrade is due to the experience gained from the first circulation. In chapter 4, we present the work of the LHC and the ATLAS experiment.

The SM shows the possibility of the self-coupling of the SM Higgs boson. Nevertheless, the cross-section of the SM Higgs boson pair production as it has been predicted by the SM is 33.41 fb [8]. The observation of this production in Run-I data was impossible as reported in Ref. [9]. However, the Higgs boson pair production can be significantly enhanced in the BSM scenario by assuming a heavy boson that decays into two SM Higgs boson. Therefore, in chapter 5 we investigate the production of two Higgs bosons at the LHC in both resonant and non-resonant productions. The search is conducted in $WW\gamma\gamma$ channel using the data collected by the ATLAS detector at a centre-of-mass energy of 13 TeV with a total integrated luminosity of 36.1 fb$^{-1}$. Monte Carlo simulation

for the signal and the considered background is also discussed. Moreover, we describe the method used to model the signal and background shape. Also a discussion of the possible uncertainty from both experimental and theoretical sides is presented, besides the statistical result. In addition, we present a prospective search using different BSM model ( see chapter 3).

After the discovery of the Higgs particle a new challenge is faced. The current goal of the collaborations is to confirm its properties via measurements of its couplings, decay width and differential distributions (of observables such as transverse momentum $p_T^h$, rapidity $y^h$ etc...). In addition, the expectation is that physics BSM might be identified with larger datasets from the LHC at the current centre-of-mass energy of $\sqrt{s} = 13$ and possibly even in the 8 TeV data. A plethora of BSM models are being considered in the literature, including additional scalar/vector bosons, fermions or exotic BSM objects. In fact, the non-zero upper limit for the neutrino mass is clearly an interesting BSM scenario for further studies both at present and future colliders [10, 11, 12, 13].

Of particular interest in this dissertation is the BSM scenario considered in Refs. [1, 14, 2, 15, 16, 17, 18] and also demonstrated in chapter 3. Scalars $H$ and $S$ were introduced to explain a number of features in the Run-I data. These include distortions of the Higgs boson transverse momentum spectrum, accompanied with an increase in the associated jet activity, elevated rate of leptons in association with $b$-tagged jets used for the search of the associated production of the Higgs boson with top quarks, and results from the search for double Higgs boson and weak boson production. In chapter 6, an effective model which is introduced in chapter 3 was tested against both the ATLAS and the CMS data. This model suggests that the production and decay modes of these scalars which could have significant signals at the LHC. The masses of these BSM scalars are constrained to $m_H = 272^{+12}_{-9}$ GeV with $m_h < m_S < m_t$, where $m_h$ and $m_t$ are the masses of the Higgs boson and the top quark, respectively. Constraints were made on the decays of $H$. For the most part, the features of the data that triggered the investigation reported in Ref. [1] remain or are magnified in the results with Run-II data reported so far, excluding $tth$ production (see Ref. [19] for a recent review).

We also study some relevant multilepton signatures of these scalars in different scenarios. Two production modes of $H$ are considered: gluon–gluon fusion (ggF), the assumed dominant production mode and top associated $H$ production ($pp \to tH, \bar{t}H$ and $pp \to t\bar{t}H$). Here we consider that the $H \to Sh$ branching ratio (BR) is 100%,[1] and that the $S \to \chi\chi$ BR is 0%. The $S$ boson is modelled in two different ways. Firstly, $S$ is considered to be Higgs-like, such that its BRs are the same as a Higgs boson with a mass $m_S$. Secondly, a model with heavy neutrinos ($N_i$) is introduced which interact with $S$ in non-standard ways. We study leptonic final states via $S \to N_i\nu_\ell$ decay modes.

In Ref. [2] emphasis is made on rare multilepton final states. These would include the production of four leptons from the production of four $W$s and the production of three same sign leptons from the production of six $W$s. We concentrate on other multilepton signatures, such as di-lepton and tri-lepton final states. Comparisons between the prediction made here and the data are made, when appropriate. We have located an

[1] In the language of Ref. [2], we are in the limit where $a_1 \to 0$.

access in the di-lepton plus jet channel ($\ell\ell + \text{jets}$), in particular leptons with a $b$-tagged jet. The compatibility of the data with the parameters obtained in Ref. [1] is discussed. Conclusions are drawn in chapter 7.

# 2

# The Standard Model of Particle Physics

The SM of particle physics is considered as our best understanding of the phenomenology of particle physics. So far the SM explains the existence of ordinary matters. However, it is yet to explain dark matters of which we can only sense its present. This chapter discusses the phenomenology of the SM which leads to the discovery of the SM Higgs boson by ATLAS and CMS in 2012.

## 2.1 Fundamental particles

Before 1978 the constituents of matter seemed to be very confusing. From theoretical as well as experimental point of view, there was a belief that the Eightfold way and the quark model were good enough to describe all fundamental particles; yet, questions arise as to why we have four leptons ($e, \nu_e$, $\mu$ and $\nu_\mu$) and only three quarks ($d, u$ and $s$), which were known at that time. Later Glashow and others provided a more specific reason for why it required having four quarks as leptons, see Ref. [20].

However, this thought was shattered by the discovery of new leptons which are the tau ($\tau$) and its associated neutrino ($\nu_\mu$). After a few years, it was realised that three more quarks existed the charm (**c**), bottom ($b$) and the top ($t$). This knowledge was gained by restoring Glashow symmetry [20], but it was hard to tell why the top quark is so heavy than the rest (40 times bigger than the bottom quarks). This was challenging due to the limitation of the experimental facilities that existed. The situation was very hostile until the era of the Electroweak (EW) theory began. The EW theory was developed by Glashow Weinberg and Salam. It is needed to offer precise prediction at relativity high energies where Fermi's theory of beta decay failed, see Ref. [21].

The EW theory predicts that there should be three carrier particles that mediate the weak interaction, i.e., the $W$s and $Z$ bosons in which their masses have been also estimated. Furthermore, Glashow, Weinberg and Salam suggested that there also should exist at least one field in the theory (nowadays known as Higgs field and hence, Higgs boson emerged). This was the beginning of the formulation of what is now known as

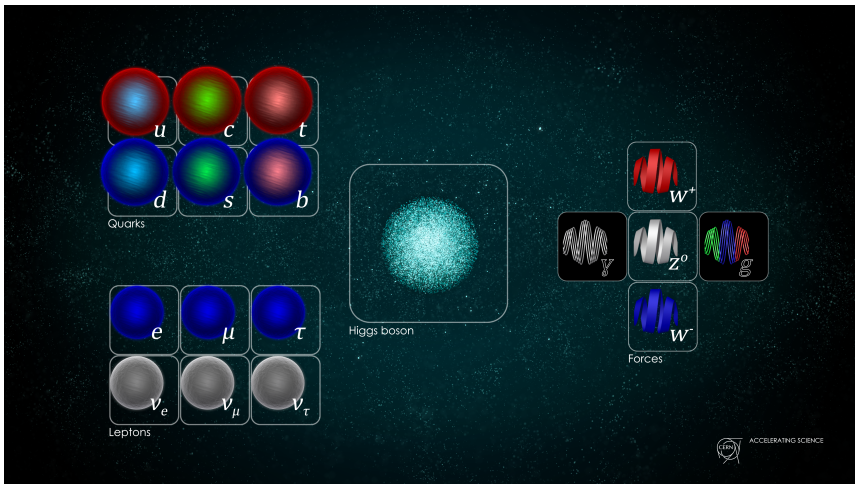


**Figure 2.1:** *The particle content of the Standard Model of particle physics [22].*

the SM of particle physics. Since 1978, the SM of particle physics has been used to describe all the known particles in nature in a very elegant way.

The particle content of the SM is shown in Figure 2.1. Where particles are classified according to their spins, masses and charges. The latter determine the properties of their interactions, as we will see later.

Fermions are divided into three generations, the lighter family is stable and the heavier families are unstable, and hence they decay to the lighter ones. All fermions are spin-1/2 particles and they are classified into two groups, namely quarks and leptons. Quarks are divided as follows: the up quark and down quark possess electromagnetic charges which are $2/3$ and $-1/3$, respectively and they are the first generation quarks. The second generation are the charm quark **c** which has a charge of $2/3$, the strange $s$ with a charge of $-1/3$, the top quark $t$ which has a charge of $2/3$ and the bottom $b$ with a charge of $-1/3$. Quarks are distinguished by their colours and they interact through strong interaction [23, 21].

There are six leptons: electron ($e$), muon ($\mu$) and tau ($\tau$), all of them have a charge of $-1$ and they organised in the first, second and the third generation, respectively. Each lepton has its associated neutrino: the electron neutrino ($\nu_e$), muon neutrino ($\nu_\mu$) and tau neutrino ($\nu_\tau$), in which they are grouped according to the lepton that they associate with. Neutrinos are neutral and they do not have any charge. All these particles have their antiparticles in which their signs are reversed. For instance, the electron has antiparticle called positron with $+1$ charge. This scenario applies to the other particles. Leptons are colourless and they interact through the weak interaction unlike quarks [23].

Vector bosons are spin-1 particles and they interact by the electromagnetic (photon is its mediator), strong (that mediates gluon) and weak interaction (which mediates $W$s and $Z$ bosons). Photon and gluon are massless particles, while $W$s and $Z$ boson are massive [23]. The Higgs boson is spin-0 particle and its existence was first suggested by

Glashow, Weinberg and Salam [24, 25]. Later Peter Higgs formulated the mechanism that gains the symmetry in the electroweak and hence, predicted the Higgs particle [26, 27].

## 2.2 The mathematics of the SM

The above mentioned particles can be described by the so-called SM of particle physics. Before we start constructing the theory of the SM, let us re-call some definition from Classical Mechanics in which we build the model on them. Consider a particle moving with a kinetic energy ($T$) in a potential energy ($U$). The best way to describe the properties (dynamics) of this particle is by writing its Lagrangian [28], which is away to describe the behaviour of the particle, the Lagrangian of such system can be defined by:

$$L = T - U. \tag{2.2.1}$$

Hence, we can get the equation of motion of this particle, let us call it "an action ($S$)". The action is just the integral of the Lagrangian with respect to the time ($S = \int L dt$) which can be used to trace the path of the particle, as particles follow the path of the least action [28]. However, if we are no longer dealing with particles and we work only with the field that the particle produces. We can use the same idea (the Lagrangian) and define a Lagrangian in terms of fields and their derivatives [28]. Now we call it a Lagrangian density $\mathcal{L}(\Phi_i(x^\mu), \partial_\mu \Phi_i(x^\mu))$ and its action is represented by:

$$S = \int \mathrm{d}^\mu x \, \mathcal{L}(\Phi_i(x^\mu), \partial_\mu \Phi_i(x^\mu)), \tag{2.2.2}$$

$\mathcal{L}(\Phi_i(x^\mu), \partial_\mu \Phi_i(x^\mu)$ can be taken as a sum of a polynomial $\vartheta(\Phi_i(x^\mu), \partial_\mu \Phi_i(x^\mu))$ values of the fields and their derivative, as:

$$\mathcal{L}(\Phi_i(x^\mu), \partial_\mu \Phi_i(x^\mu)) = \sum_k c_k \vartheta_k(\Phi_i(x^\mu), \partial_\mu \Phi_i(x^\mu)), \tag{2.2.3}$$

where $x^\mu = (x^1, x^2, x^3, x^4)$ is space-time coordinate, $\Phi_i(x^\mu)$ and $\partial_\mu \Phi_i(x^\mu)$ are general fields and their derivatives for $i = 1, 2, 3, 4$. $c_k$ are coefficients of dimension $1/\Lambda^D, D > 0$ and $\Lambda$ is an energy scale. The general field $\Phi$ can be combination of a scalar field $\phi$ or a vector field $\psi$ or both of them. The notion of particle antiparticle allow us to introduce the chirality, as it turns out that fermions correspond to left- and right-chirality [29]. Therefore, fermions come in doublet, in case of the left-chiral, and singlet, for the right-chiral, which can be combined as:

$$Q_{iL} = \begin{pmatrix} u_{iL} \\ d_{iL} \end{pmatrix}; \quad u_{iR}, d_{iR}, \tag{2.2.4}$$

$$L_{iL} = \begin{pmatrix} \nu_{iL} \\ e_{iL} \end{pmatrix}; \quad e_{iR}, \tag{2.2.5}$$

where $i = 1, 2, 3$ run over the three generations of fermions, $Q_{iL}$ are the left-chiral quarks and $L_{iL}$ are the left-chiral leptons. The right-handed quarks and leptons singlet are represented by $u_{iR}$, $d_{iR}$ and $e_{iR}$, respectively. Since the SM is a gauge theory, it should be represented by a gauge group which is a quantum field theory consists of fundamental set of particles. For instance, strong interaction is transformed under the non-abelian gauge group $SU(3)_c$ [23], where $c$ stands for colour as gluons are coloured massless particles. Also the $SU(2)_L$ is a subgroup for the weak interaction [23]. Moreover, electromagnetic interactions correspond to $U(1)_Y$, where $Y$ is the hypercharge. Therefore, the SM gauge group is:

$$G^{SM} = SU(3)_c \times SU(2)_L \times U(1)_Y. \tag{2.2.6}$$

Notice that each subgroup corresponds to a different generator. For example, the generator for $SU(3)$ is $\tau_a = \lambda_a/2, a = 1, 2, 3, \ldots, 8$ and for $SU(2)$ is $\tau_b = \sigma_b/2, b = 1, 2, 3$. $\lambda_a$ and $\sigma_b$ are Gell-Mann and Pauli matrices, respectively. The hypercharge is related to the isospin ($T_3$) and the charge ($Q$) by:

$$Q = T_3 + Y. \tag{2.2.7}$$

The most general Lagrangian for the SM, in which we call here the SM Lagrangian $\mathcal{L}^{\rm SM}$, in terms of scalars and fermions can be written as:

$$\mathcal{L}^{\rm SM}(\phi, \psi) = \mathcal{L}^{\rm SM}_{\rm kin} + \mathcal{L}^{\rm SM}_{\psi} + \mathcal{L}^{\rm SM}_{\rm Yuk} + \mathcal{L}^{\rm SM}_{\phi}, \tag{2.2.8}$$

where $\mathcal{L}^{\rm SM}_{\rm kin}$ is the kinetic term in which describes any dynamical system, the term that defines the fermions fields is $\mathcal{L}^{\rm SM}_{\psi}$ and it is a quadratic in the fields ($\psi^T\psi$, in case of Majorana mass) or ($\overline{\psi}\psi$ in case of Dirac mass), $\mathcal{L}^{\rm SM}_{\rm Yuk}$ is the Yukawa term which consists of a scalar field and two fermions fields ($\phi\overline{\psi}\psi$) and $\mathcal{L}^{\rm SM}_{\phi}$ is the part that defines the scalar fields, it could have either $\phi^2$, $\phi^3$ or $\phi^4$. The SM Lagrangian governs the interactions of the particles discussed in section 2.1. There are properties that the SM Lagrangian should preserve, one could consider them as axioms, based on the following:

1. The SM Lagrangian should be a function of the fields and their derivatives.
2. The total probability (the action) is conserved, which means that the SM Lagrangian must be real.
3. $\mathcal{L}^{SM}$ should be invariant under translation in space-time and Lorentz (Poincaré symmetry).

4. It should also be invariant under internal symmetry group which operates on the fields only.
5. For a free field, it must be polynomial which means the function of the fields should be analytic.
6. The SM Lagrangian should be renormalisable in the sense that it remain perturbative and calculable. This depends on the energy scale $\Lambda$.

## 2.3 Gauge sector

By following the properties of the SM Lagrangian, discussed above, we can now start building the Lagrangian. The $\mathcal{L}_{\psi}^{\rm SM}$ is zero, since there is no mass term for the fermions in case of Majorana and Dirac.[1] In other words all fermions have hypercharge.

Without one considering the symmetries of the fields the kinetic term of the Lagrangian can be written as:

$$\begin{aligned}\mathcal{L}_{\rm kin}^{\rm SM} = &- (\partial^{\mu}\phi)^{\dagger}(\partial_{\mu}\phi) - \overline{Q_{iL}}\,\not{\partial} Q_{iL} - i\,\overline{u_{iR}}\,\not{\partial} u_{iR} - i\,\overline{d_{iR}}\,\not{\partial} d_{iR} \\ &- i\,\overline{L_{iR}}\,\not{\partial} L_{iR} - i\,\overline{e_{iR}}\,\not{\partial} e_{iR},\end{aligned} \tag{2.3.1}$$

these are the all possible terms that can describe the free propagation of a particles related to these fields. However, these terms violate the local symmetries. For example, if we have a field $\phi \to e^{iQ\theta(x)}\phi$ and consider $x$ is space-time coordinates, this function will break under local symmetry. So to solve this problem, using the gauge symmetries we introduce a covariant derivative and the following fields strength:

$$G_a^{\mu\nu} = \partial^{\mu}G_a^{\nu} - \partial^{\nu}G_a^{\mu} - g_s f_{abc} G_b^{\mu} G_c^{\nu}, \tag{2.3.2}$$

$$W_a^{\mu\nu} = \partial^{\mu}W_a^{\nu} - \partial^{\nu}W_a^{\mu} - g\epsilon_{abc} W_b^{\mu} W_c^{\nu}, \tag{2.3.3}$$

$$A_a^{\mu\nu} = \partial^{\mu}A^{\nu} - \partial^{\nu}A^{\mu}. \tag{2.3.4}$$

where $G_a^{\mu\nu}$, $W_a^{\mu\nu}$ and $A_a^{\mu\nu}$ are a gauge fields that represent the mediators of the strong, weak and electromagnetic interactions, respectively. The sub-index "a" is the degree of freedom and the local symmetry "$SU(3) \times SU(2) \times U(1)$" force us to introduce 12 degree of freedom. $g_s$ and $g$ are the coupling strength for the strong and weak forces, respectively. $f_{abc}$ is the structure constant of $SU(3)$ and $\epsilon_{abc}$ is the structure constant for $SU(2)$.

[1] For instance, Majorana and Dirac masses can be written as follows: $\psi^T C\psi = \psi_L^T C\psi_L + \psi_R^T C\psi_R$+h.c. and $\overline{\psi}\psi = \overline{\psi_R}\psi_L + \overline{\psi_L}\psi_R$, where $C$ stands for the charge conjugation. These can have masses only under certain Lie group and will not have masses under the symmetry in which we operate ($G^{\rm SM}$) [30]. Due to the fact that right-handed neutrinos do not exist in the SM.

In addition, each field should have specific covariant derivative $D^\mu$. Using the generators for the subgroup of $SU(3)_c$ and $SU(2)_L$, the covariant derivative can be defined by:

$$
\begin{aligned}
D^\mu \phi &= \left(\partial^\mu + \frac{i}{2} g W_b^\mu \sigma_b + \frac{i}{2} g' A^\mu\right) \phi, && (2.3.5)\\
D^\mu Q_{iL} &= \left(\partial^\mu + \frac{i}{2} g_s G_a^\mu \lambda_a + \frac{i}{2} g W_b^\mu \sigma_b + \frac{i}{6} g' A^\mu\right) Q_{iL}, && (2.3.6)\\
D^\mu u_{iR} &= \left(\partial^\mu + \frac{i}{2} g_s G_a^\mu \lambda_a + \frac{2i}{3} g' A^\mu\right) u_{iR}, && (2.3.7)\\
D^\mu d_{iR} &= \left(\partial^\mu + \frac{i}{2} g_s G_a^\mu \lambda_a - \frac{i}{3} g' A^\mu\right) d_{iR}, && (2.3.8)\\
D^\mu L_{iL} &= \left(\partial^\mu + \frac{i}{2} g W_b^\mu \sigma_b - \frac{i}{2} g' A^\mu\right) L_{iL}, && (2.3.9)\\
D^\mu e_{iR} &= \left(\partial^\mu - g' A^\mu\right) e_{iR}, && (2.3.10)
\end{aligned}
$$

where $g'$ is the coupling strength associate to $U(1)_Y$. The field $\phi$ is scalar and thus it will not fail the $SU(3)$ as well as the leptons. Using Equations (2.3.6) to (2.3.10), the kinetic term in Equation (2.3.1) becomes:

$$
\begin{aligned}
\mathcal{L}_{\text{kin}}^{\text{SM}} = & - \frac{1}{4} G_a^{\mu\nu} G_{a\mu\nu} - \frac{1}{4} W_b^{\mu\nu} W_{b\mu\nu} - \frac{1}{4} A^{\mu\nu} A_{\mu\nu} - \overline{Q_{iL}}\, \not{D} Q_{iL} \\
& - i\, \overline{u_{iR}}\, \not{D} u_{iR} - i\, \overline{d_{iR}}\, \not{D} d_{iR} - i\, \overline{L_{iR}}\, \not{D} L_{iR} - i\, \overline{e_{iR}}\, \not{D} e_{iR} \\
& - (D^\mu \phi)^\dagger (D_\mu \phi)\,. \qquad (2.3.11)
\end{aligned}
$$

The possible terms for Yukawa sector can be written as:

$$
\mathcal{L}_{\text{Yuk}}^{\text{SM}} = Y_{ij}^d \overline{Q_{iL}} \phi\, d_{jR} + Y_{ij}^u \overline{Q_{iL}} \tilde{\phi}\, u_{jR} + Y_{ij}^e \overline{L_{iL}} \phi\, e_{jR} + \text{h.c.}, \qquad (2.3.12)
$$

where $\tilde{\phi} = i\sigma_2 \phi^\dagger$ and $Y_{ij}^d$, $Y_{ij}^u$ and $Y_{ij}^e$ are dimensionless Yukawa matrices ($3 \times 3$, complex and flavour dependent matrices). The h.c. is the hermitian term, it is needed because none of the terms which appear in the $\mathcal{L}_{\text{Yuk}}$ terms are self-hermitian.

## 2.4 The Brout-Englert-Higgs Mechanism

The Brout-Englert-Higgs (BEH) Mechanism focuses on the part of the Lagrangian where the $W$s and $Z$ bosons appear to be massless. This part could be considered as a potential which depends on the scalar field $\phi$, its doublet carries a hypercharge. This means we can not form a $\phi^3$ term, because we can not make a singlet out of three doublets.

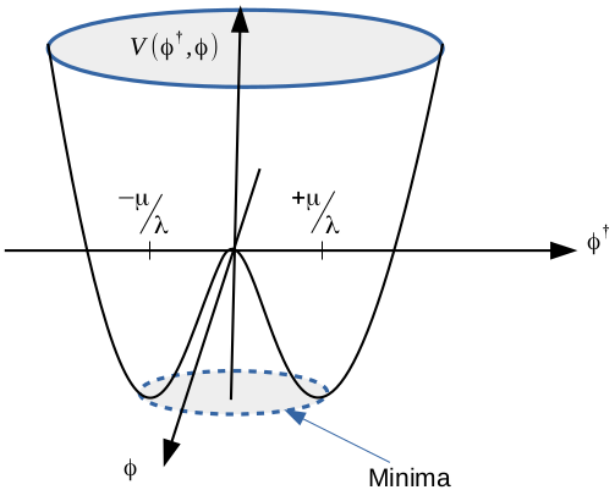


**Figure 2.2:** *Higgs potential as function of the field $\phi$ for Equation* (2.4.1).

Notice that this field is required to allow the gauge fields as well as the fermions to acquire masses. Consequently, the $SU(2)_L \times U(1)_Y$ symmetry is broken [27] unlike the $SU(3)_c$, as gluons are already massless particles. This tells us that the ground state of the universe does not respect all the symmetry of the Lagrangian, but only part of them. So we call this a spontaneous symmetry breaking (SSB), as shown in Figure 2.2, where the parameters $\mu/\lambda$ are breaking the Poincaré symmetry. Therefore, the potential is symmetric under the global transformation and Equation (2.2.7) can be used as generator for the $SU(2)_L \times U(1)_Y$, hence, the potential expressed by:

$$\mathcal{L}_{\phi}^{\mathrm{SM}} = -\mu^2 \phi^{\dagger}\phi - \lambda \left(\phi^{\dagger}\phi\right)^2, \tag{2.4.1}$$

the parameter $\lambda$ is supposed to be positive, because if it has a negative value then the potential will not be bounded from below. The parameter $\mu^2$ has two possibilities; either less than zero or greater than zero as shown in Figure 2.2. However, the square-root on the parameter is just an indication that $\mu$ has a dimension of mass squared. Let $v^2 = -\mu/\lambda$, where now $v$ is the vacuum expectation value (vev) that minimises the potential. Equation (2.4.1) can be defined in terms of the vev as:

$$\mathcal{L}_{\phi}^{\mathrm{SM}} = -\lambda \left(\phi^{\dagger}\phi - v^2/2\right)^2. \tag{2.4.2}$$

The minima of the field could be a achieved when $|\langle\phi\rangle| = v/\sqrt{2}$, see Ref [3], and depending on the choice it can be written as:

$$\langle\phi\rangle = \begin{pmatrix} 0 \\ \frac{v}{\sqrt{2}} \end{pmatrix}. \tag{2.4.3}$$

From Equations (2.3.11), (2.3.12) and (2.4.2) the SM Lagrangian can be written as:

$$\begin{aligned} \mathcal{L}^{\mathrm{SM}} = \; & - \frac{1}{4} G_a^{\mu\nu} G_{a\mu\nu} - \frac{1}{4} W_b^{\mu\nu} W_{b\mu\nu} - \frac{1}{4} A^{\mu\nu} A_{\mu\nu} - \overline{Q_{iL}}\, \not{D} Q_{iL} \\ & - i\, \overline{u_{iR}}\, \not{D} u_{iR} - i\, \overline{d_{iR}}\, \not{D} d_{iR} - i\, \overline{L_{iR}}\, \not{D} L_{iR} - i\, \overline{e_{iR}}\, \not{D} e_{iR} \\ & + Y_{ij}^d \overline{Q_{iL}} \phi\, d_{jR} + Y_{ij}^u \overline{Q_{iL}} \tilde{\phi}\, u_{jR} + Y_{ij}^e \overline{L_{iL}} \phi\, e_{jR} + \text{h.c.} \\ & - (D^\mu \phi)^\dagger (D_\mu \phi) - \lambda \left( \phi^\dagger \phi - v^2/2 \right)^2, \end{aligned} \tag{2.4.4}$$

which breaks the symmetry because of the non zero potential of the field.

## 2.5 Masses of the SM bosons

1. The Higgs boson:

   The SM Lagrangian, Equation (2.4.4), can describe all the elementary particles listed in section 2.1. Let us start by the Higgs field so we know that it is a scalar and complex field, as defined by:

$$\phi(x) = e^{[i\sigma_b \theta_b(x) - I\theta_3(x)]} \frac{1}{\sqrt{2}} \begin{pmatrix} 0 \\ v + h(x) \end{pmatrix} \Leftrightarrow \frac{1}{\sqrt{2}} \begin{pmatrix} \phi_1 + i\phi_2 \\ \phi_3 + i\phi_4 \end{pmatrix} \tag{2.5.1}$$

   where $\theta_b$; $b = 1, 2, 3$ are Goldstone bosons which emerge due to the SSB, $h$ is the Higgs boson that result from the introduction of the field [31]. Hence, applying rotation by $SU(2)_Y \times U(1)_Y$ on $\phi(x)$, of one degree of freedom, yields:

$$\phi(x) = \frac{1}{\sqrt{2}} \begin{pmatrix} 0 \\ v + h(x) \end{pmatrix}. \tag{2.5.2}$$

   Hence, $\phi^\dagger \phi$ become:

$$\phi^\dagger \phi = \frac{1}{2} \left( v^2 + 2vh + h^2 \right), \tag{2.5.3}$$

   substituting Equation (2.5.3) on Equation (2.4.2) we get:

$$\mathcal{L}_{\phi}^{\mathrm{SM}} = -\lambda v^2 h^2 - \left(\lambda v h^3 - \frac{\lambda}{4} h^4\right). \tag{2.5.4}$$

This leads us to a real scalar boson, the Higgs boson $h$, whose mass is $m_h^2 = 2\lambda v^2$. We will see how the Higgs boson is observed experimentally in section 2.6, where $\lambda$ is a parameter of the theory.

2. Vector bosons:

   By acting on the Higgs field using the definition of the covariant derivative in Equation (2.3.6), $(D_\mu \langle\phi\rangle)^\dagger (D^\mu \langle\phi\rangle)$, we get:

$$\begin{aligned} D^\mu \langle\phi\rangle &= \frac{i}{\sqrt{8}} \left(g W_b^\mu \sigma_b + g' A^\mu\right) \begin{pmatrix} 0 \\ v \end{pmatrix} \\ &= \frac{i}{\sqrt{8}} \begin{pmatrix} g W_3^\mu + g' A^\mu & g\left(W_1^\mu - i W_2^\mu\right) \\ g\left(W_1^\mu + i W_2^\mu\right) & -g W_3^\mu + g' A^\mu \end{pmatrix} \begin{pmatrix} 0 \\ v \end{pmatrix} \\ &= \frac{iv}{\sqrt{8}} \begin{pmatrix} g\left(W_1^\mu - i W_2^\mu\right) \\ -g W_3^\mu + g' A^\mu \end{pmatrix}. \end{aligned} \tag{2.5.5}$$

   Then from the last term of Equation (2.3.11) and Equation (2.5.5), we can express the mass term of the vector boson as:

$$\begin{aligned} \mathcal{L}_{M_V}^{\mathrm{SM}} &= (D_\mu \langle\phi\rangle)^\dagger (D^\mu \langle\phi\rangle) \\ &= \frac{v^2}{8} \begin{pmatrix} g\left(W_1 + i W_2\right)_\mu & -g W_{3\mu} + g' A_\mu \end{pmatrix} \begin{pmatrix} g\left(W_1^\mu - i W_2^\mu\right) \\ -g W_3^\mu + g' A^\mu \end{pmatrix} \\ &= \frac{v^2}{8} \left(g^2 (W_1 + W_2)_\mu (W_1^\mu - i W_2^\mu) + g^2 \left(W_{3\mu} - \tfrac{g'}{g} A_\mu\right)\left(W_3^\mu - \tfrac{g'}{g} A^\mu\right)\right), \end{aligned} \tag{2.5.6}$$

   if we replace $W_\mu^\pm = \frac{1}{\sqrt{2}} \left(W_1 \mp i W_2\right)_\mu$, $\tan\theta_W \equiv \frac{g'}{g}$, $Z_\mu^0 = \cos\theta_W W_{3\mu} - \sin\theta_W A_\mu$ and $B_\mu^0 = \sin\theta_W W_{3\mu} + \cos\theta_W A_\mu$ into Equation (2.5.6), we get:

$$\mathcal{L}_{M_V}^{\mathrm{SM}} = \frac{1}{4} g^2 v^2 W^{+\mu} W_\mu^- + \frac{1}{8} (g^2 + g'^2) v^2 Z^{0\mu} Z_\mu^0. \tag{2.5.7}$$

   where $W_\mu^\pm$ are charged bosons whereas $B_\mu^0$ and $Z_\mu^0$ are neutral bosons [31], their masses can be written in terms of Equation (2.5.7) as:

$$m_W^2 = \frac{1}{4} g^2 v^2, \qquad m_Z^2 = \frac{1}{4} (g^2 + g') v^2, \qquad m_B = 0. \tag{2.5.8}$$

   Similarly, one can use Equation (2.3.12) to compute the masses of the fermions.

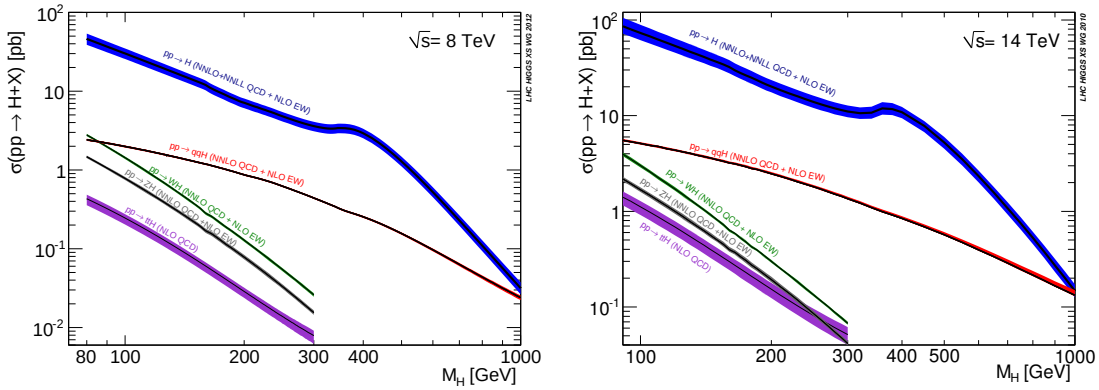


(a) (b)

**Figure 2.3:** *The production cross-section of the SM Higgs boson as a function of its mass at the LHC with centre-of-mass energy of (a) 8 TeV and (b) 14 TeV [8].*

## 2.6 The discovery of the Higgs boson

As discussed above, the SM unifies the electromagnetic and weak interactions. Moreover, it proposes the existence of a scalar and neutral boson "that is the Higgs boson", which is observed by the ATLAS and CMS experiments [5, 6]. However, the SM does not provide a prediction for the mass of the Higgs boson. This was challenging for experimentalists as it turns out that constraints for the mass has to be developed. Therefore, two types of constraints are considered. Firstly, there are experimental restrictions on the mass of the Higgs boson, where it mainly comes from experiments such as Tevatron, LEP and SLC. Figure 2.4 displays the constraints of the SM Higgs boson in which the lower bound of the Higgs mass is found to be $114^{+69}_{-45}$ [32]. Furthermore, the idea of the SM should be valid under a certain range of energy probed within some theoretical limits. For instance, the mass of the Higgs boson determine the shape of the potential, see Figure 2.2, depending on the value of the scale $\Lambda$ [33]. Figure 2.5 shows the allowed mass region for the Higgs boson mass as a function of the scale $\Lambda$.

The SM Higgs boson is produced in four production modes at the LHC as follows: gluon-gluon fusion (ggh), vector boson fusion (VBF), production with association with the $W^{\pm}$ and $Z$ bosons ($Vh$) and associated production with top quarks ($t\bar{t}h$). The deferences in their production mechanisms are shown as a function of the mass of the Higgs boson in Figure 2.3 for 8 TeV and 14 TeV. The ggh and the VBF have the largest cross-section, with the VBF being a few order of magnitude less than the ggh, as shown in Figure 2.3. While the $tth$ has the lowest cross-section among the other production mechanisms, the $Vh$ is an orders of magnitude bigger than the $tth$. Figure 2.3 also shows that the contributions coming from both the $Vh$ and $tth$ at masses greater than 300 are negligible.

The technical details of the discovery rely on the decay of the SM Higgs particle. Where manifest on the couplings of the SM Higgs boson to the SM particles. The properties

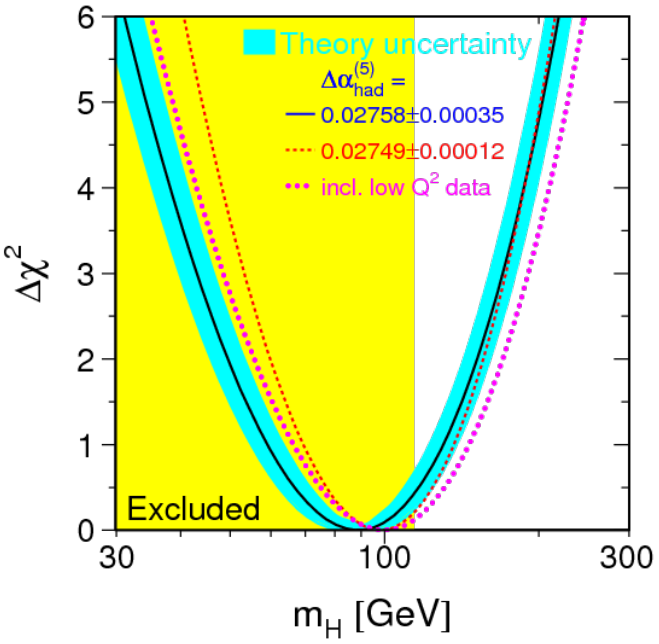


**Figure 2.4:** *Values of $\Delta\chi^2$ resulted from the fit of the electroweak precision data as a function of the mass of the Higgs boson. The blue shaded band is the theoretical uncertainty caused by missing high order correction. While the solid line denotes the measurement with full data set shown in Ref. [32]. Whereas the dashed lines express the results with the estimation of the $\Delta\alpha^{(5)}_{had}(m^2_Z)$, the plot is taken from Ref. [32]*

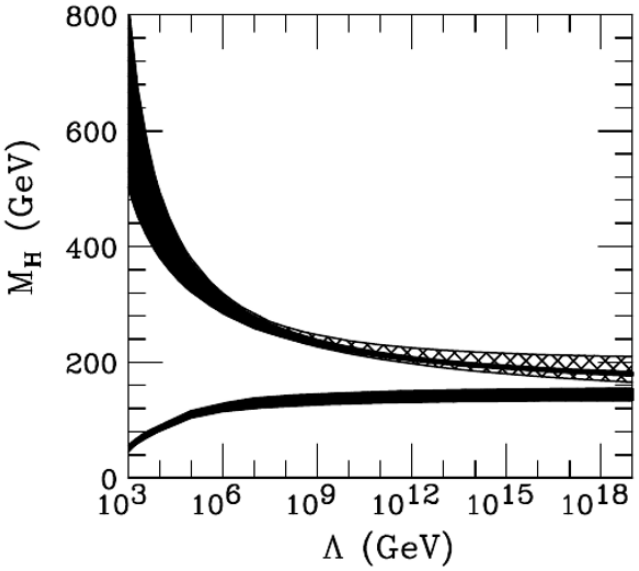


**Figure 2.5:** *Upper and lower bounds limit of the mass of the SM Higgs boson as a function of the scale $\Lambda$ [33].*

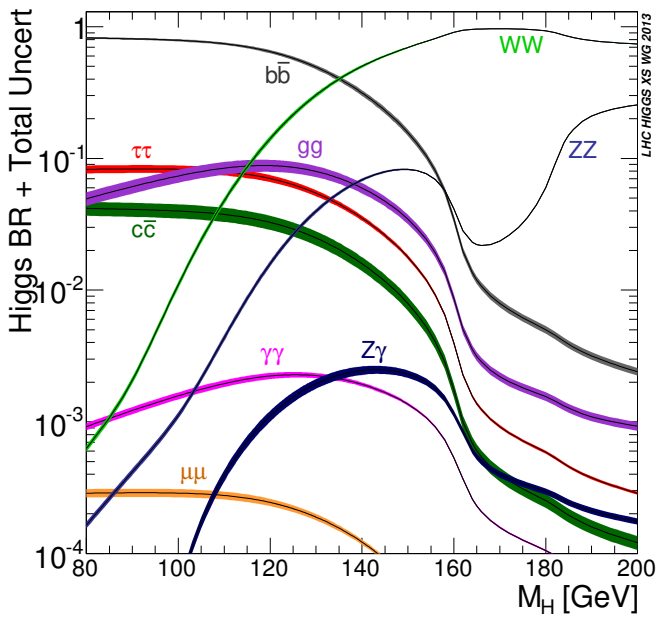


**Figure 2.6:** *The branching ratio of the Higgs boson decaying to all channels as a function of the mass of the Higgs boson [8]. These channels are referred to the SM particles that couple the SM Higgs boson, such as $WW$, $b\bar{b}$, $ZZ$, $gg$, $\tau\tau$, $c\bar{c}$, $Z\gamma$, $\gamma\gamma$ and $\mu\mu$.*

of the Higgs boson decay are determined by the particles that it interacts with, as the Higgs boson has a very short life time of about $10^{-22}$ s. For example, Equation 2.5.8 shows that the coupling strength is directly proportional to the masses of the vector bosons. The computed branching ratios of the decay of the Higgs boson to other SM particles are in Figure 2.6. We can divide Figure 2.6 into lower (lighter Higgs boson, $100 < m_h < 130$ GeV) and higher mass (heavy Higgs boson, $140 < m_h > 200$ GeV) regions. Therefore, at lower mass region about 80% of the Higgs boson decays to $b\bar{b}$ ($h \to b\bar{b}$) and 9% to $\tau\tau$ ($h \to \tau\tau$). At higher mass region $W$ boson dominates and its fraction is about 98%. While only about 2% of the Higgs boson goes to $ZZ$.

In addition, channels coming from other sources should be considered as background during the analysis. The observation of a neutral scalar boson with a mass of $126.0^{\pm 0.4}_{\pm 0.4}$ GeV was reported by the ATLAS detector in Ref [5]. It has been measured with a significant of 5.9 standard deviations [5]. Combined results, for 7 TeV and 8 TeV, and results for the $h \to ZZ^*$, $h \to \gamma\gamma$ and $h \to WW$ are shown in Figure 2.7.

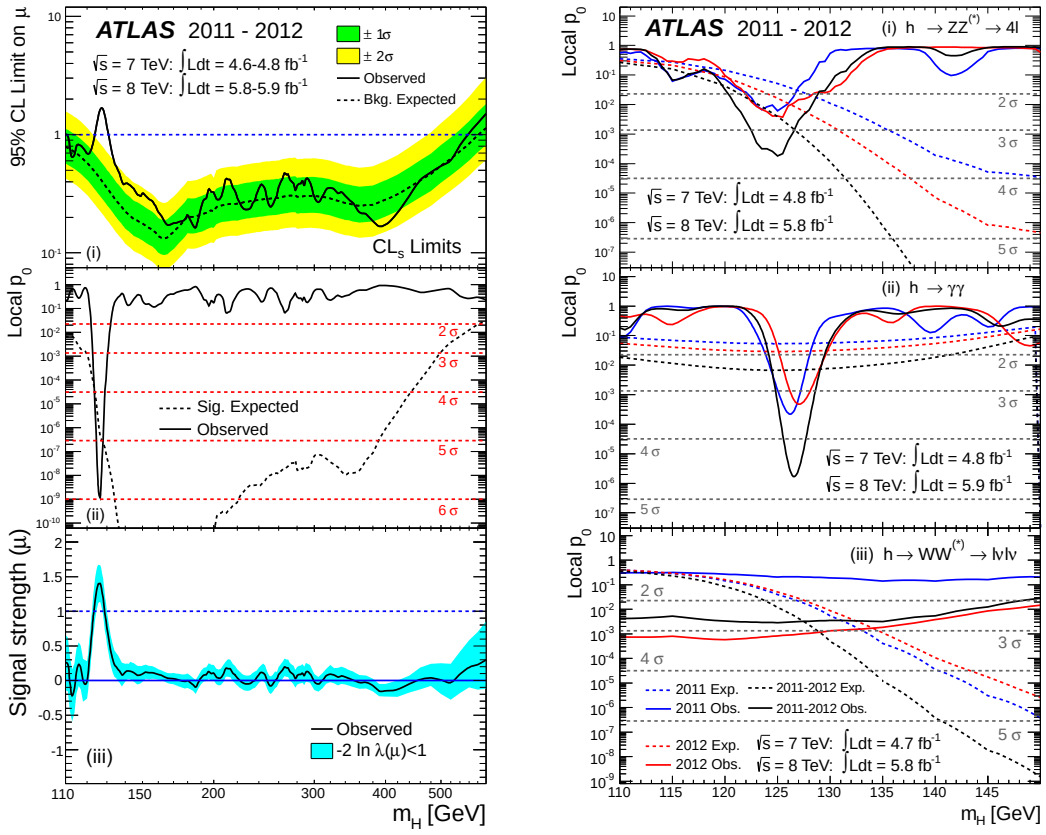


(a) (b)

**Figure 2.7:** *In Figure (a) A combined results for $WW$, $b\bar{b}$, $ZZ$, $gg$, $\tau\tau$, $c\bar{c}$, $Z\gamma$, $\gamma\gamma$ and $\mu\mu$ channels are shown. Where (i) The signal strength at 95% confidence limit (CL) of the observed (solid line) and the dashed line is the expected background-only; the bands correspond to the uncertainty, (ii) the local $p_0$ for the observed (solid) and the expected signal (dashed) and (iii) the best fit of the signal strength. Figure (b) is the local $p_0$ for (i) $h \to ZZ^* \to 4\ell$, (ii) $h \to \gamma\gamma$ and (iii) $h \to WW^* \to \ell\nu\ell\nu$. Each sub-plots is displayed as a function of the mass of the SM Higgs boson [5].*

## Summary

In this chapter, we reviewed the content of the SM of particle physics. We also looked at each sector in the SM such as the gauge sector, Yukawa sector and the Higgs sector. In addition, we discussed the BEH Mechanism which explains the EW interactions. Where the introduction of a scalar field is needed in the theory, which means the existence of a new particle (Higgs boson). Hence, we build the SM Lagrangian which is invariant under Lorentz transformation. Later the SM Higgs boson was discovered by both ATLAS and CMS experiments. Although the SM is successful on its prediction, there are reasons to think that it is not a complete theory. Searches for physics BSM have been carried by both theorists and experimentalists which will be discussed next chapter.

# 3

# Extending the Higgs Sector

We have seen in chapter 2 that the SM has been very successful in explaining the particles which we observe in nature. There we assumed a scalar field which transforms under $SU(2)$ doublet. However, there are several reasons to believe the SM is just the lower energy regime and its scalar sector is not complete. For example, in the fermions representations of the $SU(3)_c$ the parity is conserved, but it is not in the $SU(2)_L \times U(1)_Y$ representation. Also there is unexplained large differences of the fine structure constant between the strong, electroweak and electromagnetic interactions. In addition, there are no right-handed neutrinos in the SM that is why neutrinos in the SM have small masses [34].

In this chapter, we discuss theories that go beyond the SM of particle physics (BSM). In particular, the two-Higgs-doublet model (2HDM) is reviewed and a possible extension for the 2HDM with an additional singlet scalar is addressed.

## 3.1 Two-Higgs-doublet model

The general Lagrangian for the 2HDM can be expressed by:

$$\mathcal{L}^{\text{2HDM}} = \mathcal{L}^{\text{2HDM}}_{\text{kin}} + \mathcal{L}^{\text{2HDM}}_{\text{Yuk}} + \mathcal{L}^{\text{2HDM}}_{\phi}, \tag{3.1.1}$$

where $\mathcal{L}^{\text{2HDM}}_{\text{kin}}$, $\mathcal{L}^{\text{2HDM}}_{\text{Yuk}}$ and $\mathcal{L}^{\text{2HDM}}_{\phi}$ are the kinetic, Yukawa and the scalar field of the 2HDM Lagrangian. These terms depend on the component of the scalar field which will be introduced. Mostly the Yukawa and the potential term will be affected when we move the scalar part of the kinetic term to the Higgs scalar term, as shown in Refs. [35, 36]. The Higgs sector can be written as:

$$\mathcal{L}^{\text{2HDM}}_{\phi} = (D^{\mu}\phi_1)^{\dagger}(D_{\mu}\phi_1) + (D^{\mu}\phi_2)^{\dagger}(D_{\mu}\phi_2) - V(\phi_1, \phi_2), \tag{3.1.2}$$

where $\phi_1$ and $\phi_2$ are a complex scalar fields, same as Higgs field, notice that these doublets have same hypercharge +1. Therefore, the 2HDM potential can be written in away similar to Equation (2.4.1) as follows:

$$\begin{aligned} V(\phi_1,\phi_2) &= m_{11}^2\phi_1^\dagger\phi_1 + m_{22}^2\phi_2^\dagger\phi_2 - m_{12}^2\left(\phi_1^\dagger\phi_2 + \phi_2^\dagger\phi_1\right) + \frac{\lambda_1}{2}\left(\phi_1^\dagger\phi_1\right)^2 \\ &+ \frac{\lambda_2}{2}\left(\phi_2^\dagger\phi_2\right)^2 + \lambda_3\left(\phi_1^\dagger\phi_1\right)\left(\phi_2^\dagger\phi_2\right) + \lambda_4\left(\phi_1^\dagger\phi_2\right)\left(\phi_2^\dagger\phi_1\right) + \frac{\lambda_5}{2}\left(\phi_1^\dagger\phi_2\right)^2 \\ &+ \left[\frac{\lambda_5^*}{2}\left(\phi_2^\dagger\phi_1\right)^2 + \lambda_6\left(\phi_1^\dagger\phi_1\right)\left(\phi_1^\dagger\phi_2\right) + \lambda_7\left(\phi_2^\dagger\phi_2\right)\left(\phi_1^\dagger\phi_2\right)\right. \\ &+ \left.\text{h.c.}\right], \end{aligned} \tag{3.1.3}$$

where $m_{11}$, $m_{22}$ and $\lambda_{1\,\text{to}\,4}$ are real parameters. While $m_{12}$ and $\lambda_{5\,\text{to}\,7}$ are complex parameters. Since we have too many parameters (14 real and complex parameters) the minimisation of the potential will be rather difficult. Therefore, to ensure that the potential must be bounded from below and all the vevs are real and positive, the following assumption have been made:

1. In the Higgs fields the CP is required to be conserved and not spontaneously broken.

2. The parameters in Equation (3.1.3) must be reduced. This is attained by assuming that $\lambda_6 = \lambda_7 = 0$. In addition, the $\lambda$s should satisfy the following conditions [37]:

$$\lambda_1 > 0, \quad \lambda_2 > 0, \quad \lambda_3 > -\sqrt{\lambda_1\lambda_2}, \quad \lambda_3 + \lambda_4 \pm |\lambda_5| > -\sqrt{\lambda_1\lambda_2} \tag{3.1.4}$$

3. The introduction of two doublets field causes the Higgs field to emit flavour-charging current neutral, which implies that Yukawa matrices in Equation (2.3.12) will no longer be simultaneously diagonalised. This is known as the FCNC problem in the 2HDM. However, to avoid this problem one might consider a continuous or discrete symmetries, where the quartic transform under $Z_2$ symmetry:

$$Z_2: \quad \phi_1 \to \phi_1, \quad \phi_2 \to -\phi_2, \tag{3.1.5}$$

   where $\phi_1$ and $\phi_2$ are defined by:

$$\phi_a = \begin{pmatrix} \phi_a^+ \\ \frac{v_a+\rho_a+i\eta_a}{\sqrt{2}} \end{pmatrix}, \quad a = 1,2, \tag{3.1.6}$$

4. The parameter $m_{12}^2$ and $\lambda_5$ can alter the $Z_2$ symmetry as follows: If $m_{12}^2 = 0$, the symmetry will not be affected by this choice. However, if they are non-zeros the symmetry will acquire an additional global symmetry ($U(1)$), that sponta-

neously breaks the $Z_2$ symmetry. This symmetry break is known as Peccei-Quinn symmetry [38].

The minimisation of the potential can be written as:

$$\langle\phi_1\rangle = \begin{pmatrix} 0 \\ \frac{v_1}{\sqrt{2}} \end{pmatrix}, \quad \langle\phi_2\rangle = \begin{pmatrix} 0 \\ \frac{v_2}{\sqrt{2}} \end{pmatrix}. \tag{3.1.7}$$

After applying the conditions summarised above, we are left with 8 parameters. Three of these parameters are absorbed to give masses to the three vector bosons, the $W^{\pm}$ and the $Z$ bosons. The other Higgs fields parameters give rise to the two neutral bosons, the SM Higgs (lighter) and Higgs boson (heavier than the SM Higgs boson). Therefore, the spectrum of the 2HDM can be computed using the extrema of the potential, and the set-up of the parameters can be given as:

$$\begin{aligned} \left.\frac{\partial V(\phi_1,\phi_2)}{\partial \phi_1^{\dagger}}\right|_{(\phi_1=\langle\phi_1\rangle,\phi_2=\langle\phi_2\rangle)} &= 0\,. \\ \left.\frac{\partial V(\phi_1,\phi_2)}{\partial \phi_2^{\dagger}}\right|_{(\phi_1=\langle\phi_1\rangle,\phi_2=\langle\phi_2\rangle)} &= 0\,. \end{aligned} \tag{3.1.8}$$

Hence one can get the following:

$$\begin{aligned} m_{11}^2 &= m_{12}^2\frac{v_2}{v_1} - \frac{\lambda_1}{2}v_1^2 - (\lambda_3+\lambda_4+\lambda_5)\frac{v_2^2}{2}, \\ m_{22}^2 &= m_{12}^2\frac{v_1}{v_2} - \lambda_2\frac{v_2^2}{2} - (\lambda_3+\lambda_4+\lambda_5)\frac{v_1^2}{2}, \end{aligned} \tag{3.1.9}$$

by substituting Equation (3.1.9) and (3.1.9) into Equation (3.1.3) we get the following mass terms [7]:

$$\mathcal{L}_{\phi^{\pm}}^{2HDM} = \left[m_{12}^2 - (\lambda_4+\lambda_5)\,v_1v_2\right](\phi_1^-,\phi_2^-)\begin{pmatrix} v_2/v_1 & -1 \\ -1 & v_1/v_2 \end{pmatrix}\begin{pmatrix}\phi_1^+\\ \phi_2^+\end{pmatrix}, \tag{3.1.10}$$

$$\mathcal{L}_{\eta}^{2HDM} = \frac{m_A^2}{v_1^2+v_2^2}(\eta_1,\eta_2)\begin{pmatrix} v_2 & -v_1v_2 \\ -v_1v_2 & v_1 \end{pmatrix}\begin{pmatrix}\eta_1\\ \eta_2\end{pmatrix}, \tag{3.1.11}$$

$$\mathcal{L}_{\rho}^{2HDM} = -(\rho_1,\rho_2)\begin{pmatrix} m_{12}^2\frac{v_2}{v_1}+\lambda_1v_1^2 & -m_{12}^2+\lambda' v_1v_2 \\ -m_{12}^2+\lambda' v_1v_2 & m_{12}\frac{v_1}{v_2}+\lambda_2v_2^2 \end{pmatrix}\begin{pmatrix}\rho_1\\ \rho_2\end{pmatrix}, \tag{3.1.12}$$

where $\lambda' = \lambda_2+\lambda_3+\lambda_5$. Let us define $v = \sqrt{v_1^2+v_2^2}$, $v_1 = v\cos\beta$, $v_2 = \sin\beta$ and $\tan\beta = v_2/v_1$ to obtain;

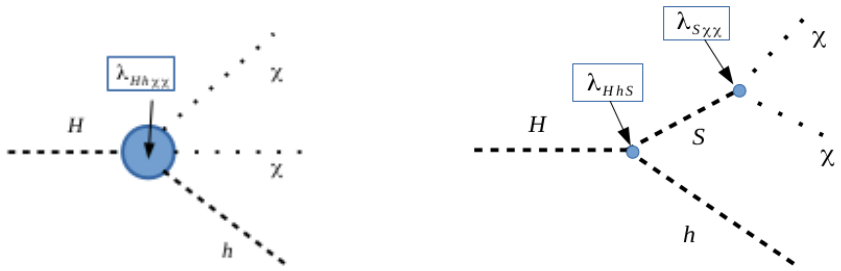


(a) (b)

**Figure 3.1:** *Sketch describing the effective Lagrangian in Equation (3.3.5) when (a) adding a singlet scalar $\chi\chi$ to the 2HDM which interact with the $H$ and $h$ throught a quartic coupling $\lambda_{Hh\chi\chi}$ and (b) after adding a CP-even scalar as an intermediate scalar $S$ which couples to the $H$, $h$ and $\chi\chi$ through $\lambda_{HhS}$ and $\lambda_{S\chi\chi}$, respectively.*

$$\begin{pmatrix} H_1 \\ H_2 \end{pmatrix} = \begin{pmatrix} \cos\beta & \sin\beta \\ -\sin\beta & \cos\beta \end{pmatrix} = \begin{pmatrix} \phi_1 \\ \phi_2 \end{pmatrix} \tag{3.1.13}$$

in which $\beta$ represents the angle of rotation that diagonalises the mass-matrix of the charged scalar and psudoscalar. The square-mass of the charged scalar ($m^2_{\phi^\pm}$) and pseudoscalar ($m^2_A$) can be written as in Ref. [7]:

$$m^2_{\phi^\pm} = (v_1^2 + v_2^2)\left(\frac{m^2_{12}}{v_1 v_2} - \lambda_4 - \lambda_5\right), \tag{3.1.14}$$

$$m^2_A = (v_1^2 + v_2^2)\left(\frac{m^2_{12}}{v_1 v_2} - 2\lambda_5\right), \tag{3.1.15}$$

Equation (3.1.14) demonstrates the observed parameters which let the charged $W^\pm$ bosons acquire masses. This comes from the digonalisation of the $2 \times 2$ matrix in Equation (3.1.11), which corresponds to so-called Goldstone boson $G^\pm$. It is associated with a zero eigenvalue which express the neutral $Z^0$ boson. The pseudoscalar is originated from the diagonalisation of the $2 \times 2$ matrix of Equation (3.1.12). While Equation (3.1.12) diagonalisation produces the light scalar $h$ and the heavy scalar $H$. An additional scalar is added to the 2HDM in order to handle some of the problems that the 2HDM is facing. This is known as the Madalla hypothesis which is the 2HDM plus a scalar boson $S$ (2HDM+S).

## 3.2 The Madala hypothesis

The 2HDMs introduce scalars to the Higgs sector in an attempt to explain the phenomenology that SM has failed to accommodate. However, several points still need to

| No. | Scalar particles | Decay mode |
|---|---|---|
| 1. | $h$ | $b\bar{b}$, $\tau^+\tau^-$, $\mu^+\mu^-$, $s\bar{s}$, $\mathbf{c\bar{c}}$, $gg$, $\gamma\gamma$, $Z\gamma$, $W^+W^-$, $ZZ$ |
| 2. | $H$ | The decay mode of $h$, $hh$, $SS$, $Sh$ |
| 3. | $A$ | The decay mode of $h$, $t\bar{t}$, $Zh$, $ZH$, $ZS$, $W^\pm H^\mp$ |
| 4. | $H^\pm$ | $W^\pm h$, $W^\pm H$, $W^\pm S$ |
| 5. | $S$ | The decay mode of $h$, $\chi\chi$ |

**Table 3.1:** *Table shows list of the particles content and the possible decay modes of the 2HDM+S [2].*

be understood. For instance, the source of dark matter and the origin of mass for the neutrinos. In this section, we discuss a 2HDMs based model that suggests additional scalars to the 2HDMs. We refer to this model as the Madala hypothesis (MH) which was introduced in Ref. [2]. In this model, a singlet scalar is added to the Higgs sector which satisfies all the assumptions discussed above. This new field interacts with the SM Higgs boson, heavy Higgs boson, pseudoscalar and charged Higgs boson, as shown in Figure 3.1(a). The phenomenology of this scalar is studied in Ref. [2], and it is beyond the scope of this dissertation. Similarly, a CP-even scalar has been also added to act like a mediator to the fields. This new scalar could be considered as SM Higgs-like that couples to all SM particles, as shown in Figure 3.1(b). The potential in Equation (3.1.3) can be re-written for the new CP-even scalar:

$$\begin{aligned} V(\phi_1,\phi_2,S) &= V(\phi_1,\phi_2) + \frac{1}{2}m_S^2S^2 + \frac{\lambda_{S_1}}{2}\phi_1^\dagger\phi_1 S^2 + \frac{\lambda_{S_2}}{2}\phi_2^\dagger\phi_2 S^2 \\ &+ \frac{\lambda_{S_3}}{4}\left[\phi_1^\dagger\phi_2 + \text{h.c.}\right]S^2 + \frac{\lambda_{S_4}}{4!}S^4 + \mu_1\phi_1^\dagger\phi_1 S + \mu_2\phi_2^\dagger\phi_2 S, \\ &+ \mu_3\left[\phi_1^\dagger\phi_2 + \text{h.c.}\right]S + \mu_S S^3, \end{aligned} \tag{3.2.1}$$

where the coupling of Equation (3.2.1) and the interactions vertices have been computed in Ref. [2]. In this dissertation, we focus on process where the heavy boson $H$ decays into SM Higgs boson $h$ and scalar boson $S$. Other possible decay mode for the $S$ is shown in Table 3.1. In the MH we assume that the BR of $H$ to $Sh$, $hh$ or $SS$ is dominant and the BR of $H$ to SM particles is very small.

The production and decay modes of $H$ make use of an effective field theory (EFT) approach. $S$, on the other hand, is considered to be produced dominantly through the decay of $H$. The nature of the $S$ decay modes should include multiple leptons, but we still have to assume how it decays in order to reduce the number of free parameters it introduces in the model. As in Refs. [1, 14, 2, 15, 16, 17, 18], the mass ranges for the new scalars are as follows:

- Light Higgs-boson ($h$): $m_h = 125$ GeV (as the SM Higgs-boson),
- Heavy Higgs-boson ($H$): $2m_h < m_H < 2m_t$, where $m_t$ is the top-quark mass, and

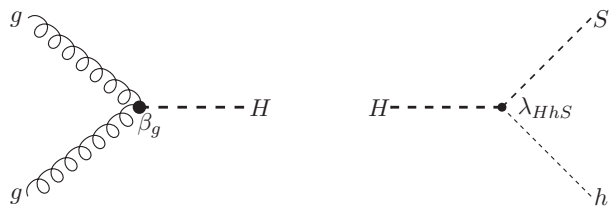


(a) (b)

**Figure 3.2:** *Feynman diagrams contributing to (a) the dominant production mode of $H$ ($g\,g \to H$), and (b) the dominant decay mode ($H \to Sh$). The coupling parameters $\beta_g$ and $\lambda_{HhS}$ are defined in Equations (3.3.1) and (3.3.10).*

- Higgs-like scalar ($S$):[1] $m_h \lesssim m_S \lesssim m_H - m_h$,

## 3.3 Effective field theory of $H$ and $S$

Following an EFT approach, and after electroweak symmetry breaking (EWSB), the required vertices for this study are:

$$\mathcal{L}_{\rm G} = -\frac{1}{4}\,\beta_g \kappa^{\rm SM}_{hgg}\, G_{\mu\nu}G^{\mu\nu}H + \beta_V \kappa^{\rm SM}_{hVV}\, V_\mu V^\mu H, \tag{3.3.1}$$

$$\mathcal{L}_{\rm Y} = -\frac{1}{\sqrt{2}}\left[y_{ttH}\bar{t}tH + y_{bbH}\bar{b}bH\right], \tag{3.3.2}$$

$$\mathcal{L}_{\rm T} = -\frac{1}{2}\,v\lambda_{Hhh}Hhh, \tag{3.3.3}$$

$$\mathcal{L}_{\rm Q} = -\frac{1}{4}\lambda_{HHhh}HHhh, \tag{3.3.4}$$

where $\beta_g = y_{ttH}/y_{tth}$ is a scale factor with respect to the SM Yukawa top coupling for $H$, and therefore multiplies the effective $ggH$ coupling. In Ref. [1], for Run-I fit results, $\beta_g$ was constrained to be $1.5 \pm 0.6$. A similar factor $\beta_V$ is used for $VVH$ couplings, where $V = W^\pm$ and $Z$ bosons. $\kappa^{\rm SM}_{hgg}$ is the SM ggh coupling and $v$ is the standard vev. These interactions are independent of the SM Lagrangian ($\mathcal{L}^{\rm SM}$), that we deliberated on in chapter 2, and the Higgs sector is given by:

$$\mathcal{L}_H = \frac{1}{2}\partial_\mu H\partial^\mu H - \frac{1}{2}m_H^2 HH + \mathcal{L}_{\rm G} + \mathcal{L}_{\rm Y} + \mathcal{L}_{\rm T} + \mathcal{L}_{\rm Q}. \tag{3.3.5}$$

Similarly the Lagrangian for the singlet real scalar $S$ can be written as:

[1] Note that this range is not strictly adhered to, since the original idea was to keep the $H \to Sh$ decay mode on-shell. While off-shell decays not studied here since it deserve especial consideration.

$$\mathcal{L}_S = \mathcal{L}_{\rm K} + \mathcal{L}_{SVV'} + \mathcal{L}_{Sf\bar{f}} + \mathcal{L}_{hHS}, \tag{3.3.6}$$

where

$$\mathcal{L}_{\rm K} = \frac{1}{2}\partial_\mu S \partial^\mu S - \frac{1}{2} m_S^2 SS, \tag{3.3.7}$$

$$\begin{aligned}\mathcal{L}_{SVV'} &= \frac{1}{4}\kappa_{_{Sgg}}\frac{\alpha_s}{12\pi v} S G^{a\mu\nu} G^a_{\mu\nu} + \frac{1}{4}\kappa_{_{S\gamma\gamma}}\frac{\alpha}{\pi v} S F^{\mu\nu} F_{\mu\nu} \\ &+ \frac{1}{4}\kappa_{_{SZZ}}\frac{\alpha}{\pi v} S Z^{\mu\nu} Z_{\mu\nu} + \frac{1}{4}\kappa_{_{SZ\gamma}}\frac{\alpha}{\pi v} S Z^{\mu\nu} F_{\mu\nu} \\ &+ \frac{1}{4}\kappa_{_{SWW}}\frac{2\alpha}{\pi s_w^2 v} S W^{+\mu\nu} W^-_{\mu\nu},\end{aligned} \tag{3.3.8}$$

$$\mathcal{L}_{Sf\bar{f}} = -\sum_f \kappa_{_{Sf}}\frac{m_f}{v} S\bar{f}f, \tag{3.3.9}$$

$$\begin{aligned}\mathcal{L}_{HhS} &= -\frac{1}{2}\, v\Big[\lambda_{_{hhS}} hhS + \lambda_{_{hSS}} hSS + \lambda_{_{HHS}} HHS \\ &+ \lambda_{_{HSS}} HSS + \lambda_{_{HhS}} HhS\Big],\end{aligned} \tag{3.3.10}$$

The notation of $V$ here differs slightly from what is seen before. In this case, $V \equiv g, \gamma, Z, W^\pm$ and $W^\pm_{\mu\nu} = D_\mu W^\pm_\nu - D_\nu W^\pm_\mu$, $D_\mu W^\pm_\nu = [\partial_\mu \pm ieA_\mu] W^\pm_\nu$. $\alpha_s$ and $\alpha$ are the strong and weak couplings respectively. Other possible self interaction terms for $S$ are omitted here since they are not of any phenomenological interest for this study. The total effective Lagrangian is therefore,

$$\mathcal{L}_{\rm tot} = \mathcal{L}^{\rm SM} + \mathcal{L}_H + \mathcal{L}_S. \tag{3.3.11}$$

As mentioned above, the dominant production mechanism for $H$ is assumed to be $gg$F, and the dominant decay mode is $H \to Sh$. The Feynman diagrams for this production and decay chain can be seen in Figure 3.2.

## 3.4 Modelling the decays of $S$

Of particular interest in this research is the ability of the BSM scenario we consider to produce multiple leptons. Since the process $pp \to H \to Sh$ is considered, one would be able to produce multileptonic signatures through the decay of $S$, while the Higgs boson decays dominantly to $b$-quarks. In an attempt to model this, we have considered two different models for the decay of $S$.

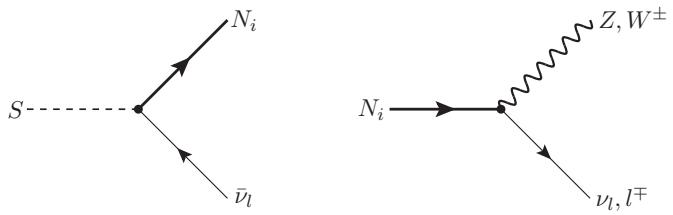


(a) (b)

**Figure 3.3:** *The vertices that build the decay chain of $S$ in the HNM. (a) The decay $S \to N_i \bar{\nu}_l$, and (b) the decay $N_i \to Z\nu_l$, $N_i \to W^{\pm} l^{\mp}$.*

### 3.4.1 The Higgs-like $S$ model

Following the logic of Ref. [2], the decays of $S$ can be made simple through the assumption that it has Higgs-like couplings. These couplings are assumed to be suppressed, such that $S$ is not directly produced with a large cross-section. However, its BRs should be the same as those for a SM-like Higgs boson with a higher mass. This greatly reduces the number of free parameters in the model. If this is the case, then the $S$ should decay more dominantly to $W$ and $Z$ boson pairs as its mass gets closer to $\sim 2\, m_W$. Therefore, the $S$ becomes a source of multiple leptons through the decays of the gauge bosons.

### 3.4.2 The heavy neutrino model

As mentioned above, we have also taken an opportunity to study the possibilities of heavy neutrinos at the LHC. Thus, we introduce the interactions discussed in Refs. [10, 11, 12, 13], where heavy mass neutrino eigenstates $N_i$ couple to the EW bosons $Z, W^{\pm}$ and $S$ via mixing with left-handed (LH) neutrinos $\nu_L$.

Following the notation used in Ref. [10], the flavour state $\nu_l$ in the mass basis is expressed as:

$$\nu_l = \sum_{m=1}^{3} U_{lm} \nu_m + \sum_{m'=1}^{n} V_{lm'} N^c_{m'}, \tag{3.4.1}$$

where $U_{lm}$ and $V_{lm'}$ are the observed light neutrino mixing and active-heavy mixing matrices, respectively. Considering only one heavy mass eigenstate $N$, for simplicity, the interaction Lagrangian with the electroweak bosons is given by:

$$\begin{aligned}\mathcal{L}_{\text{int}} &= -\frac{g}{\sqrt{2}}W_\mu^+\sum_{l=e}^{\tau}\sum_{m=1}^{3}\bar{\nu_m}U_{lm}^*\gamma^\mu P_L l^- - \frac{g}{\sqrt{2}}W_\mu^+\sum_{l=e}^{\tau}\bar{N^c}V_{lN}^*\gamma^\mu P_L l^- \\ &- \frac{g}{2\,\cos\theta_W}Z_\mu\sum_{l=e}^{\tau}\sum_{m=1}^{3}\bar{\nu_m}U_{lm}^*\gamma^\mu P_L\nu_l - \frac{g}{2\,\cos\theta_W}Z_\mu\sum_{l=e}^{\tau}\bar{N^c}V_{lN}^*\gamma^\mu P_L\nu_l \\ &- \frac{gm_N}{2M_W}S\sum_{l=e}^{\tau}\bar{N^c}V_{lN}^*\gamma^\mu P_L\nu_l + \text{h.c.} \qquad (3.4.2)\end{aligned}$$

The precise values of $V_{lN}$ are model dependent. These are constrained by $0\nu\beta\beta$-decays, oscillation and collider experiments and tests of lepton universality, as discussed in Refs. [10, 39, 40].

In the Heavy Neutrino Model (HNM), $S$ is still a source of leptons due to the interaction between the heavy neutrinos and the gauge bosons. The Feynman diagrams showing the decay chain of $S$ in the heavy HNM can be seen in Figure 3.3. The mass of the HNM ($N_i$), however, is not as well constrained and therefore has been considered in the range $m_N = 100 - 1000$ GeV.

## Summary

In summary, we discussed the Higgs sector of the 2HDM. This is done by considering the assumptions presented above. We explored a possible extension of the 2HDM, where we introduced a singlet scalar into the Higgs sector of the 2HDM. As a consequence, two new scalar bosons $S$ and $H$ appear in the extended 2HDM. Furthermore, we introduce a new decay mode for the $S$ in addition to the decay modes shown in Table 3.1. In chapter 5 and 6 we focus on the future of the $S$ in this extended 2HDM model.

# 4 The Large Hadron Collider and the ATLAS Detector

This chapter discusses the experimental setup of the Large Hadron Collider, how it operates, and the ATLAS detector which is within the scope of this dissertation.

## 4.1 The Large Hadron Collider

The Large Hadron Collider (LHC) is the biggest and powerful machine that humanity has ever made. LHC is made as a discovery machine that was built on the experience learned from colliders such as Tevatron, HERA and Sp$\bar{p}$S [41]. It was established by CERN, the European Laboratory for Particle Physics.

The LHC is biggest in accelerator complex at CERN. It is about 27 kilometres in circumference and 75 meters under-ground. It is filled with superconducting magnets that have accelerating points that boosts the energy of the circulating beam of particles up to 7 TeV. Within this ring there are two vacuum pipes that the beam of protons will be injected to. One of these beams goes clockwise and the other counter-clockwise, counter-rotating in four points. These points are place-holders for four huge and important experiment facilities. These are a Large Ion Collider Experiment (ALICE) [42], A Toroidal LHC Apparatus (ATLAS) [43], Compact Muon Solenoid (CMS) [44] and LHC-beauty (LHCb) [45], which is the smallest of them [46].

The LHC receives particles from Super Proton Synchrotron (SPS), that is 7km in circumference [47]. The SPS is designed to accelerate the proton beams to 450 GeV. The LHC is designed to collide a beam of about $10^{11}$ protons. This collision happens 40 millions times per second, which produce 13 TeV of proton-proton collision with an instantaneous luminosity of $10^{34}$ cm$^{-2} \cdot$ s$^{-1}$. Although LHC is designed to collide protons, it can also accommodate heavy ions [41].

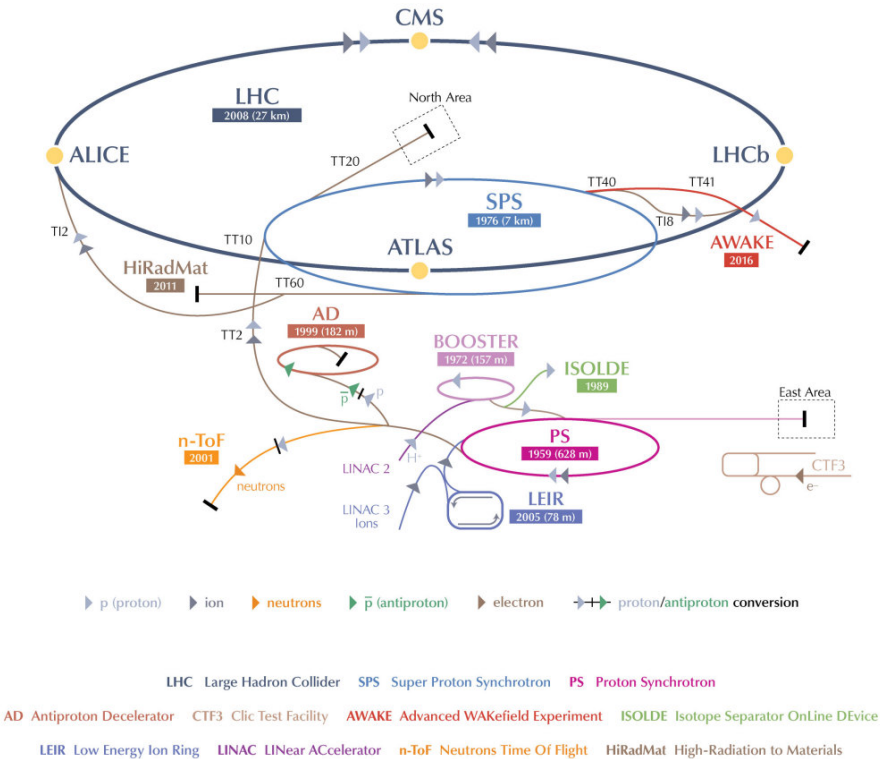


**Figure 4.1:** *CERN's accelerator complex [48].*

### 4.1.1 How does the LHC work

There are four stages that the proton beam has to go through before it ends up colliding in one of the detector experiments:

1. Hydrogen atoms are injected into the Linear accelerator (LINAC 2), see Figure 4.1. Where the electrons will be pulled out of the LINAC 2 chamber, this leaves only the protons which have positive charges. That can be accelerated in an electric field. At this stage the particles will be accelerated up to one third of the speed of light and their energy reach 50 MeV [49], hence the protons are then sent to stage 2.

2. The Proton Synchrotron Booster (PSB), as shown in Figure 4.1, is 175 meters in circumference and consists of four rings which maximise the intensity of the energy beam that comes from LINAC 2, this raises the energy of protons to 1.4 GeV. The PSB accelerates the protons to 91.6% of the speed of light [50] and deliver them to the next step.

3. The Proton Synchrotron (PS), see Figure 4.1, is 628 meters in circumference and is responsible of accelerating the protons package to 99.9% of the speed of light. Here the protons reach the speed limit and, therefore, start getting heavier. The mass of each proton becomes 25 times bigger [51], and then they will be sent to the last stage.

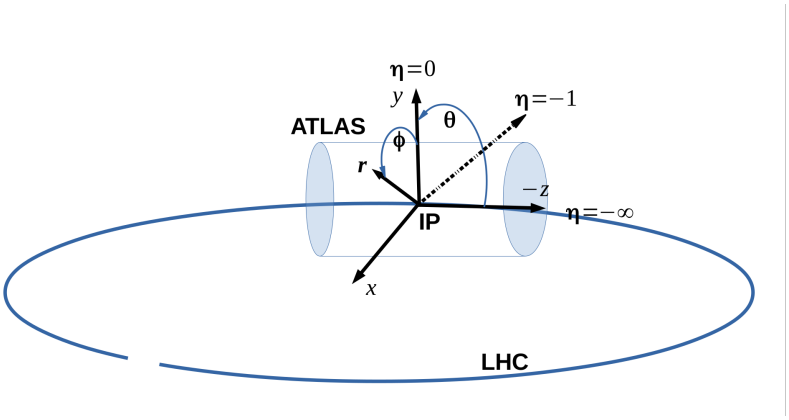


**Figure 4.2:** *A right-handed Cartesian and cylindrical coordinate used by the ATLAS detector.*

4. The Super Proton Synchrotron (SPS) increases the energy of the beam up to 450 GeV and then delivers them to the main gigantic LHC ring, see Figure 4.1 for both SPS and LHC.

5. In the LHC particles are accelerated up to 7 TeV per side, the beam get another boost and will be split into two beams moving away from each other. The velocity of the beams now reach 99.9999% of the speed of light, and hence they cross at 14 TeV in the interaction point of the four experiment.

This is the case where the injected particles are protons, however, same procedures apply for the heavy ion. For the heavy ion collider, the linear accelerator (LINAC 3) point is used and instead of protons lead (Pb) ion is used.

## 4.2 The ATLAS Experiment

ATLAS experiment is a multi-purpose detector and the second-largest experiment in the LHC. The weight of the ATLAS is 7000 tonne and it is 46 meters in length and 25 meters in hight and width. It has been made to explore the products of the proton-proton (p–p) and ion-ion (Pb–Pb) collisions from the LHC. ATLAS uses a right-handed Cartesian coordinate system. The origin of the detector is considered to be the interaction point (IP). The beam direction lays in the horizontal plane and is defined by the $z$-axis, as shown in Figure 4.2. The $x$-axis points from the IP toward the centre of the LHC. While the $y$-axis points upward, the $x-y$ plane is the plane transverse to the direction of the beam and is perpendicular the direction of the pipe. The cylindrical coordinate is defined by:

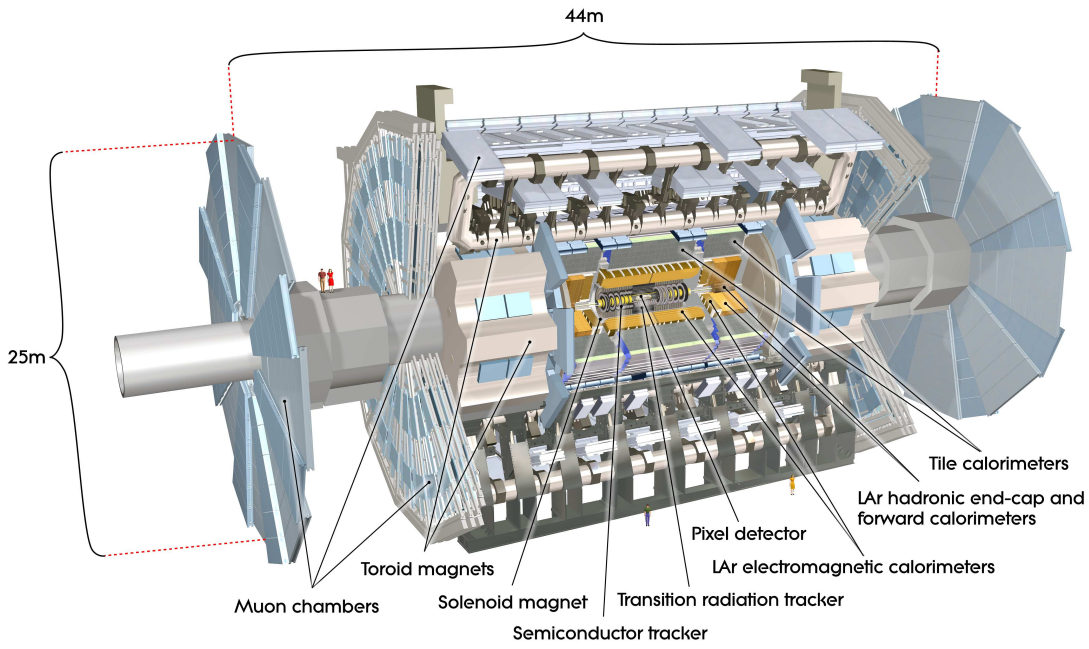


**Figure 4.3:** *CERN's accelerator complex [52].*

$$r = \sqrt{x^2 + y^2}, \tag{4.2.1}$$

$$\phi = \arctan\left(\frac{y}{x}\right), \tag{4.2.2}$$

$$\theta = \arctan\left(\frac{r}{z}\right), \tag{4.2.3}$$

$$\eta = -\ln\left(\tan\left(\frac{\theta}{2}\right)\right), \tag{4.2.4}$$

where $\phi$ is azimuthal angle, which is measured around the beam line from the $x$-axis, $r$ is the radius measured from the beam and $\theta$ measures the angle from the beam and the momentum of the flaying particles. The ATLAS experiment like the other LHC experiments is designed to measure the tracks and energies of scattered particles. It consists of sub-detesters which surround the IP each corresponding to specific measurements. These are the Inner Detector (ID), Calorimeter and the Muon detector, which are explained briefly below.

### 4.2.1 The Inner Detector

The ID is covered by a 2 T solenoid field, it measures the tracks and momentum of charged particles, such as electron and muons. It is a composite of Pixel detector, Silicon microstrip (SCT) tracker and Transition radiation tracker (TRT) as shown in Figure 4.4. The Pixel detector and SCT consist of very sensitive sensors that measure

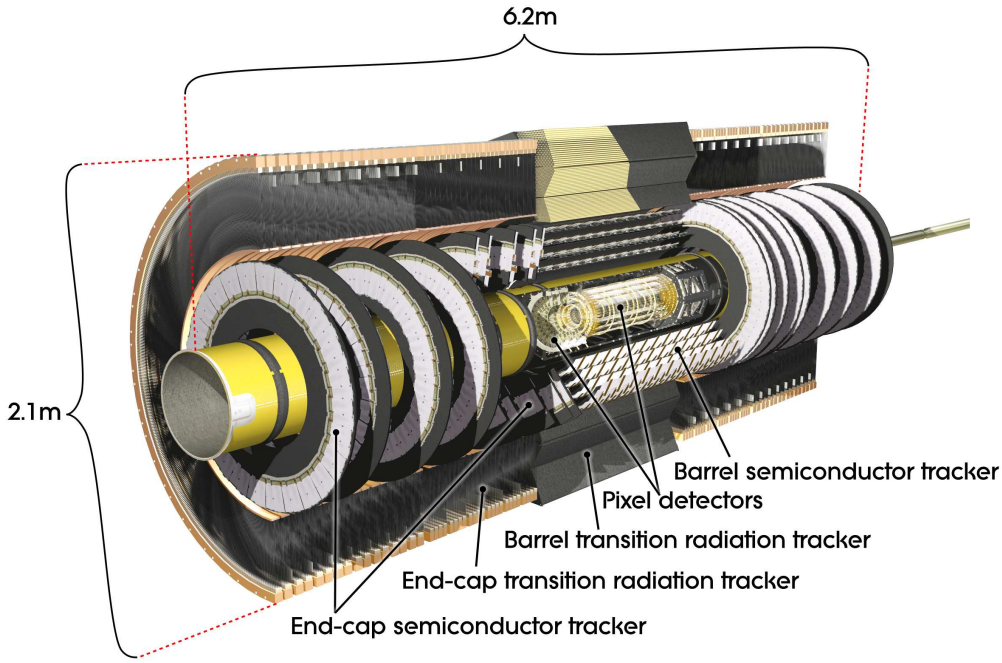


**Figure 4.4:** *A 3D cut-away view of the ID detector and its sub-systems [52].*

the position of particles with a precision of the order of 50 micro-meters. TRT provides an accurate identification of particles by measuring their transition radiation [53, 52]. The Pixel detector, SCT and TRT can measure particles up to $|\eta| = 2.5$.

### 4.2.2 The Calorimeter System

The ATLAS calorimeter system consists of a Liquid Argon (LAr) Electromagnetic calorimeter, Tile Hadronic Calorimeter (TileCal), Endcap and Forward cap Calorimeter. The main goal of these calorimeters is to measure the energy of hadrons, electrons and photons. Figure 4.5 displays the calorimeter and sub-calorimeter systems. They are specific in terms of the region of the pesudorapidity that they cover. For instance, the LAr Electromagnetic calorimeter and TileCal cover the range $|\eta| < 3.2$ and $|\eta| < 1.7$, respectively. While the Endcap and the Forward cap Calorimeter measure particles span the range of $3.1 < |\eta| < 4.9$ ($1.7 < |\eta| < 3.2$). This means that the calorimeter systems cover 4.9 of the pseudorapidity.

### 4.2.3 The Muon Spectrometer

The Muon Spectrometer represents the outer shell of the ATLAS detector. It is designed to measure any charged particles escaping from the end-cap Calorimeter. The Muon System can measure these particles in the range of $|\eta| < 2.7$. In addition, it acts as a trigger on particles spanning the range of $|\eta| < 2.4$.

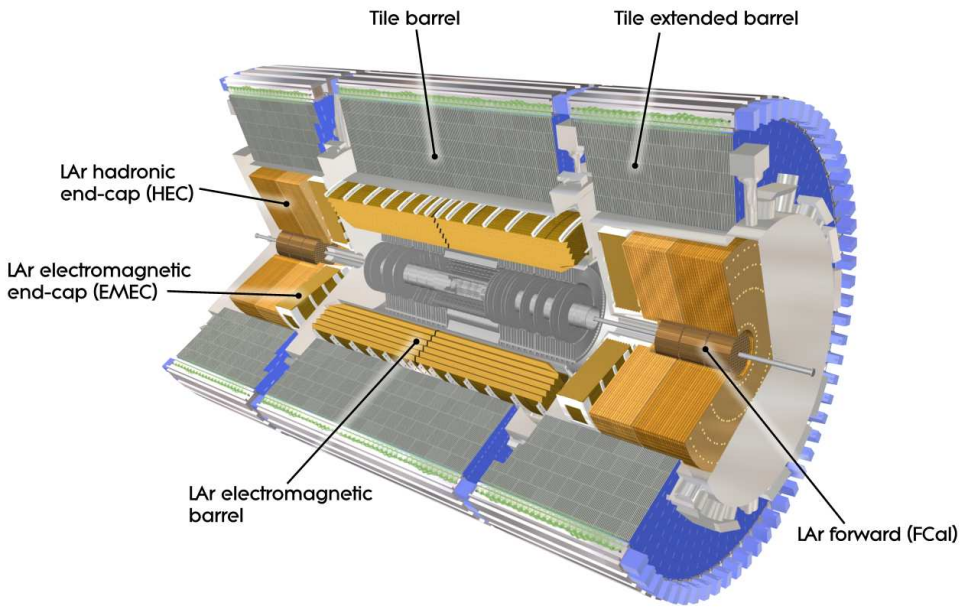


**Figure 4.5:** *A three dimensional view of the ATLAS Calorimeter System and its subsystems [52].*

## Summary

In this chapter we discussed the LHC and how it collides proton–proton to achieve a large centre-of-mass energy. Furthermore, the ATLAS detector, which is one of the LHC experiments, is summarised. Data collected from the ATLAS is analysed or simulated in chapters 5 and 6, along with MC simulated data.

# 5

# Search for Higgs Pair Production in $WW\gamma\gamma$ Channel

This chapter is fully based on our work that is presented in Refs. [54, 55]. It discusses the semi-leptonic $WW^*\gamma\gamma$ final state from a Higgs pair decay, where two photons from $h$, two jets and one charged lepton together with missing energy from $h$ is considered. $W$s bosons decay semileptonically and hadronically. The non-resonant ($gg \to hh \to WW^*\gamma\gamma \to l\nu jj\gamma\gamma$) and the resonant (as in $gg \to H \to hh \to WW^*\gamma\gamma \to l\nu jj\gamma\gamma$) processes are discussed. In addition, a possible search for a heavy boson based on the model discussed in chapter 3 is also presented.

## 5.1 Data samples

The data samples used in this analysis correspond to the data taken by ATLAS throughout 2015 and 2016, which sums up to an integrated luminosity of 36.1 fb$^{-1}$. The whole dataset is recorded with all of ATLAS subsystems operational.

## 5.2 Monte Carlo samples

Monte Carlo simulation is used to simulate the SM Higgs background and the signal. Data-driven method is used to determine the continuum background of the multi-photons and multi-jets processes. The production cross-section of the Higgs pair at $\sqrt{s} = 13$ TeV in gluon–gluon fusion ($gg \to hh$) is 33.41 fb [8].

### 5.2.1 Signal samples

The resonant and non-resonant signal samples are generated at next-to-leading-order (NLO) by using MadGragh5_aMC@NLO [56]. The production of these events are performed with a Higgs Effective Field Theory (HEFT) model [57]. These events are hadronised by Herwig++ with UEEE5 [58] tune and CTEQL1 PDF set [59]. The

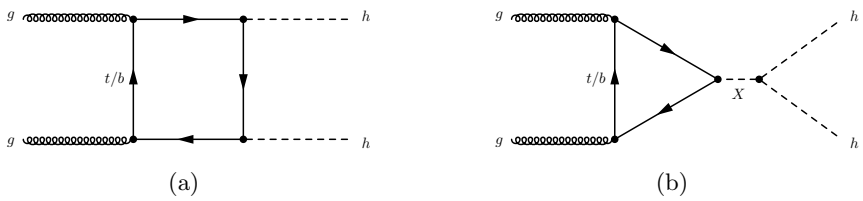


**Figure 5.1:** *Feynman diagrams for leading-order Higgs boson pair production in the SM through (a), a heavy-quark loop and (b) an intermediate heavy resonant.*

masses of the heavy boson $X$ at the generation level are set to be: 260 GeV, 300 GeV, 400 GeV and 500 GeV. This is done by assuming a narrow decay width for $X$ which is set to be 10 MeV. The heavy boson $X$ is forced to decay to a pair of SM Higgs, one of them decays to $WW$ bosons and the other SM Higgs boson decays into two photons.

The $WW\gamma\gamma$ kinematic distributions for particles for signal samples are shown for the resonant and non-resonant. Figure 5.4, 5.3 and Figure 5.4 show the kinematic distributions for the photons, jets and leptons, respectively. They displace the transverse momentum of the leading and the sub-leading of the photons, jets and leptons.

### 5.2.2 Background samples

Since we consider a heavy boson $X$ decaying into two SM Higgs boson $hh$, SM Higgs bosons which come from other sources should be taken into account. Therefore, five production channels are regarded as SM Higgs background. These channels are the gluon-gluon fusion $gg \to h$ (ggh), vector-boson fusion $q\bar{q} \to q\bar{q}h$ (VBF), Higgs production in association with the $W^{\pm}$ and $Z$ bosons $q\bar{q} \to Wh/Zh$ and the associated production with a top quarks $gg/q\bar{q} \to t\bar{t}h$ ($t\bar{t}h$). A prediction of the cross-sections calculated at next-to-next-to-leading order (NNOL) in case of VBF, $Vh$ and $t\bar{t}h$ and next-to-next-to-next-to-leading order (N$^3$LO) for the ggh are summarised in Table 5.1. The ggh is simulated by using Powheg NNLOPS [60]. The VBF events are mimicked at NLO by Powheg and the cross-section is computed in QCD and electroweak (EW) corrections [61, 62]. The processes of $Vh$ are generated, including QCD and EW up to NNLO corrections [63, 64], by Powheg MiNLO. MadGragh5_aMC@NLO [56] is used to generate the contributions from $t\bar{t}h$. The (PDF) sets that are used for the generation are PDF4LHC15 and NNPDF3.0 for the processes ggh, VBF and $Vh$ and $t\bar{t}h$, respectively. There are also particles in the final states, such as $pp \to \ell\nu jj\gamma\gamma$ and $pp \to jjj\gamma\gamma$, that contaminate our signal. Here we refer them as continuum backgrounds. $\ell\nu jj\gamma\gamma$ events are simulated using MadGragh5_aMC@NLO which interfaced with Phyia8, accompanied by AU2 tune and NN23LO1ME PDF set. The computed cross-section of these event is 31.739 fb. Sherpa is used to generate the $jjj\gamma\gamma$ events with CT10 tune, where the cross-section is found to be 40.127 pb.

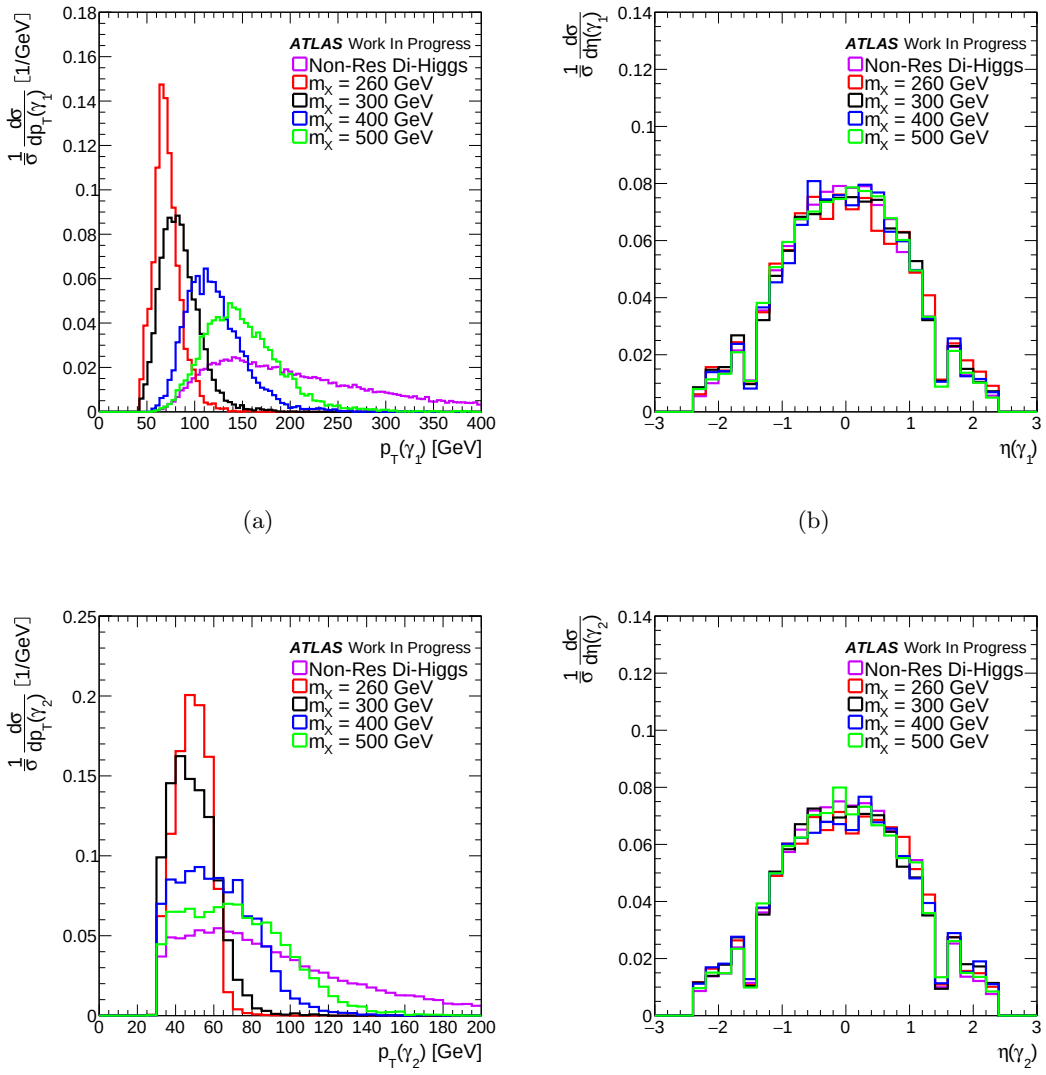


(a) (b)

(c) (d)

**Figure 5.2:** *Distributions of the MC simulation for $WW\gamma\gamma$ of the di-Higgs production. (a) and (c) are the transverse momentum $p_T$ of the leading and sub-leading photon, respectively. (b) and (d) are the pseudorapidity $\eta$ of the leading and sub-leading photon, respectively.*

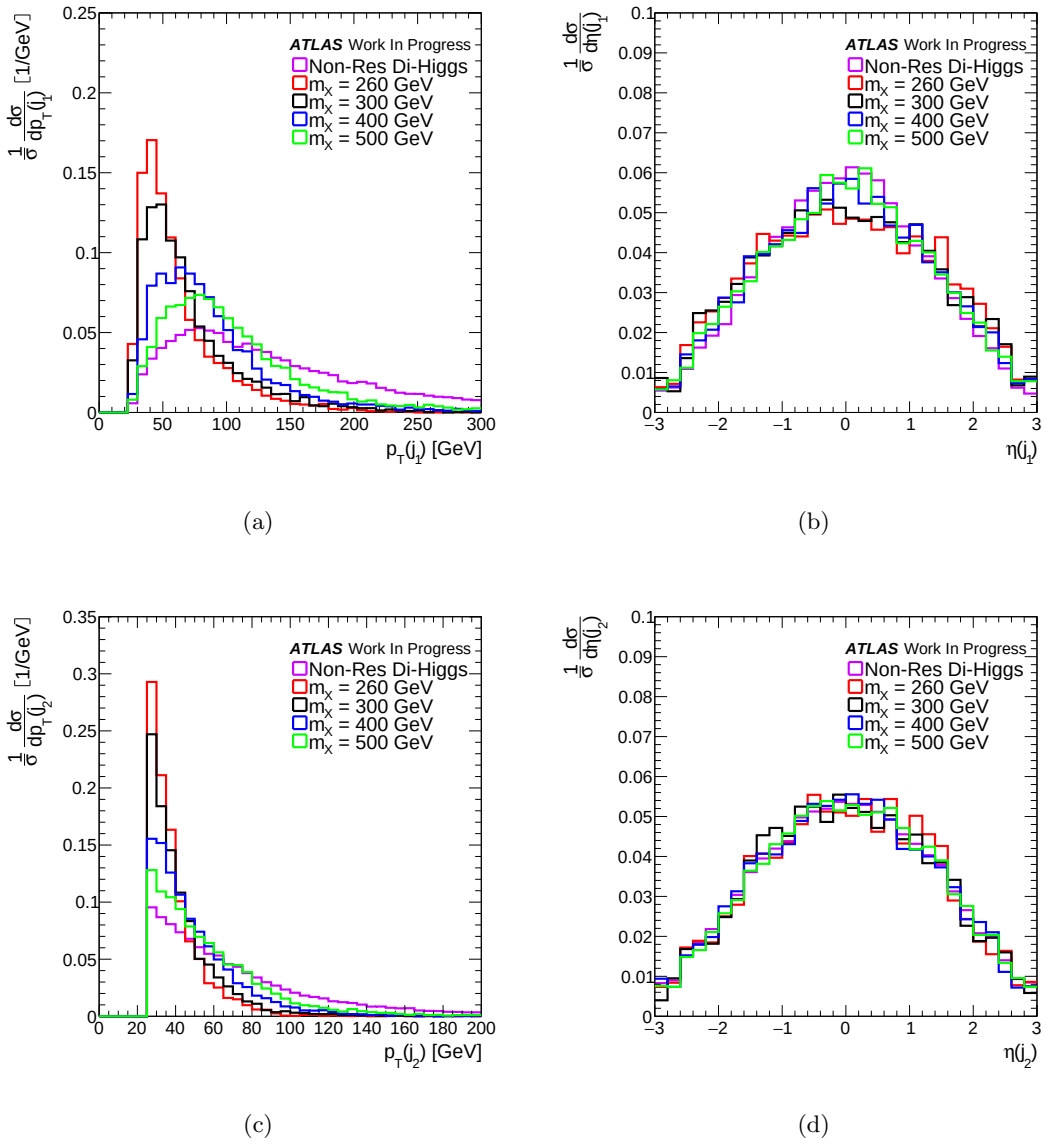


**Figure 5.3:** *Distributions of the MC simulation for $WW\gamma\gamma$ of the di-Higgs production. (a) and (c) are the transverse momentum $p_T$ of the leading and sub-leading jet (at $p_T^{sub\text{-}leading} > 30$ GeV), respectively. (b) and (d) are the pseudorapidity $\eta$ of the leading and sub-leading jet, respectively.*

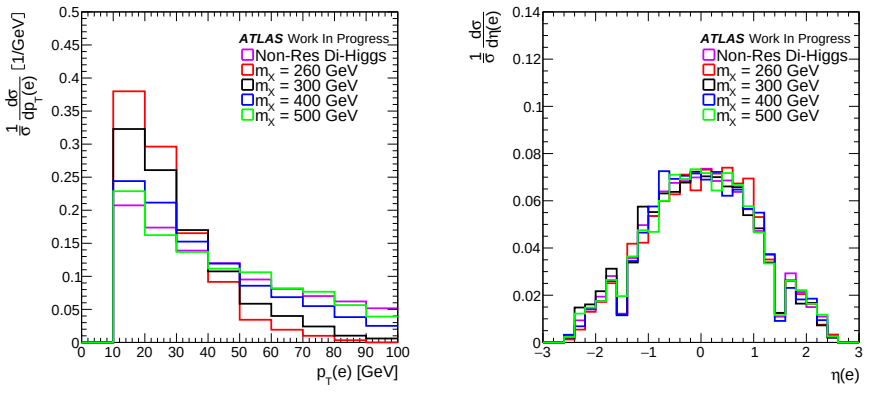


(a)




(b)

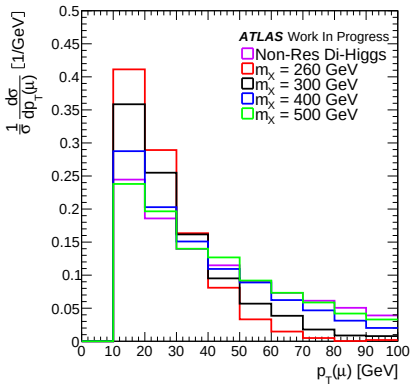


(c)

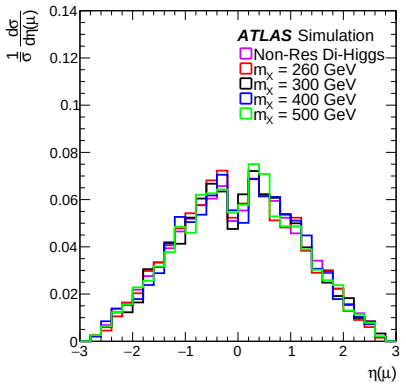


(d)

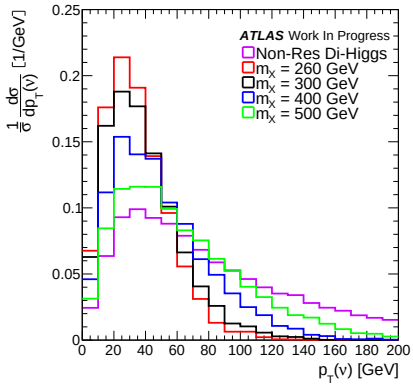


(e)

**Figure 5.4:** *Distributions of the MC simulation for $WW\gamma\gamma$ of the di-Higgs production. (a) and (c) are the transverse momentum $p_T$ of the electron and muon, respectively. (b) and (d) are the pseudorapidity $\eta$ of the electron and muon, respectively. (e) Corresponds to the transverse momentum of neutrino.*

| Processes | Cross-section [pb] |
|---|---|
| ggh | 48.5200 |
| VBF | 3.7790 |
| $W^+h$ | 0.8379 |
| $W^-h$ | 0.5313 |
| $Zh$ | 0.8839 |
| $ggZh$ | 0.7600 |
| $t\bar{t}h$ | 0.5065 |

**Table 5.1:** *The production cross-sections of the SM Higgs boson background for* $m_h = 125$ *GeV [65].*

## 5.3 Object reconstruction and identification

Photons are reconstructed based on the energy deposited in the electromagnetic calorimeter (EM), as described in Ref. [66]. These photons must be in the pseudorapidity of $|\eta| < 2.37$, excluding the crack region of the detector between $1.37 < |\eta| < 1.5$. To suppress the fake photons, the selected photons should pass the tight identification in the inner detector (ID) cut [67]. Tight ID refer to the method that used to separate the converted and unconverted photons. This gives a photon identification efficiency of about 85% for photons with $E_{\mathrm{T}} > 40$ GeV and background with rejection factor of 5000. The transverse momentum of the isolated photon $\mathbf{p}_{\mathrm{T}}^{\mathrm{iso}}$ is required to be inside a cone of $\Delta R = \sqrt{(\Delta\eta)^2 + (\Delta\phi)^2} = 0.2$. Moreover, the diphoton invariant mass should be in the range of $(106, 160)$ GeV.

Electrons are formed by matching an energy deposit in the EM calorimeter to a track in the inner detector. The identification of electrons from jets or non-prompt electron is performed by a set of likelihood-base algorithm [68]. Electrons are required to have a transverse energy $E_{\mathrm{T}} > 10$ GeV and pseudorapidity $|\eta| < 2.47$, excluding the part of the calorimeter between $1.37 < |\eta| < 1.52$. leptons are required to be isolated within a cone of $\Delta R = 0.2$.

Muons are reconstructed incorporating tracks in the ID with that of muon spectrometer (MS) [69]. Muons are required to have $p_{\mathrm{T}} > 10$ GeV and $|\eta| < 2.7$. A cone with $\Delta R = 0.3$ is used to isolate muons.

Jets are reconstructed by using the Anti-$k_t$ algorithm [70] with distance parameter $R = 0.4$. The transverse momentum of jets must be greater than 25 GeV, and they should be within $|\eta| < 2.5$. A multivariate technique (MV2c10) [71, 72] is used to classify the $b$-tagged jets, with an efficiency of 70%. Jet vertex tagger was used to reject jets which are coming from pileup. This was applied for jets with $p_{\mathrm{T}} < 60$ GeV and $|\eta| < 2.4$.

Missing transverse energy ($E_{\mathrm{T}}^{\mathrm{miss}}$) is defined as the negative sum of the transverse momentum $p_{\mathrm{T}}$ of all reconstructed charged or neutral particles, such as electrons, muons, jets and photons.

| Samples / Cuts | Non-resonant | Resonance Mass | | | |
|---|---|---|---|---|---|
| | | **260 GeV** | **300 GeV** | **400 GeV** | **500 GeV** |
| All Events | 100.0% | 100.0% | 100.0% | 100.0% | 100.0% |
| Duplicate | 100.0% | 100.0% | 100.0% | 100.0% | 100.0% |
| GRL | 100.0% | 100.0% | 100.0% | 100.0% | 100.0% |
| Pass Trigger | 73.8% | 68.5% | 69.4% | 71.8% | 74.4% |
| Detector Quality | 73.8% | 68.5% | 69.4% | 71.8% | 74.4% |
| has PV | 73.8% | 68.5% | 69.4% | 71.8% | 74.4% |
| 2 loose photons | 59.0% | 56.3% | 55.8% | 57.2% | 59.5% |
| Trig Match | 58.8% | 56.0% | 55.5% | 56.8% | 59.2% |
| Tight ID | 48.6% | 45.3% | 44.7% | 46.8% | 49.4% |
| Isolation | 43.9% | 38.5% | 38.5% | 41.9% | 44.9% |
| Rel.Pt cuts | 40.4% | 36.1% | 35.0% | 38.2% | 41.7% |
| $105 < m_{\gamma\gamma} < 160$ GeV | 40.2% | 36.0% | 34.9% | 38.0% | 41.5% |
| At least 1 lepton | 17.5% | 16.5% | 15.8% | 17.4% | 17.9% |
| At least 2 central jets | 11.0% | 6.40% | 7.54% | 10.3% | 11.9% |
| B-veto | 10.4% | 6.08% | 7.11% | 9.66% | 11.2% |
| $p_{\mathrm{T}}(\gamma\gamma) > 100$ GeV | 8.63% | - | - | 7.82% | 10.4% |

**Table 5.2:** *The accumulative cut efficiency for the non-resonant and resonant signal samples.*

Overlap removal technique was applied to ensure that we did not count the event twice. The removal is defined by the value of $\Delta R$, as follows: electrons and jets are removed if their distance to photon is smaller than 0.4 in $\Delta R$, namely $\Delta R(e,\gamma) < 0.4$ and $\Delta(\gamma,\mathrm{jet}) < 0.4$. Also jets and muons with $\Delta R(\mu,\gamma)$ and $\Delta(\mu,\mathrm{jet})$ less than 0.4 are removed. In addition, jets with $\Delta(\mathrm{jet},e) < 0.2$ are also removed.

## 5.4 Event selection

Events are required to have two photons, as explained in section 5.3. The selection of these photons is performed according to the selection in Ref. [73]. The leading and sub-leading photon must have $E_{\mathrm{T}}$ satisfying $E_{\mathrm{T}}^{\gamma}/m_{\gamma\gamma} > 0.35$ and 0.25, respectively. In addition to the two photons selections, events with at least two jets are required to have $p_{\mathrm{T}} > 25$ GeV and $|\eta| < 2.5$. Also, an event will be rejected if any $b$-tagged jet is found in the events. A $b$-tagger (MV2c10) with a $b$-tagging efficiency of 70% is used to suppress the contribution coming from $t\bar{t}h$. Moreover, the number of leptons in the final state should be at least one lepton and it could be either a muon or an electron.

The continuum background is suppressed, to enhance the non-resonant and the resonant Higgs, by cutting on the diphoton transverse momentum $p_{\mathrm{T}}^{\gamma\gamma}$. For the non-resonant and resonant Higgs boson pair production with $m_X < 400$ GeV the transverse momentum is required to be greater than 100 GeV, as shown in Figure 5.5.

The selection efficiencies for the signal samples as a function of the mass of $X$ are shown in Table 5.2. Where the selection efficiency at the diphoton invariant mass

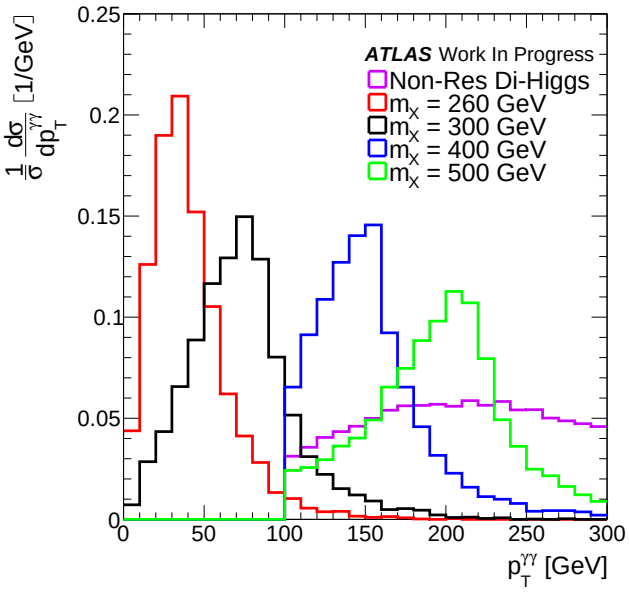


**Figure 5.5:** *Kinematic distributions of the transverse momentum of two photons system $p_T^{\gamma\gamma}$; for the signal in case of the non-resonant di-Higgs and when the mass of the heavy boson $X$ is 260 GeV, 300 GeV, 400 GeV and 500 GeV. A cut on $p_T^{\gamma\gamma} > 100$ is applied for the non-resonant and resonant with mass of 400 GeV and 500 GeV.*

($m_{\gamma\gamma}$) cut is 40.2%, 36.0%, 34.9%, 38.0% and 41.5% for the non-resonant and resonant with 260 GeV, 300 GeV, 400 GeV and 500 GeV, respectively. After additional cuts, the selection efficiencies for the signal are 8.63%, 7.82% and 10.4% for the non-resonant and for the resonant with masses 400 GeV and 500 GeV, respectively. In cases where the mass of $X$ is lower than 400 GeV, the efficiency becomes 6.08% for $m_X = 260$ GeV and 7.11% for $m_X = 300$ GeV.

## 5.5 Signal and background estimation

### 5.5.1 Signal modelling and estimation

A double-sided Crystal Ball (DSCB) is used to model the shape of the signal. The DSCB is used to fit the MC simulation of the non-resonant and resonant di-Higgs production with $m_h = 125$ GeV and different resonant masses, to the distribution of the invariant mass of the two photons. The DSCB is defined as:

| Cuts \ Samples | ggh | VBF | $W^+h$ | $W^-h$ | $Zh$ | $ggZh$ | $t\bar{t}h$ |
|---|---|---|---|---|---|---|---|
| All Events | 100.0% | 100.0% | 100.0% | 100.0% | 100.0% | 100.0% | 100.0% |
| Duplicate | 100.0% | 100.0% | 100.0% | 100.0% | 100.0% | 100.0% | 100.0% |
| GRL | 100.0% | 100.0% | 100.0% | 100.0% | 100.0% | 100.0% | 100.0% |
| Pass Trigger | 59.9% | 61.0% | 55.6% | 60.4% | 57.1% | 67.7% | 73.5% |
| Detector Quality | 59.9% | 61.0% | 55.6% | 60.4% | 57.1% | 67.7% | 73.5% |
| has PV | 59.9% | 61.0% | 55.6% | 60.4% | 57.1% | 67.7% | 73.5% |
| 2 loose photons | 49.8% | 50.8% | 43.2% | 48.1% | 46.0% | 56.2% | 59.1% |
| Trig Match | 49.7% | 50.7% | 43.1% | 48.0% | 45.9% | 56.0% | 58.6% |
| Tight ID | 43.2% | 43.8% | 37.0% | 41.1% | 39.4% | 48.1% | 48.6% |
| Isolation | 38.6% | 39.6% | 32.6% | 36.2% | 34.7% | 43.2% | 40.3% |
| Rel.Pt cuts | 35.8% | 36.0% | 29.9% | 33.1% | 31.7% | 39.4% | 36.7% |
| $105 < m_{\gamma\gamma} < 160$ GeV | 35.8% | 36.0% | 29.7% | 33.0% | 31.6% | 39.2% | 36.3% |
| At least 1 lepton | 0.0266% | 0.0355% | 5.24% | 5.66% | 2.30% | 3.09% | 11.4% |
| At least 2 central jets | 0.00381% | 0.00789% | 0.715% | 0.791% | 0.426% | 0.936% | 10.6% |
| B-veto | 0.00317% | 0.00694% | 0.683% | 0.748% | 0.386% | 0.856% | 1.97% |
| $p_{\mathrm{T}}(\gamma\gamma) > 100$ GeV | 0.000873% | 0.00404% | 0.373% | 0.367% | 0.186% | 0.643% | 1.10% |

**Table 5.3:** *The selection efficiency for the SM Higgs background samples of the ggh, VBF, $W^+h$, $W^-h$, $Zh$, $ggZh$ and $t\bar{t}h$.*

$$CB(m_{\gamma\gamma}) = N \times \begin{cases} e^{-\frac{t^2}{2}}, & \text{if } -\alpha_{\text{low}} \leq t \leq \alpha_{\text{high}} \\ \dfrac{e^{-\frac{1}{2}\alpha_{\text{low}}^2}}{\left[\frac{1}{\frac{n_{\text{low}}}{\alpha_{\text{low}}}}\left(\frac{n_{\text{low}}}{\alpha_{\text{low}}} - \alpha_{\text{low}} - t\right)\right]^{n_{\text{low}}}}, & \text{if } t < -\alpha_{\text{low}} \\ \dfrac{e^{-\frac{1}{2}\alpha_{\text{high}}^2}}{\left[\frac{1}{\frac{n_{\text{high}}}{\alpha_{\text{high}}}}\left(\frac{n_{\text{high}}}{\alpha_{\text{high}}} - \alpha_{\text{high}} - t\right)\right]^{n_{\text{high}}}}, & \text{if } t > \alpha_{\text{high}} \end{cases} \tag{5.5.1}$$

where $t = (m_X - \mu_{CB})/\sigma_{CB}$, $\mu_{CB}$ is the Gaussian distribution peak and $\sigma_{CB}$ is the width of the DSCB Gaussian core. The parameters $\alpha_{\text{low}}$ and $\alpha_{\text{high}}$ are the exponent high of the low mass and exponent high of the high mass, respectively. $n_{\text{low}}$ and $n_{\text{high}}$ are the power-low and power-high of the exponent tile, respectively. MC samples are used to compute the expected events of the non-resonant and resonant signals. This is performed by assuming the cross-section for the non resonant to be $\sigma(pp \to hh) = 1$ pb and in the resonant case $\sigma(pp \to X) \times \text{BR}(X \to hh) = 1$ pb.

### 5.5.2 Background modelling and estimation

The single SM Higgs boson is considered as background and its contribution to the $m_{\gamma\gamma}$ distribution is estimated by using MC simulation. Table 5.3 displays the cut efficiencies for the SM background. It shows that most of the contribution comes from the $t\bar{t}h$, this

is assignable to the lepton which comes from the decay of the top quark and the high jet multiplicity. The continuum background contribution to the $m_{\gamma\gamma}$ is estimated from the fit to the diphoton invariant mass. Where several functions are examined to model the continuum background. The test and the computation of the continuum background are given below.

**Spurious signal**

The spurious signal method is important in helping us decide which PDF will be suitable for our study. In addition, it allows us to describe the continuum background and to estimate the fluctuation in the continuum background.

The spurious signal is computed only on the range of the SM Higgs boson signal $m_{\gamma\gamma}$. The model used for the fitting is signal plus background ($S$+$B$), which has the composite PDF form:

$$N_S \times \mathrm{PDF}_S + N_B \times \mathrm{PDF}_B. \tag{5.5.2}$$

Where $N_S$, $\mathrm{PDF}_S$, $N_B$ and $\mathrm{PDF}_B$ are number of signal, PDF of the signal, number of background and PDF of the background, respectively. The PDF of the signal is already stored in the workspace and the PDF of the continuum background is to be determined by this study. The selection of the continuum background PDF is performed by HGamTool. HGamTool is a software package that inherent from HGamAnalysisFramework that is used by the HGam group. as follows:

- A fit of $(S+B)$ will be done first on the input MC, so that we can get the number of the signal for all the selected background PDF's.
- The maximum fitted signal will be computed in the SM Higgs boson mass signal ($N_S$).
- Then we apply selection as to whether to accept or reject a certain PDF. The acceptance of the PDF is achieved by selecting the maximum signal over the error to be less than 20%, $\max(N_S/\Delta N_S) < 20\%$. Where $\Delta N_S$ is the systematic uncertainty of the spurious signal.
- The PDF is chosen if it passed the condition above. However, if all the selected functions passed the selection criteria, then the PDF with less parameters will be selected by the tool.
- In the configuration file, the integrated luminosity of the input dataset has to be consistent with the luminosity of the computed yield.
- The lower and upper end of the window to maximise over to compute the spurious signal is (Higgs mass signal $\pm$ 8 GeV).
- Exponential, ExpPoly2, Poly1 and Poly2 are the PDF functions that are to be tested.

| Function | Max($N_S$) | Max($N_S/\Delta N_S$) | Result | Function | Max($N_S$) | Max($N_S/\Delta N_S$) | Result |
|---|---|---|---|---|---|---|---|
| Exponential | 0.81309 | 16.08% | pass | Exponential | 0.82685 | 16.25% | pass |
| ExpPoly2 | −0.43869 | −10.51% | pass | ExpPoly2 | −0.45901 | −10.90% | pass |
| Poly1 | −1.69689 | −44.85% | fail | Poly1 | −1.73049 | −45.43% | fail |
| Poly2 | −1.11274 | −29.16% | fail | Poly2 | −1.13824 | −29.63% | fail |
| For $m_X = 260$ GeV | | | | For $m_X = 300$ GeV | | | |
| Exponential | 0.245930 | 10.53% | pass | Exponential | 0.240416 | 10.55% | pass |
| ExpPoly2 | −0.264615 | −10.61% | pass | ExpPoly2 | −0.259126 | −10.74% | pass |
| Poly1 | −0.272567 | −11.83% | pass | Poly1 | −0.269504 | −12.05% | pass |
| Poly2 | −0.277345 | −11.86% | pass | Poly2 | −0.253425 | −11.07% | pass |
| For $m_X = 400$ GeV | | | | For $m_X = 500$ GeV | | | |
| Exponential | 0.243031 | 10.56% | pass | | | | |
| ExpPoly2 | −0.260077 | −10.64% | pass | | | | |
| Poly1 | −0.274957 | −12.10% | pass | | | | |
| Poly2 | −0.261354 | −11.31% | pass | | | | |
| Non-resonant | | | | | | | |

**Table 5.4:** *Spurious signal computation and the selection result of the PDF function for the background. The examined PDF functions are Exponential, ExpPoly2, Poly1 and Poly2. $N_S$ is the amount of the spurious signal around the $m_{\gamma\gamma}$ and $\Delta N_S$ is the systematic uncertainty in the signal. The value of Max($N_S/\Delta N_S$) $< 20\%$ is the criteria used to make judgement, as to whether the PDF function should pass or not.*

- The scan range has been set to be between the range of $(115 - 135)$ GeV.
- The scan is performed by taking 0.5 GeV as interval between the scan points.

The input dataset for the test is generated by merging the $\gamma\gamma$ background samples. That is to be used as an input file for the spurious signal study. Each sample has been normalised by its number of events in the control region (side-band). The samples are smoothened by an exponential function, then merged. The reason for smoothing the samples is that the samples do not have enough number of entries. So the only way to avoid the MC fluctuation is to smooth single samples and fit them because we use a non-binned likelihood estimator. Then the spurious test is only testing the difference between the mixed function and the single final fit function. The result of the $(S + B)$ fit parameters for the background is shown in Table 5.4. The table shows results for the non-resonant and the resonant Higgs boson pair production.

## 5.6 Systematic uncertainties

A combined uncertainties from different sources could severely affect the measurements. Therefore, we consider different uncertainties that can have a huge impact on our measurements. For instance, the uncertainty in the measurement of the delivered luminosity is systematic uncertainty.

| Processes | +QCD Scale | −QCD Scale | $PDF$ | $\alpha_s$ |
|---|---|---|---|---|
| $ggh$ | +3.9% | −3.9% | ±1.9% | ±2.6% |
| VBF | +0.4% | −0.3% | ±2.1% | ±0.5% |
| $W^+h$ | +0.5% | −0.7% | ±1.7% | ±0.9% |
| $W^-h$ | +0.5% | −0.7% | ±1.7% | ±0.9% |
| $Zh$ | +0.5% | −0.6% | ±1.7% | ±0.9% |
| $ggZh$ | +25.1% | −18.9% | ±1.8% | ±1.6% |
| $t\bar{t}h$ | +5.8% | −9.2% | ±3.0% | ±2.0% |

**Table 5.5:** *Theoretical uncertainties for the production of the SM Higgs boson with $m_h = 125$ GeV. These uncertainties are for the QCD scale, PDF uncertainties and the coupling constant ($\alpha_s$) which are taken from [65].*

### 5.6.1 Theoretical uncertainties

These uncertainties come from theoretical models such as the SM and its extensions. Where the determination of their fundamental parameters plays a crucial role. In this work, theoretical uncertainties are considered for the QCD scale, QCD coupling constant and PDF uncertainties. For a single SM Higgs boson production the recommended uncertainties are shown in Table 5.5, as provided in Ref. [65]. And the theoretical uncertainties for the di-Higgs production are given in Table 5.6, as recommended by Ref. [8]. The uncertainties in the continuum background are estimated as explained in section 5.5.2. Where the uncertainties range from 2.6% to 4.6% as shown in the highlighted area in Table 5.4.

### 5.6.2 Experimental uncertainties

In Run-I data taking period it is found that the uncertainty for 22.7 fb$^{-1}$ of pp collision delivered to ATLAS at $\sqrt{s} = 8$ TeV is ±1.9% [74]. Following similar arguments the luminosity uncertainty in Run-II is found to be 2.1% for 36.1 fb$^{-1}$ luminosity of pp collision at $\sqrt{s} = 13$ TeV.

The uncertainty of the diphoton trigger is computed to be 0.4%, as reported by Ref. [75]. A maximum uncertainty of 1.7% is estimated for misidentification of photons that come from the radiative $Z$ boson, including $\gamma$ events and events that come from $Z \to e^+e^-$ [67]. There is also uncertainty due to the photon track isolation which mainly comes from the measurements of the data to simulation efficiency, and it is about 1%. Moreover, the measurement of the photon energy resolution can have impact on the efficiency of the event selections and it ranges from 1.2% to 2.0%.

Jet energy scale uncertainties are estimated from Run-I and Run-II data, which are found to affect the selection of the event from 3.5% to 5.2%. In addition, uncertainty from the resolution of the jet energy is found to have a value of 0.2% to 8.0%. Electrons and muons are found to have uncertainties coming from their reconstructions, identification and isolation of about 1%. Uncertainties arising from pileup re-weighting, to

| $\sqrt{s}$ | $\sigma^{NNLO}_{gg\to hh}$ | Scale | $\pm PDF$ % | $\pm\alpha_s$ % | EFT |
|---|---|---|---|---|---|
| 13 TeV | 33.41 fb | +4.3% -6.0% | ±2.1% | ±2.3% | ±5% |

**Table 5.6:** *Theoretical uncertainties for the di-Higgs production in gluon–gluon fusion (ggh), taken from Ref. [8].*

differentiate the events distribution per bunch crossing, range from 2.0% to 1.8%. A summary of these uncertainties are provided in Table 5.7.

## 5.7 Statistical model

A likelihood function to the parameters to the data is used to perform the fit of diphoton invariant mass and its form (see Ref. [76]) is given by:

$$\mathscr{L}(\mu,\theta) = \begin{array}{l}\prod_i (N_{\text{BSM}}(\mu,\theta)\times f_{\text{DSCB}}(m^i_{\gamma\gamma},\theta) + N_{\text{SM}}(\theta)\times f_{\text{DSCB}}(m^i_{\gamma\gamma},\theta) \\ +N_{\text{Cont}}\times f_{\text{Cont}}(m^i_{\gamma\gamma},\theta) + N_{SS}\times f_{\text{DSCB}}(m^i_{\gamma\gamma},\theta))\prod \text{Norm}(\theta|0,1)\end{array}, \quad (5.7.1)$$

where $N_{\text{BSM}}$ and $N_{\text{SM}}$ are the expected signal yield and expected events of single Higgs boson, respectively; $f_{\text{DSCB}}$ is a double-sided crystal ball for both SM and BSM signal. $N_{\text{Cont}}$ is the events number of the continuum background, $f_{\text{Count}}$ is a second order exponential PDF function that describes the continuum background and $N_{SS}$ is the estimated spurious signal. The number of events of spurious signal and the PDF functions are shown in Table 5.4. $\mu$ represents the cross-section for the non-resonant case, and the cross-section times the branching ratio in the resonant case. The nuisance parameters ($\theta$) are estimated by using the Norm (probability density function), and $i$ is the index of the event. Finally there are normalisation terms that pull the value of nuisance parameters to their best value. The best fit is performed by setting an upper limit Ref. [76] which is defined by:

$$\tilde{q}_\mu = \begin{cases} -2\ln\frac{\mathscr{L}(\mu,\hat{\hat{\theta}}(\mu))}{\mathscr{L}(0,\hat{\hat{\theta}}(0))} & \text{if } \hat{\mu} < 0 \\ -2\ln\frac{\mathscr{L}(\mu,\hat{\hat{\theta}}(\mu))}{\mathscr{L}(\hat{\mu},\hat{\theta})} & \text{if } 0 \le \hat{\mu} \le \mu \\ 0 & \text{if } \hat{\mu} > \mu \end{cases} \quad (5.7.2)$$

where $\mathscr{L}$ is the likelihood function in Equation 5.7.1, $\mu$ and $\theta$ are same as in Equation 5.7.1.

| Source of uncertainties | | Non-resonant $hh$ | $X \to hh$ | Single-$h$ bkg $p_{\mathrm{T}}^{\gamma\gamma} > 100$ GeV | Single-$h$ bkg No $p_{\mathrm{T}}^{\gamma\gamma}$ selection |
|---|---|---|---|---|---|
| Luminosity 2015+2016 | | 2.1 | 2.1 | 2.1 | 2.1 |
| Trigger | | 0.4 | 0.4 | 0.4 | 0.4 |
| Pileup re-weighting | | 0.5 | 0.9 | 0.7 | 0.6 |
| Event statistics | | 1.7 | 2.2 | 1.6 | 1.3 |
| Photon | energy resolution | 7.7 | 5.1 | 11.4 | 9.3 |
| | energy scale | 0.5 | 0.4 | 0.5 | 0.5 |
| | identification | 1.7 | 1.4 | 0.8 | 0.8 |
| | isolation | 0.8 | 0.7 | 0.4 | 0.4 |
| Jet | energy resolution | 0.1 | 1.6 | 0.5 | 1.0 |
| | energy scale | 4.0 | 9.9 | 2.4 | 2.6 |
| $b$-tagging | $b$-hadron jets | 0.06 | 0.09 | 3.8 | 3.6 |
| | $c$-hadron jets | 1.5 | 1.0 | 0.7 | 0.6 |
| | light-hadron jets | 0.3 | 0.3 | 0.1 | 0.1 |
| | extrapolation | 0.02 | 0.001 | 0.1 | 0.08 |
| Lepton | electron | 0.5 | 0.7 | 0.2 | 0.2 |
| | muon | 0.5 | 0.7 | 0.3 | 0.5 |
| Theory | PDF on $\sigma$ | 2.1 | - | 3.4 | 3.4 |
| | $\alpha_S$ on $\sigma$ | 2.3 | - | 1.3 | 1.3 |
| | scale on $\sigma$ | 6.0 | - | 0.9 | 0.9 |
| | HEFT on $\sigma$ | 5.0 | - | - | - |
| | Scale on $Acc$ | 3.4 | 4.1 | - | - |
| | PDF on $Acc$ | 3.0 | 2.4 | - | - |
| | PS on $Acc$ | 7.8 | 29.6 | - | - |
| | jet multiplicity | - | - | 6.3 | 6.3 |
| | BR($h \to \gamma\gamma$) | 2.1 | 2.1 | 2.1 | 2.1 |
| | BR($h \to WW^*$) | 1.5 | 1.5 | 1.5 | 1.5 |
| Total | | 14.8 | 32.4 | 14.8 | 13.2 |

**Table 5.7:** *Summary of systematic uncertainties propagated to the yields in percentage. Entries marked by '-' indicate that the systematic uncertainty is not applicable for the corresponding process. The extrapolation uncertainties in b-tagging include two components: one is from the extrapolation to high-$p_T$ ($p_T > 300$ GeV) jets and the other one is from extrapolating c-jets to $\tau$-jets. The resonant numbers shown here assume $m_X$=260 GeV.*

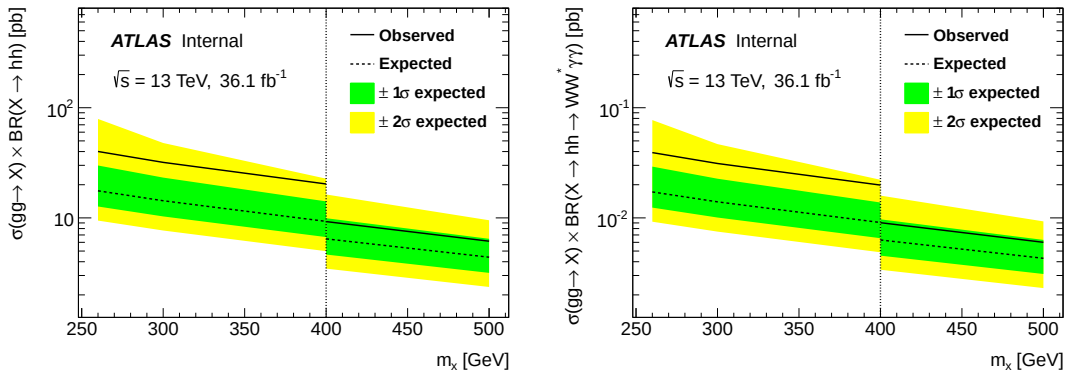


(a) (b)

**Figure 5.6:** *Upper limit at 95% confidence level of the resonant di-Higgs production cross-section multiplied by the branching ratio of $X \to hh$ as a function of the mass of the $X$. (a) Without considering the SM branching ratio of $h \to WW^*$ and $h \to \gamma\gamma$. (b) Considering the SM branching ratio of $h \to WW^*$ and $h \to \gamma\gamma$. The solid line is the expected limit and the dashed line is the expected. The green and yellow band are correspond to $1\,\sigma$ and $2\,\sigma$ interval on the expected limit, respectively. The region on the right hand of the dashed-vertical line at $m_X = 400\,GeV$ was evaluated with $p_T^{\gamma\gamma} >$ 100 GeV cut in both plots, but not the one on left hand of the dashed-vertical line.*

## 5.8 Results

Following Ref. [77], a frequentist approach $CL_s$ is adopted to compute 95% confidence-level (CL) exclusion limits that yield the expected 1 $\sigma$ and 2 $\sigma$ band. The results are shown for the non-resonant and resonant di-Higgs production with and without $p_T^{\gamma\gamma} >$ 100 GeV cut, as described in section 5.4. It is hardly worth mentioning excess in the data associated to the expected total background. The resonant with $m_{\gamma\gamma} = 400$ GeV reports substantial variation from the background-only hypothesis. This deviation corresponds to a $2.0\,\sigma$ effects. The expected cross-section of the non-resonant di-Higgs production is 5.4 pb, while the observed cross-section is 7.7 pb giving a small excess in the data. The expected cross-section times the branching ratio of $(X \to hh)$ is 17.6 to 4.4 pb, meanwhile, for the the mass of the resonant between 260 and 500 GeV the observed cross-section times the branching ratio is in the range of 40 pb to 6.1 pb. This was unaccompanied by the branching ratio of the SM Higgs boson to $WW^*$ and $\gamma\gamma$, as shown in Figure 5.6(a). However, by including the branching ratio of the SM Higgs boson to $WW^*$ and $\gamma\gamma$, the expected cross-section times the branching ratio of $hh \to WW^*\gamma\gamma$ for the non-resonant is 5.3 fb, and the observed limit is 7.6 fb. In the resonant case the the expected cross-section times $hh \to WW^*\gamma\gamma$ limit ranges 16.8 fb to 4.2 fb and the observed limit is 38.2 fb to 5.9 fb, as shown in Figure 5.6(b). The invariant mass of the diphoton $m_{\gamma\gamma}$ derived using the statistical model described in section 5.7 is shown in Figure 5.7.

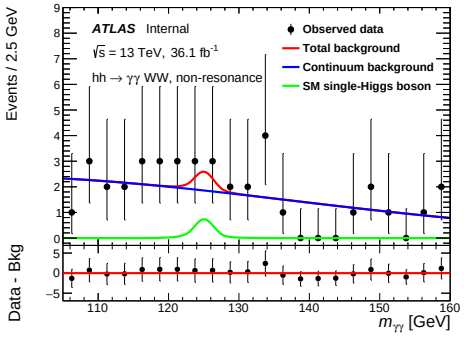


(a)

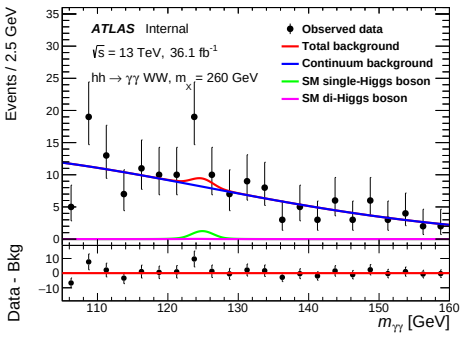


(b)

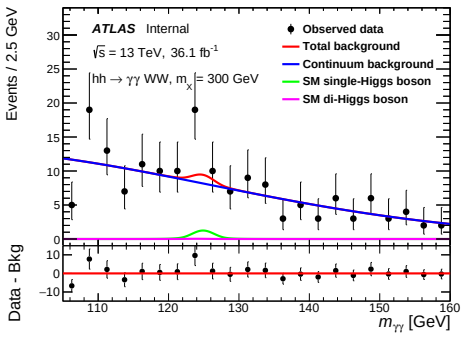


(c)

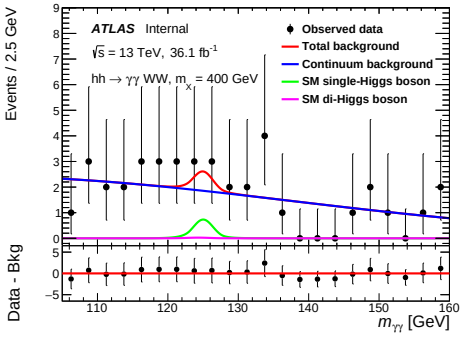


(d)

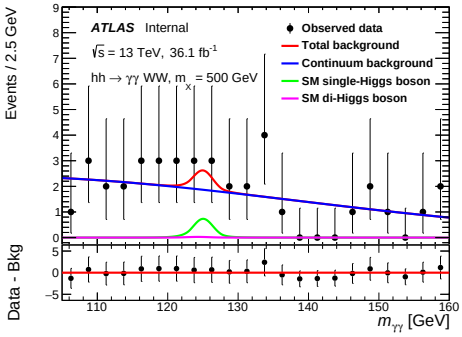


(e)

**Figure 5.7:** *Kinematic distributions of the selected events ($\ell\nu jj\gamma\gamma$) of the diphoton invariant mass for data and MC simulation. The fit is performed for (a) non-resonant and the resonant masses (b) $m_X = 260\ GeV$, (c) $m_X = 300\ GeV$, (d) $m_X = 400\ GeV$ and (e) $m_X = 500\ GeV$. (b) and (c) are evaluated with $p_T^{\gamma\gamma} > 100\ GeV$ cut.*

## Summary

In this chapter we investigated the SM Higgs boson pair production in the $WW\gamma\gamma$ channel with one lepton, two jets and two photons in the final states. The search is carried out on pp collision data that is collected by the ATLAS experiment in the data taking period of 2015-2016. The analysis is performed at luminosity of 36.1 $fb^{-1}$ at centre-of-mass energy of 13 TeV. The non-resonant and resonant di-Higgs production are studied. It is found that the main source of the uncertainty is coming from the resolution of jet energy which have value of 0.2% to 8.0%. No significant deviation from the SM prediction is observed in the data.

# 6

# Multilepton Signatures at the LHC

Leptons have very distinct signatures in particle physics detectors, such as ATLAS and CMS detectors. In this chapter, the phenomenology of a heavy boson which decays to a scalar boson and a SM Higgs boson is studied in a BSM scenario. Furthermore, we analyse the results of the di-lepton invariant mass that are reported by ATLAS and CMS collaborations. In addition, a study of three leptons final states is also reported.

This chapter is largely based on the work descried in Ref. [78], which uses the effective models explained in chapter 3. Details about simulation, phenomenology and analysis of the BSM signals are illustrated in chapter 1. The focus of this chapter is at the production of the heavy boson in gluon-gluon fusion.

## 6.1 Simulation and analysis

Monte Carlo (MC) events were generated and analysed in order to study the cross-sections and kinematics of the BSM scenario that we have discussed in this chapter. Firstly, model files were built based on the Lagrangian described in Equations (3.3.5), (3.3.11) and (3.4.2) using the FeynRules package [79]. The various processes were simulated by using MG5_aMC@NLO [80]. These hard scatter events were passed to Pythia8 [81] for the parton shower (PS) and hadronisation; with NNPDF2.3QCD+QEDLO [82] PDF set, and thereafter through Delphes3 [83] to estimate the detector response for both ATLAS and CMS. Jets were clustered using FastJet [84] with the anti-$k_T$ algorithm [70] using the distance parameter $R = 0.4$. For $b$-tagged jets $p_{\mathrm{T}} > 25\,\mathrm{GeV}$ within $|\eta| < 2.4$ were used. Only signal processes were generated for this study; all contributing backgrounds were extracted from the relevant ATLAS and CMS papers, as referenced in the text. We have considered direct production mechanisms of $H$ through ggF ($gg \to H \to Sh$) and the production of the $H$ in association with the top quarks ($t(tt)H \to Sh$).

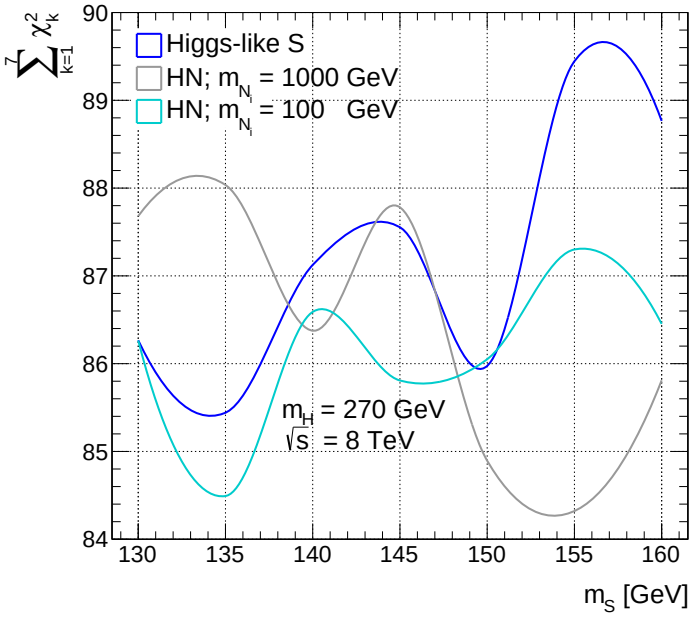


**Figure 6.1:** *Distributions of the $\chi^2$ sum of the di-lepton invariant mass of ATLAS and CMS data [85, 86, 87, 88, 89] comparing to the Higgs-like $S$, HNM with $m_{N_i} > m_S$ and HNM with $m_{N_i} < m_S$; as a function of the mass of the scalar boson ($m_S$). These measurements resulted from the analysis of the di-lepton invariant mass of the ATLAS and CMS data (see appendices A, B and C).*

## 6.2 Data and background samples

The analysis is based on the data collected by both the ATLAS and CMS experiments [85, 86, 87, 88, 89] through Run-I data-taking period. This corresponds to a centre-of-mass energy of 8 TeV with integrated luminosity of 20.3 fb$^{-1}$ for ATLAS data and 19.4 fb$^{-1}$ for CMS data. Currently no results are available with 2016 data.

## 6.3 Method for determining the best fit mass points of $S$

Based on the analysis of the di-lepton invariant mass,[1] we studied the masses of the $S$ that can fit the data in Refs. [85, 86, 87, 88, 89] best. As explained in chapter 3, we scan the mass of the $S$ in the range between $(130, 160)$ GeV; taking 5 GeV as a step. Hence, each mass point is added (in the BSM scenario) to the SM backgrounds described in Refs. [85, 86, 87, 88, 89]. Then $\chi^2$ values (defined in Equation A.1.1) are calculated after fitting the di-lepton invariant mass spectrum ($m_{\ell\ell}$). The sum of the $\chi^2$ for all the ATLAS and CMS measurements ($\sum_{k=1}^{7} \chi^2_k$) is shown in Figure 6.1. This figure

[1] More information about these analysis are provided in appendices A, B and C.

shows that the Higgs-like $S$ and the HNM ($m_{N_i}$ is on-shell) follow the same pattern. They have the same minima at $m_S = 135$ GeV and maxima approximately around $m_S = 155$ GeV. However, the HNM with $m_{N_i}$ off-shell ($m_{N_i} > m_S$) deviates from the latter two by 5 GeV. This gave the HNM two local minimus at $m_S = 140$ GeV and $m_S = 155$ GeV, and maximum at $m_S = 132$ GeV. To simplify the analysis we will use $m_S = 135, 140$ and 150 GeV. These masses will be compared to the ATLAS and CMS data and SM background in Refs. [85, 86, 87, 88, 89].

## 6.4 Direct production of $H$

As mentioned above, we assume that the $H$ is produced primarily through ggF, and has a 100% BR to $Sh$. Thereafter, $h$ is allowed to decay to all possible modes according to the available phase space. The scalar boson $S$, on the other hand, decays according to the two scenarios discussed in chapter 3. Firstly, through SM-like Higgs boson decay modes, $S$ decays into all possible SM final states. Secondly, $S$ decays through $N_i$ to leptons and missing transverse energy ($E_{\mathrm{T}}^{\mathrm{miss}}$) in the HNM (as shown in Figure 3.3).

By considering $S$ to be a Higgs-like scalar boson, the number of free parameters is drastically reduced. For this reason, we consider the Higgs-like $S$ model for comparisons to data and fitting the masses of $H$ and $S$. This choice also enhances the number of leptons via the decay of $S$, since for a Higgs-like scalar boson with a mass near $2\,m_W$, the BR for $S \to W^+W^-$ becomes dominant.

In contrast with this, the HNM produces $N_i$, which naturally gives leptonic signatures either through charged or neutral leptons in association with $W^\pm$ and $Z$ bosons. We also note that for $m_{N_i} > m_S$ the $N_i$ become off-shell, as shown in Figures 6.2(c) and 6.2(d). This affects the features of the kinematic observables as opposed to the case where $m_{N_i} < m_S$ is on-shell as shown in Figures 6.2(a) and 6.2(b).

### 6.4.1 Di-lepton final states

There are two natural signatures that arise from event selections based on the sign of leptons. These are opposite-sign (OS) and same-sign (SS) di-leptons. We have only considered $e^\pm$ and $\mu^\pm$ as leptons, barring possibilities from $\tau^\pm$ leptons. In OS the selection we have required $e^\pm e^\mp$, $\mu^\pm\mu^\mp$ or $e^\pm\mu^\mp$ pairs, and for SS pairs we have required $e^\pm e^\pm$, $\mu^\pm\mu^\pm$ or $e^\pm\mu^\pm$. The event selection based on kinematic cut is the same for both cases, and it is as follows: electrons should satisfy $|\eta^e| < 2.47$ and excluding the transition region of the calorimeter $1.57 < |\eta^e| < 1.37$. Muons are selected if $|\eta^\mu| < 2.4$. Jets must have transverse momentum $p_{\mathrm{T}}^{\mathrm{jet}} > 25$ GeV and must be in the pseudorapidity $|\eta^{\mathrm{jet}}| < 4.5$. Events must have exactly two leptons with OS or SS leptons and should satisfy the selection criteria described above. The leading and the sub-leading leptons are required to have transverse momentum $p_{\mathrm{T}}^{\mathrm{lead}} > 25$ GeV and the sub-leading $p_{\mathrm{T}}^{\mathrm{sub\text{-}lead}} > 15$ GeV. These selections are summarised in Table 6.2 for OS leptons and in Table 6.1 for SS leptons.

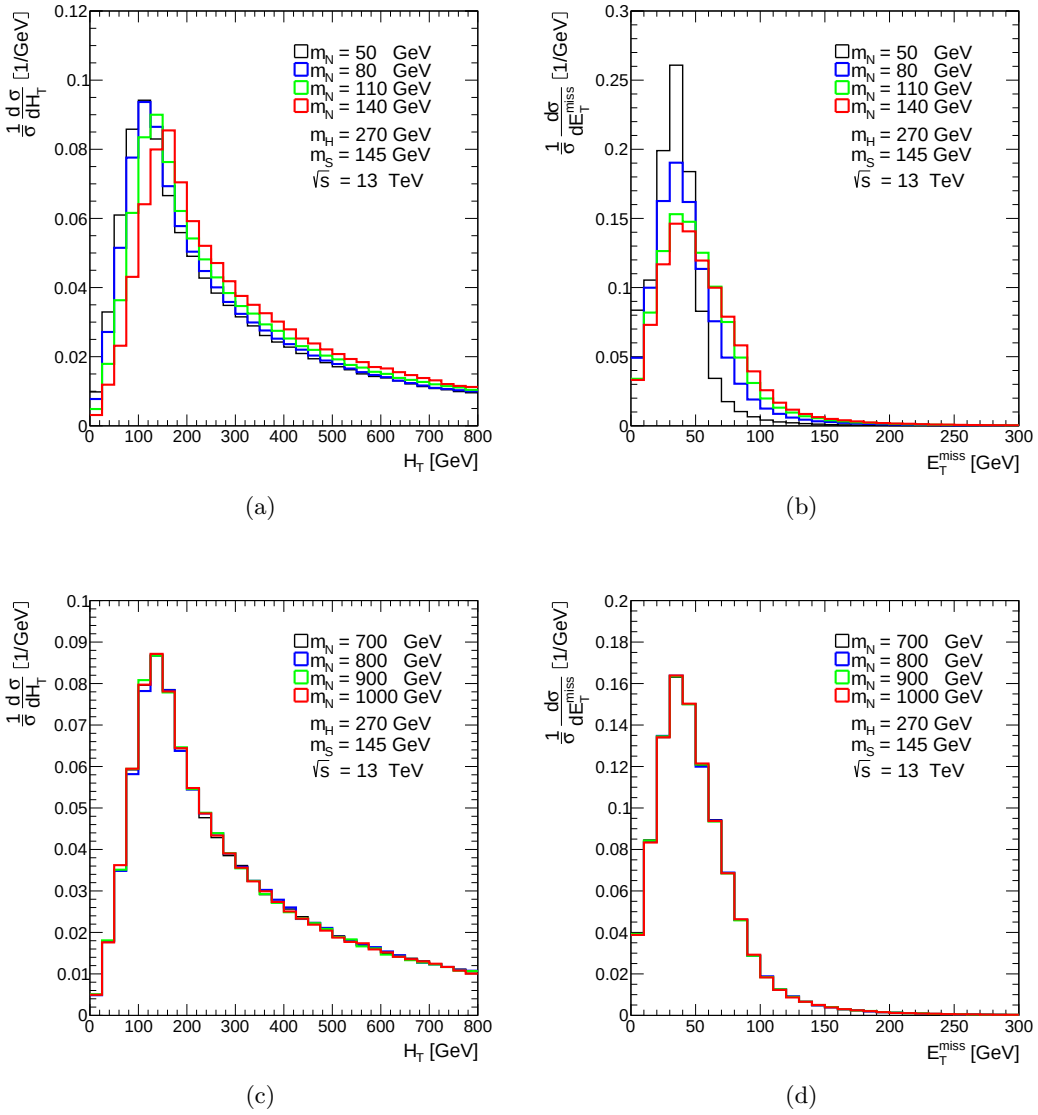


**Figure 6.2:** *Kinematic distributions of the HNM for the off shell and on shell effect of the mass of the HNM $m_{N_i}$. For $m_{N_i} < m_S$ (a) The scalar sum of all final states particles transverse momentum $H_T$ and (b) The missing transverse energy. In case of $m_{N_i} > m_S$ (c) The scalar sum of all final states particles transverse momentum $H_T$ and (d) The missing transverse energy.*

| | Higgs-like S | HNM with $m_{N_i} = 1000$ GeV | HNM with $m_{N_i} = 100$ GeV |
|---|---|---|---|
| All events | 2000000 | 2000000 | 2000000 |
| $e^{\pm}e^{\pm}/\mu^{\pm}\mu^{\pm}/e^{\pm}\mu^{\pm}$ | 7301 | 206443 | 209451 |
| $p_{\mathrm{T}}^{\text{lead}} > 25$ GeV | 6144 | 187646 | 182472 |
| $p_{\mathrm{T}}^{\text{sub-lead}} > 15$ GeV | 5042 | 164825 | 154735 |
| Efficiency | 0.002521 | 0.0824125 | 0.0773675 |

**Table 6.1:** *Cutflow for MC simulation of the event selections of two SS leptons ($e^{\pm}e^{\mp}/\mu^{\pm}\mu^{\mp}/e^{\pm}\mu^{\mp}$) for the SM background, Higgs-like $S$ and the HNM. Two cases, depending on the mass of the HNM $m_{N_i}$, are considered for the HNM.*

| | SM | Higgs-like S | HNM with $m_{N_i} = 1000$ GeV | HNM with $m_{N_i} = 100$ GeV |
|---|---|---|---|---|
| All events | 2000000 | 2000000 | 2000000 | 2000000 |
| $e^{\pm}e^{\mp}/\mu^{\pm}\mu^{\mp}/e^{\pm}\mu^{\mp}$ | 102538 | 31619 | 412713 | 418597 |
| $p_{\mathrm{T}}^{\text{lead}} > 25$ GeV | 86625 | 27064 | 376229 | 367165 |
| $p_{\mathrm{T}}^{\text{sub-lead}} > 15$ GeV | 69265 | 22526 | 324992 | 297133 |
| $E_{\mathrm{T}}^{\text{miss}} > 20$ | 39134 | 15715 | 284717 | 261284 |
| Efficiency | 0.019567 | 0.0078575 | 0.142358 | 0.130642 |

**Table 6.2:** *Cutflow for MC simulation of the event selections of two OS leptons ($e^{\pm}e^{\mp}/\mu^{\pm}\mu^{\mp}/e^{\pm}\mu^{\mp}$) for the SM background, Higgs-like $S$ and the HNM. Two cases, depending on the mass of the HNM $m_{N_i}$, are considered for the HNM.*

Based on the above requirements, basic kinematic distributions are shown in Figures 6.3, 6.4 and 6.5 for $m_H = 270$ GeV, $m_S = 145$ GeV, $m_{N_i} = 100$ GeV and $m_{N_i} = 1000$ GeV. A SM prediction is also shown for the OS di-leptonic events, whereas for the SS selection the SM acceptance was far too low to generate a reasonable amount of statistics. Even if the SM can produce a few SS di-leptonic events, they are constructed from fake leptons and should be ignored.

A number of features deserve discussion. As opposed to the production of the SM Higgs boson via ggF, the direct production of di-leptons with $H \to Sh$ displays significantly larger jet multiplicity (6.3(a) and 6.3(c)). Di-leptons are studied at ATLAS and CMS within the context of $h$-related measurements and the measurement of the non-resonant $WW$ production by applying restrictions on the number of hadronic jets and $b$-tagged jets. In this context it would be interesting to study the di-lepton invariant distributions in events with more than one hadronic jet and with the application of a veto on $b$-tagged jets. OS di-leptons display the feature that about a third of the events contain at least one $b$-tagged jet, where top-related backgrounds contribute strongly (see section 6.4.2). The production mechanism of $S$ suggested here is distinct from the potential direct production via gluon-gluon fusion due to the significantly enhanced jet activity and the associated production of $b$-tagged jets.

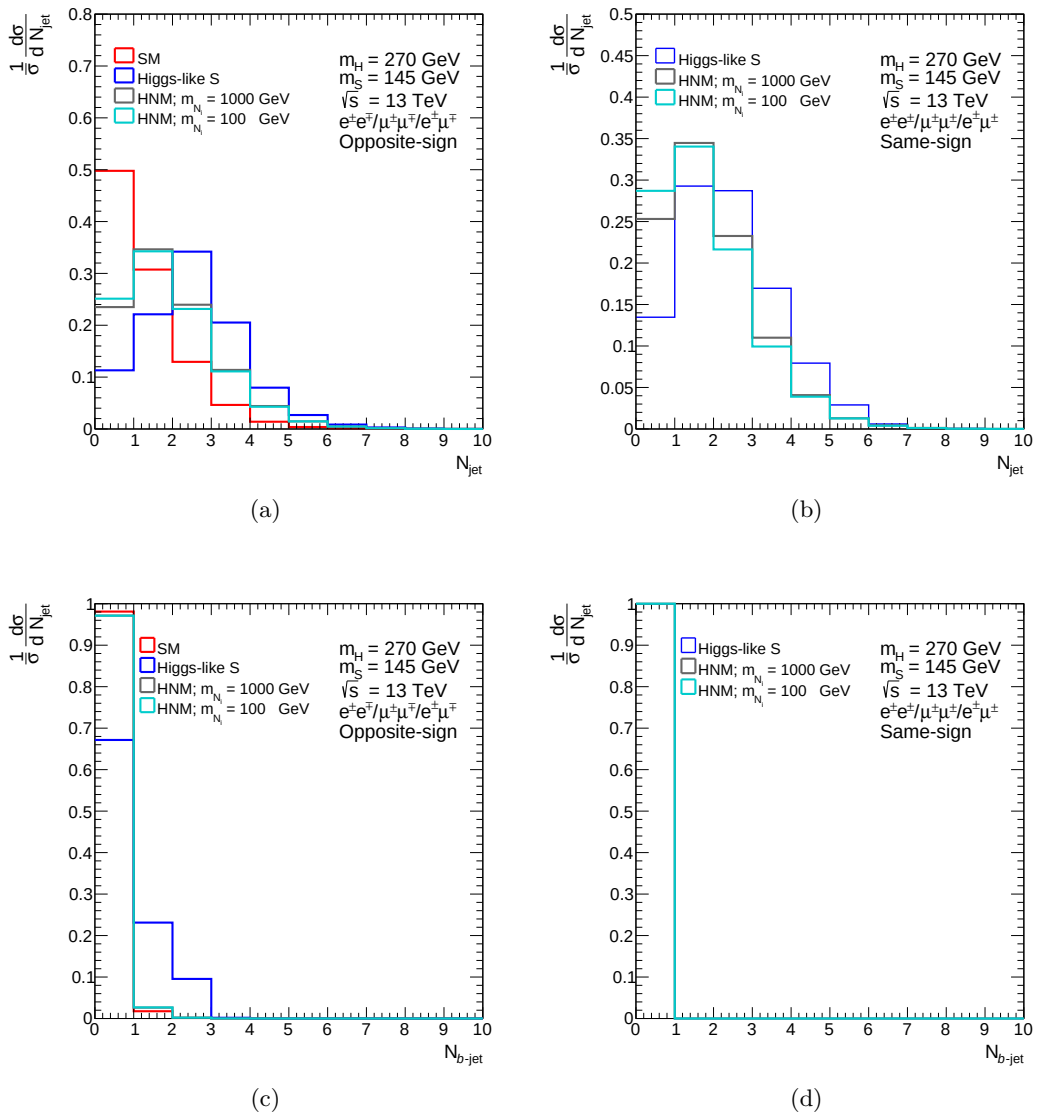


**Figure 6.3:** *Normalised distributions of (a), (b) jet and (c), (d) b-tagged jet multiplicities for the event pre-selection in case of OS (left) and SS (right) channels, where the process is $gg \to H \to Sh$.*

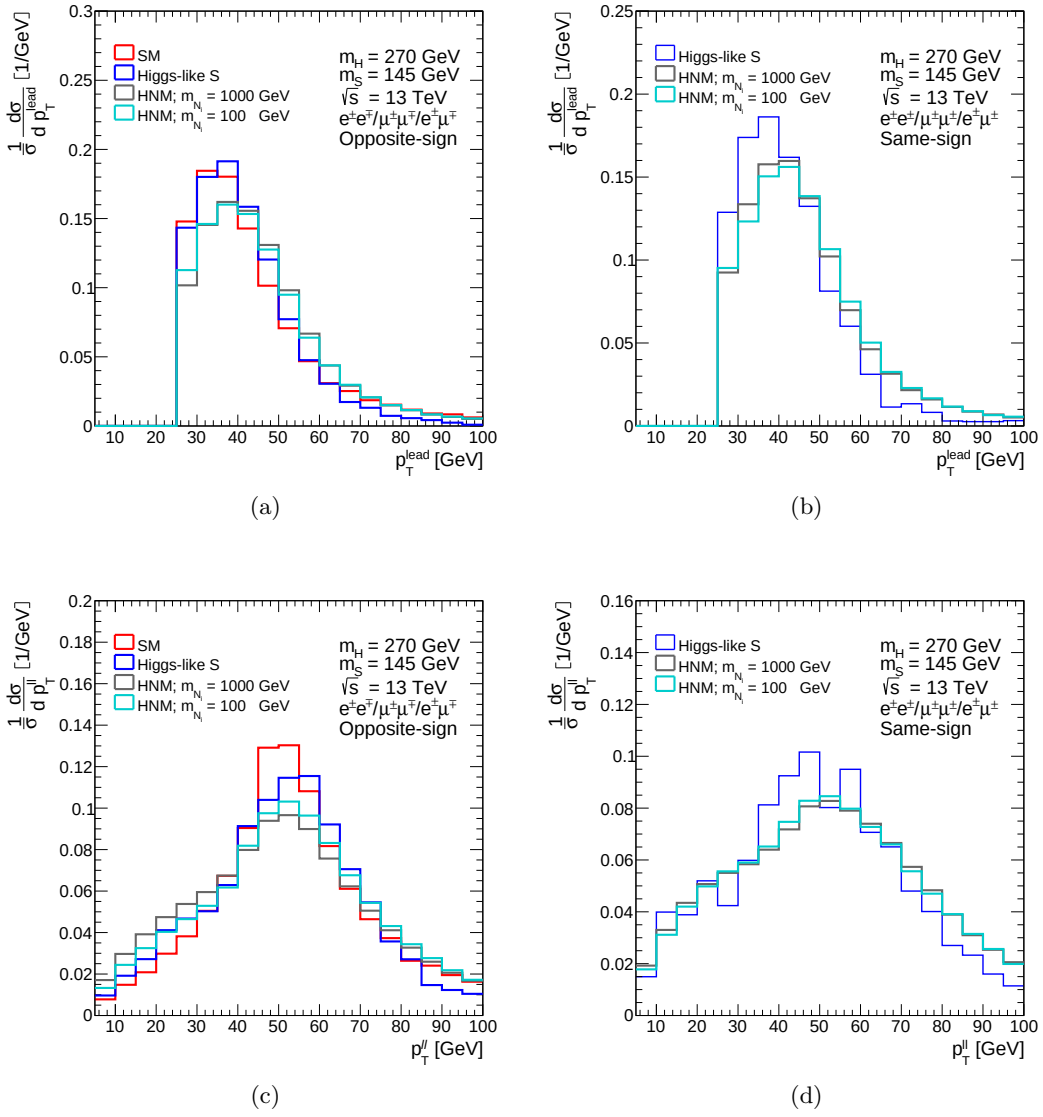


**Figure 6.4:** *Normalised distributions of (a), (b) leading-lepton $p_T$ and (c), (d) $p_T$ of di-lepton system for the event pre-selection in case of OS (left) and SS (right) channels, where the process is $gg \to H \to Sh$.*

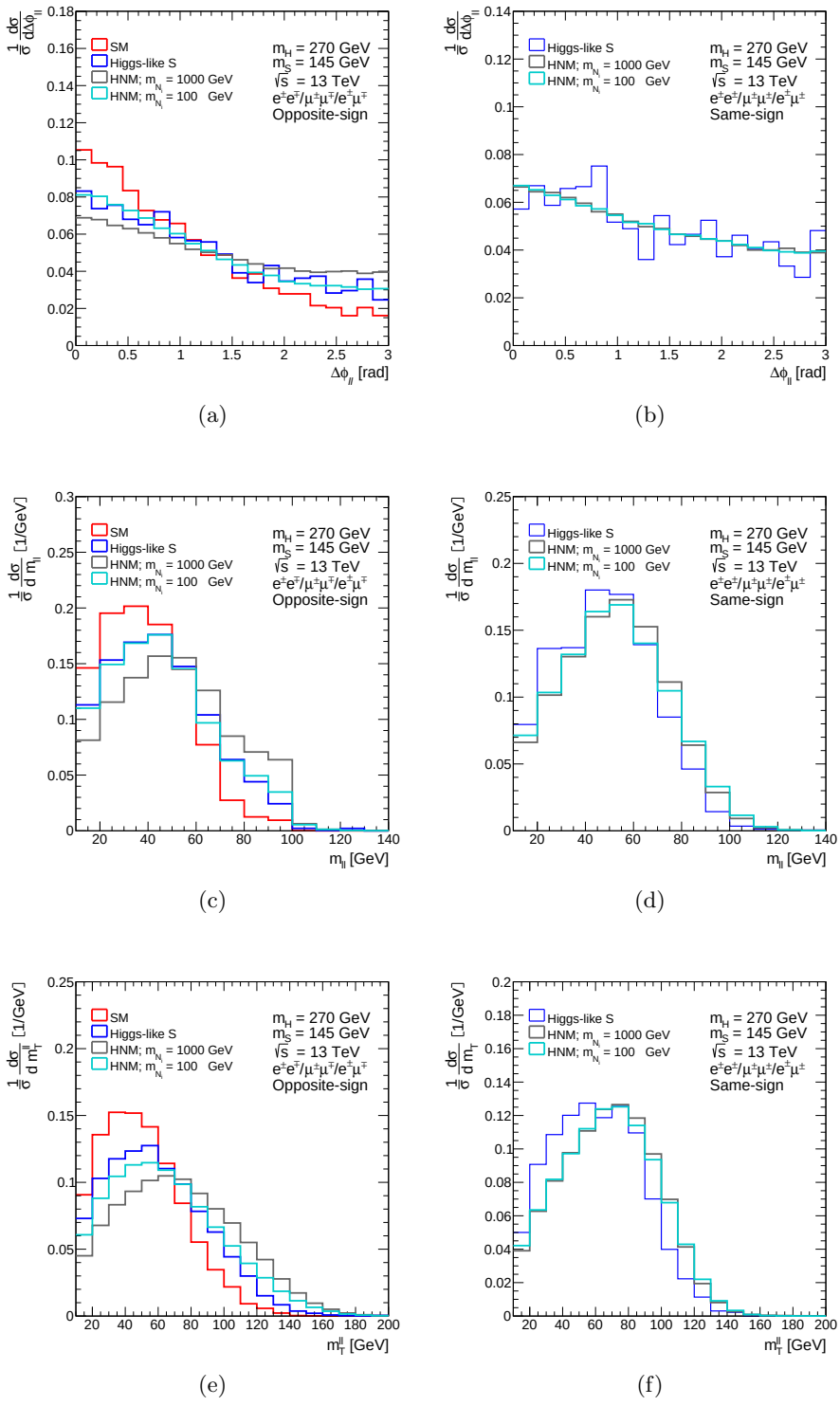


**Figure 6.5:** *Normalised distributions of (a), (b) $\Delta\phi$; (c), (d) invariant-mass of di-lepton system and (e), (f) invariant transverse-mass of di-lepton system for the event pre-selection in case of OS (left) and SS (right) channels, where the process is $gg \to H \to Sh$.*

| Measurement | Reference | Expected events | Post-fit event yield | $\beta_g^2$ | $\chi^2_{\text{SM}} - \chi^2_{\text{SM+BSM}}$ |
|---|---|---|---|---|---|
| ATLAS, 20.2 fb$^{-1}$<br>$e^{\pm}\mu^{\mp}$<br>$N_{b\text{-jet}} \geq 1$ | [85] | $112 \pm 26$ | $397 \pm 93$ | $4.89 \pm 1.15$ | 12.11 |
| ATLAS, 20.3 fb$^{-1}$<br>$e^{\pm}\mu^{\mp}$<br>$N_{\text{jet}} = 0$ | [86] | $28 \pm 6$ | $48 \pm 46$ | $2.37 \pm 2.27$ | 0.43 |
| ATLAS, 20.3 fb$^{-1}$<br>$e^{+}e^{-}$, $\mu^{+}\mu^{-}$<br>$N_{\text{jet}} = 0$ | [86] | $16 \pm 4$ | $82 \pm 20$ | $7.07 \pm 1.73$ | 7.31 |
| ATLAS, 20.3 fb$^{-1}$<br>$e^{\pm}\mu^{\mp}$<br>$N_{\text{jet}} = 1$ | [87] | $70 \pm 16$ | $20 \pm 36$ | $0.39 \pm 0.71$ | 0.16 |
| CMS, 19.4 fb$^{-1}$<br>$e^{+}e^{-}$, $\mu^{+}\mu^{-}$, $e^{\pm}\mu^{\mp}$<br>$N_{\text{jet}} = 0$ | [88] | $46 \pm 11$ | $136 \pm 58$ | $4.08 \pm 1.74$ | 3.31 |
| CMS, 19.4 fb$^{-1}$<br>$e^{+}e^{-}$, $\mu^{+}\mu^{-}$, $e^{\pm}\mu^{\mp}$<br>$N_{\text{jet}} = 1$ | [88] | $111 \pm 26$ | $46 \pm 43$ | $0.57 \pm 0.53$ | 0.58 |
| CMS, 5.3 fb$^{-1}$<br>$e^{+}e^{-}$, $\mu^{+}\mu^{-}$, $e^{\pm}\mu^{\mp}$<br>$N_{\text{jet}} \geq 2$, $N_{b\text{-jet}} \geq 2$ | [89] | $25 \pm 6$ | $17 \pm 58$ | $0.94 \pm 3.20$ | $-0.04$ |

**Table 6.3:** *Best fits to the di-lepton invariant mass spectra reported by ATLAS and CMS at a proton-proton centre of mass of $\sqrt{s} = 8$ TeV. The post-fit event yield reflects the number of BSM events required to fit the data (in excess of the SM prediction). The value of $\beta_g^2$ corresponding to the post-fit event yield is reported along with the test statistic $\chi^2_{SM} - \chi^2_{SM+BSM}$ in order to gauge the significance of the fit. The mass of the heavy scalar is fixed at $m_H = 270$ GeV and the mass of $S$ is allowed to vary, where the best fit is found for $m_S = 150$ GeV. For simplicity, it is assumed that $H$ decays exclusively into $Sh$. The higher value for the statistic is more evidence for the BSM physics.*

### 6.4.2 Comparison with ATLAS and CMS OS di-lepton invariant mass spectra

The BSM scenario discussed here is of particular interest with regards to several ATLAS and CMS SM measurements of di-lepton invariant mass spectra, since the BSM OS di-leptonic signature has some sensitivity towards them. For this reason, various 8 TeV ATLAS and CMS results were selected for study. The BSM signal was generated according to the event selections described in the publications by collaborations, and then added to the SM prediction. A best fit event yield was calculated by varying the BSM normalisation and fitting the SM+BSM prediction to the data, using the $\chi^2$ approach described in appendix A. A list of the measurements that were considered can be seen in Table 6.3. The SM MCs are normalised to the data in the region of the di-lepton mass, $m_{\ell\ell} > 110$ GeV, where the signal is expected to be negligible (see Figure 6.5). The data with $m_{\ell\ell} < 100$ GeV is compared to the re-scaled SM MC plus the BSM signal. The mass of the heavy scalar is set to $m_H = 270$ GeV and the mass of $S$ is varied. This is motivated by the fact that the di-lepton invariant mass is not significantly sensitive to $m_H$.

As discussed in chapter 3, the cross-section of the BSM signal is proportional to $\beta_g^2$, which is a free parameter. Therefore, from the fits of the invariant mass spectra (shown in Figures 6.6 and 6.7), the value of $\beta_g^2$ can be calculated along with its standard deviation. In addition to this, a test statistic can be used to determine the significance of the BSM signal's improvement on the SM-only hypothesis. The test statistic that was considered is $\Delta\chi^2 \equiv \chi^2_{\text{SM}} - \chi^2_{\text{SM+BSM}}$.[2] The combined best fit is obtained for $m_S = 150 \pm 5$ GeV, as shown in Figure 6.1. The results of the individual fits are compared with the prediction of the direct production of $H \to Sh$. The cross-section is estimated by using a combined value of $\beta_g^2 = 1.38 \pm 0.32$. The latter is obtained from different Higgs boson signal strengths reported so far (see Ref. [19]). Results are reported in Table 6.3. In order to present the numbers in Table 6.3, the di-lepton invariant mass distributions are used. Those differential distributions are shown in Figure 6.6 and Figure 6.7 with the best fit data points from ATLAS and CMS, respectively. It is very interesting to point out that ATLAS with a luminosity of 20.2 fb$^{-1}$ has a statistic at 12.

A combined fit is performed with a common value of $\beta_g^2$. This tests the ability of the simplified model to describe the data. The best fit obtained here corresponds to $\beta_g^2 = 1.22 \pm 0.38$. This corresponds to a significance of 3.2 standard deviations. The value of $\beta_g^2$ obtained in this section is in good agreement with the combined value discussed above. A few remarks are in order here: A simplified assumption is made here whereby the BSM contribution arises solely from the direct production of $H \to Sh$. A non-trivial contribution from $H \to hh$ is expected, as detailed in Refs. [1, 14, 2]. This contribution can impact the di-lepton invariant mass distributions. To date, no complete set of results with the data taken in 2016 is available to give a more reliable estimate than that given in Ref. [1]. As a result, the $hh$ decay is not taken into account here. The contribution from OS di-leptons from the associated production of $H$ (see section 6.5) is neglected here. The contribution from the decay $H \to WW \to \ell\nu\ell\nu$ is also neglected. As the mass of $H$ becomes less than $m_h + m_S$, the di-boson decay includes off-shell effects. This is expected to have a non-trivial impact on the expected yields of the di-leptons and hadronic jets, including $b$-tagged jets. This effect is not studied here. A method for calculating $\beta_g^2$ is shown in appendix A, where we extracted the combined $\beta_g^2$ for $m_S = 145$ GeV and $m_S = 135$ GeV.

[2] The analysis of the results reported in Ref. [85] is sensitive to the assumed systematic uncertainty. The latter is obtained from the different MC predictions of the shape of the di-lepton invariant spectrum reported there. The analysis of the rest of the results is largely insensitive to the assumed systematic error. A systematic error of 2% is assumed there.

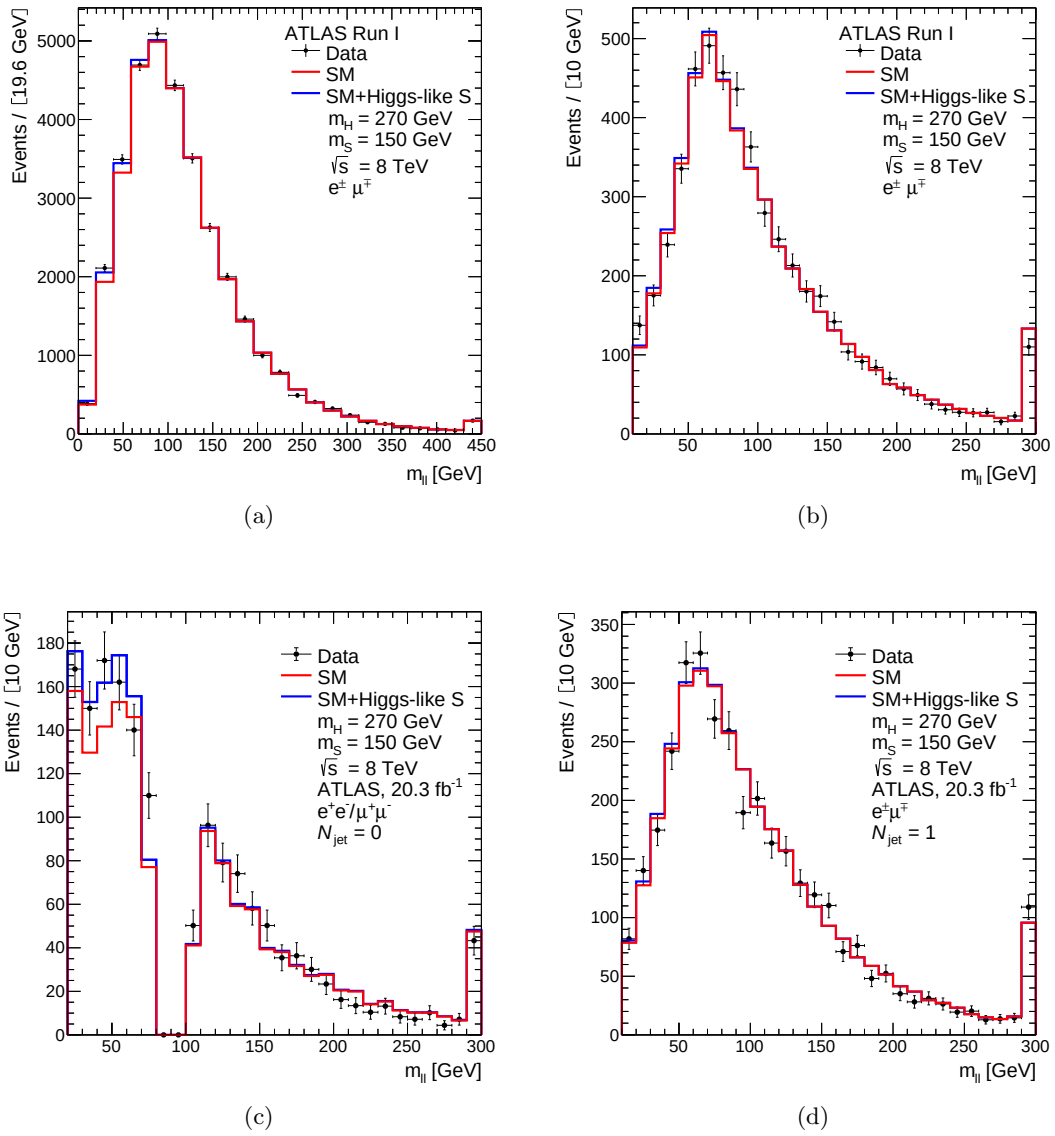


**Figure 6.6:** *Distributions of the ATLAS data and SM background comparing to the BSM signal (Higgs-like S boson) for the di-lepton invariant mass. In (a) events are required to have two opposite-charge leptons (e, μ) with at least one b-tagged jet [85]. For (b) events are required to have two opposite-charge leptons with different-flavour (eμ) and (c) with same-flavour (ee/μμ), where both analysis require zero jets [86]. In case of (d) events are required to have two opposite-charge leptons (e, μ) with exactly one jet. The data used here is from pp collision collected by the ATLAS experiment at* $\sqrt{s} = 8$ *TeV with luminosity of 20.3* $fb^{-1}$ *for (b), (c) and (d), and 20.2* $fb^{-1}$ *for (a).*

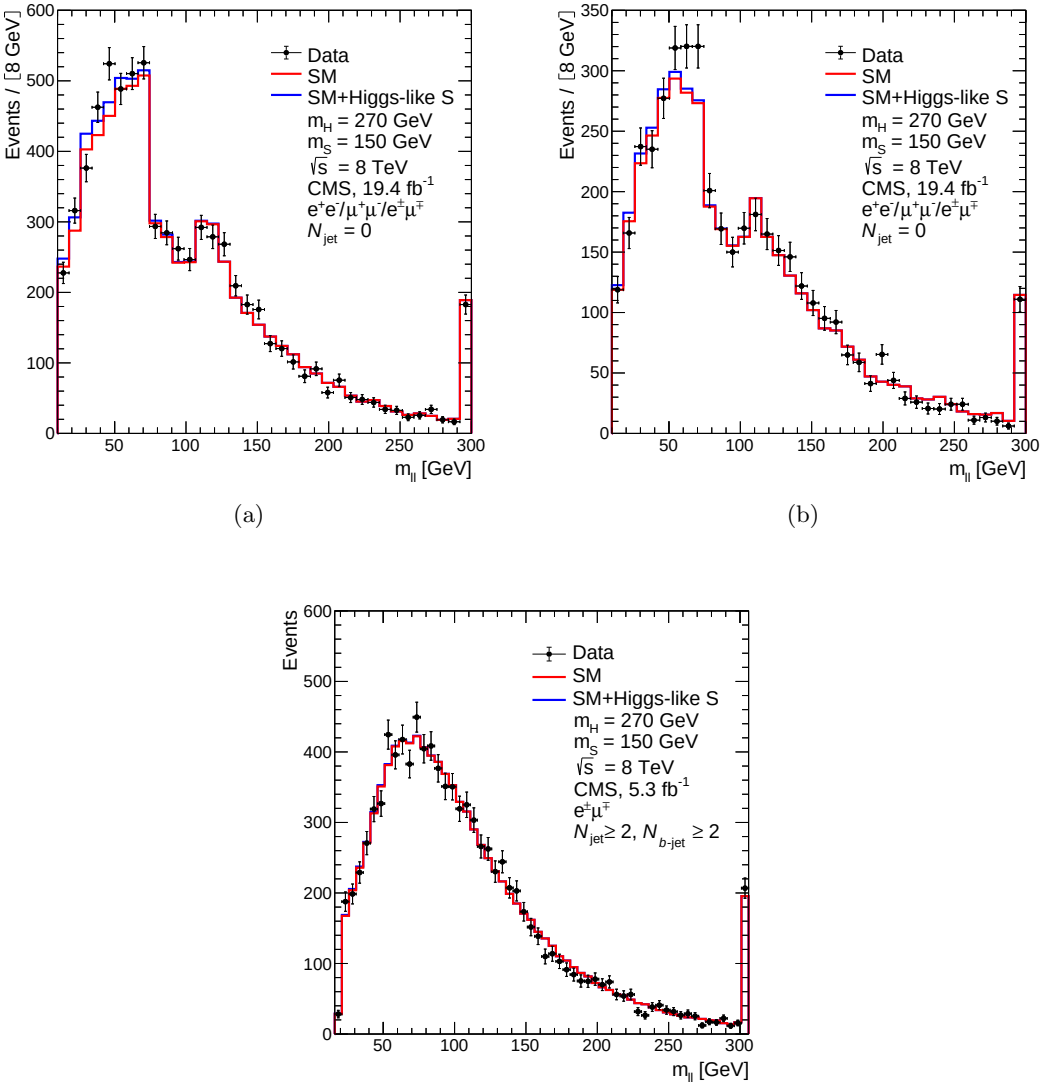


**Figure 6.7:** *Distributions of the CMS data and SM background comparing to the BSM signal (Higgs-like $S$ boson) for the di-lepton invariant mass ($m_{\ell\ell}$). Events are required to have two opposite-charge leptons with (a) zero-jet, (b) one-jet [88] and (c) $e\mu$ channel [89] with at least two jets and one b-tagged jet. The data used here, are from the measurement of the $W^+W^-$ and $t\bar{t}$ production cross-section in $p--p$ collision at $\sqrt{s} = 8$ TeV with luminosity of 19.4 $fb^{-1}$ and 5.3 $fb^{-1}$ for top and bottom plots, respectively.*

| Channel | Number of BSM candidate events | $\beta_g^2$ |
|---|---|---|
| $e\mu$ | $37.04 \pm 12.10$ | $3.03 \pm 0.99$ |
| $\mu\mu$ | $37.22 \pm 17.52$ | $4.25 \pm 2.00$ |
| Tri-lepton | $6.00 \pm 5.52$ | $0.75 \pm 0.69$ |
| **Combined** | | $1.69 \pm 0.54$ |

**Table 6.4:** *The number of BSM candidate events and the corresponding values of $\beta_g^2$ for each channel in the CMS Run-II search in Ref. [90]. The combined result is calculated as the error weighted mean of the individual values calculated for each channel [78].*

## 6.5 Production of $H$ in association with top quarks

Although the production of $H$ in association with top quark ($ttH$) is 100 times less than its production by the gluon-gluon fusion, experimental results in Ref. [91] show a non-negligible deviation from the SM. Therefore, by following same procedure applied on the direct production of $H$ explained before, we can try to explain the excess in the data.

The signal that has been studied in Ref. [78] is $H \to Sh$, where the $H$ is simulated to be produced by the disturbance in the top quark field. Notice that, $H$ originated from both single ($tH$) and double ($ttH$) top quarks. Hence, the Higgs-like S signal is compared, with relevant analysis, to the CMS data [90]. The measurements that have been taken into account for the comparison are the azimuthal angle $\Delta\phi_{\ell\ell}$ between the leading same-sign pair, pseudorapidity and jet multiplicities. The masses that are used in this analysis for the heavy boson $H$ and the scalar boson $S$ are 270 GeV and 150 GeV, respectively. The values of $\beta_g^2$ and the number of the BSM signal in different channels are shown in Table 6.4. The combined $\beta_g^2$ is found to be $\beta_g^2 = 1.69 \pm 0.54$, which is in agreement with the value of $\beta_g^2$ obtained with the same mass point in section 6.4.2.

### 6.5.1 Tri-lepton final states

Another important final state to check is the production of three leptons with a total charge of $\pm 1$, since the prediction of the model is not excluded by the existing data. Therefore, pre-selections are applied for the leptons and jets as follows: Both electrons and muons should have $p_{\mathrm{T}} > 15$ GeV and they must be within $|\eta^e| < 1.37$ or $1.52 < |\eta^e| < 2.47$ ($\eta^\mu < 2.5$) for the electrons (muons). Jets are required to have $p_{\mathrm{T}} > 25$ GeV and pseudorapidity $|\eta| < 4.5$.

Events are required to have exactly three leptons in the final-state ($eee, \mu\mu\mu, e\mu\mu$ or $ee\mu$) and satisfy the selection criteria described above. We consider a phase space where the kinematics of final-state lepton associated with the $ZW^\pm$ bosons decay. Two leptons with same-flavour (SF) and OS which have invariant mass consistent with the $Z$ boson mass are selected and the last lepton assumed to decay from the $W^\pm$ bosons; at least one of these leptons should have $p_{\mathrm{T}} > 25$ GeV. To suppress the background coming from the misidentification of the jets as lepton, the transverse momentum of the lepton

| | SM | Higgs-like S | HNM with $m_{N_i} = 1000$ GeV | HNM with $m_{N_i} = 100$ GeV |
|---|---|---|---|---|
| All events | 2000000 | 2000000 | 2000000 | 2000000 |
| $eee/\mu\mu\mu/ee\mu/\mu\mu e$ | 46764 | 16540 | 552094 | 486334 |
| $\lvert m_{\ell\ell} - m_Z \rvert < 15$ GeV | 12042 | 3914 | 139513 | 84242 |
| $p_{\mathrm{T}}^{\geq 1\mathrm{lep}} > 25$ GeV | 11973 | 3901.00 | 139189.00 | 84025.00 |
| $p_{\mathrm{T}}^{3^{rd}\mathrm{lep}} > 20$ GeV | 6179 | 2625 | 98833 | 55318 |
| $m_{\mathrm{T}}^{W^\pm} > 30$ GeV | 4174 | 1977 | 74035 | 41697 |
| Efficiency | 0.002087 | 0.000885 | 0.0370175 | 0.0208485 |

**Table 6.5:** *Cutflow for MC simulation of the event selections of three leptons ($eee, \mu\mu\mu, e\mu\mu$ or $ee\mu$) for the SM background, Higgs-like S and the HNM. Two cases, depending on the mass of the HNM $m_{N_i}$, are considered for the HNM.*

associated with the $W^\pm$ bosons must be greater than 20 GeV. The transverse mass of the $W^\pm$ boson is defined by:

$$m_{\mathrm{T}}^{W^\pm} = \sqrt{2 \cdot E_{\mathrm{T}}^{\mathrm{miss}} \cdot p_{\mathrm{T}}^{\ell} \left[1 - \cos(\Delta\phi(\ell, \nu))\right]}, \tag{6.5.1}$$

where $\Delta\phi(\ell, \nu)$ is the difference of the azimuthal angle between lepton associated with the $W^\pm$ bosons and neutrino. The transverse mass of the $W^\pm$ bosons are required to be greater than 30 GeV. Cutflow of the events after each cut is shown in Table 6.5. Figure 6.8 shows the kinematic distributions of the $W^\pm$ bosons transverse mass, transverse mass of the $ZW^\pm$ bosons system, the invariant mass; the transverse momentum of the $Z$ boson ($p_{\mathrm{T}}^{Z}$) and the azimuthal angle of the lepton associated with the $W^\pm$ bosons and the neutrino.

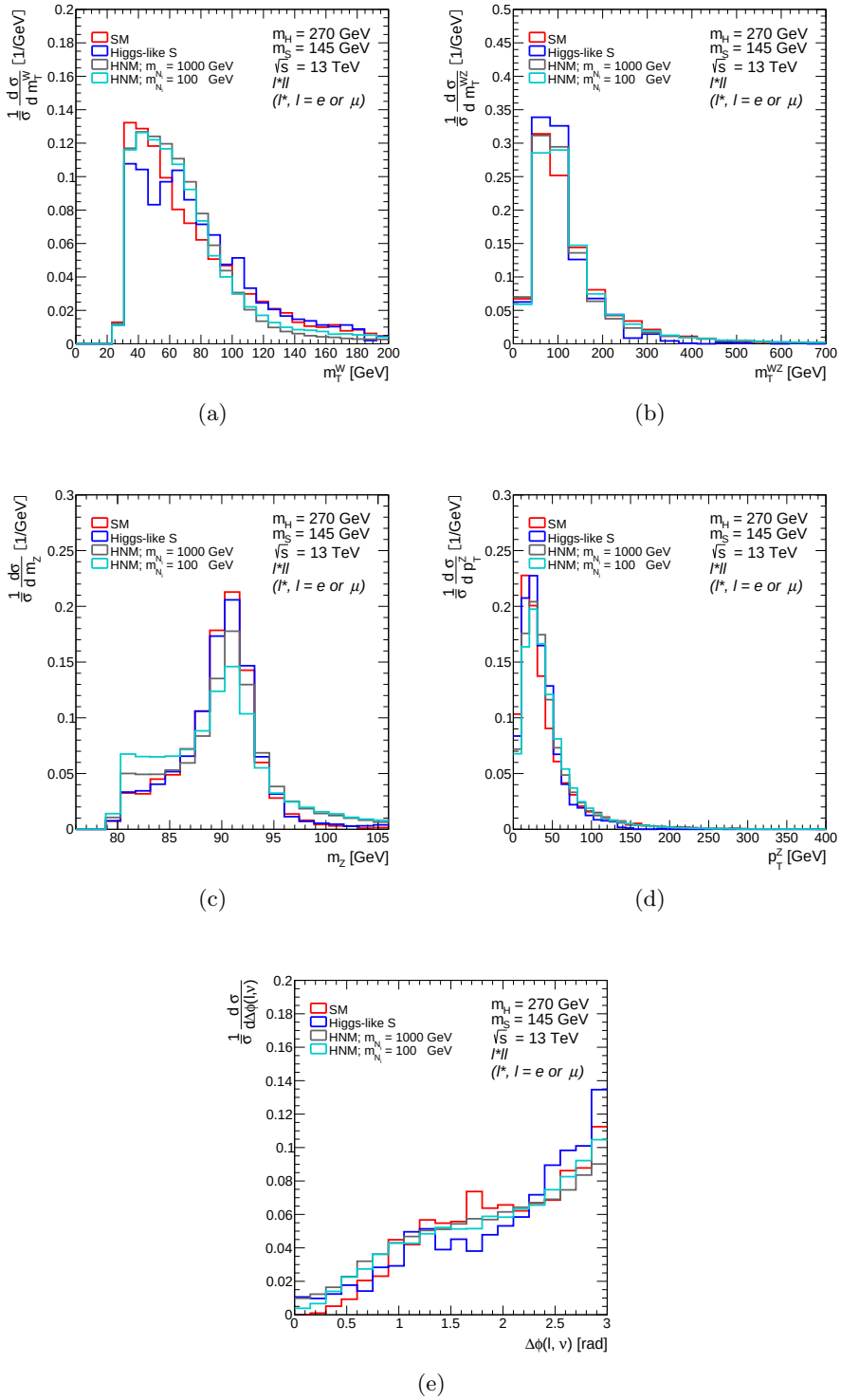


**Figure 6.8:** *Normalised distributions of (a) transverse-mass of reconstructed $W^{\pm}$-boson, (b) transverse-mass of reconstructed $ZW^{\pm}$-boson system, (c) reconstructed mass of $Z$-boson, (d) $p_T$ of $Z$-boson and (e) $\Delta\phi$ between leading lepton and missing energy for the event pre-selection for the tri-leptons channel, where the process is $gg \to H \to Sh$.*

| **Dataset** | **Extracted $\beta_g^2$** | **Standard deviations** |
|---|---|---|
| Higgs boson signal strength | $1.38 \pm 0.32$ [19] | 4.3 |
| Leptons with $b$-tagged jets | $1.69 \pm 0.54$ [78] | 3.1 |
| Di-lepton with jets | $1.22 \pm 0.38$ | 3.2 |
| **Combined** | $1.38 \pm 0.22$ | 6.3 |

**Table 6.6:** *Summary of the combined $\beta_g^2$ values and the significance for different datasets.*

## Summary

In this chapter we discussed the phenomenology of multilepton that arises from the decay of the scalar boson $S$. In particular, special attention has been given to di-lepton final states. We compared the di-leptons signal of the BSM to the ATLAS and CMS data. This was done in order to understand the excess in the di-leptons results. The scale factor (the combined $\beta_g^2$ for different datasets) is used to make judgement of how the BSM signal performs. The combined $\beta_g^2$ calculated from the di-leptons invariant mass of $H \to Sh$ signal with ATLAS and CMS data is found to be $\beta_g^2 = 1.22 \pm 0.38$ which corresponds to $3.2\,\sigma$ for $m_H = 270$ GeV and $m_S = 150$ GeV. This result is in good agreement with the scale factor extracted from the collected data so far. In Refs. [19, 78] the combined $\beta_g^2$ values for the Higgs boson signal strength and leptons with $b$-tagged jets are $\beta_g^2 = 1.69 \pm 0.54$ and $\beta_g^2 = 1.22 \pm 0.38$, respectively. Combining these results together using Equation A.7.5 we get $\beta_g^2 = 1.38 \pm 0.22$. This corresponds to a 6.3 standard deviations. A summary of the combined $\beta_g^2$ and the significance for different datasets is given in Table 6.6. Also we looked at three lepton final states showing an interesting kinematic distributions.

# 7 Conclusions

## 7.1 Overview of this research

In chapter 2 we first review the SM and we built the SM Lagrangian which describes the particles we observed in nature. Secondly, we explained the discovery of the SM Higgs boson and the channels of the discovery. In chapter 3 we illustrated the 2HDMs and their possible extension. The latter is the focus of this dissertation, which introduces two scalars bosons $S$ and $H$ to the 2HDMs. The scalar boson $S$ which originated from introducing a CP-odd scalar field to the 2HDMs. The particle contents of this extension, which we call the Madala hypothesis, are the SM Higgs $h$, heavy Higgs $H$, pseudoscalar $A$, the charged Higgs boson $H^{\pm}$ and the scalar boson $S$. In this dissertation, we focused on the $H$ where its decay modes could be either $hh$, $SS$ or $Sh$ we only studied the $Sh$ process. In contrast, the $S$ could decay to a two dark matter candidates and can have Higgs-like nature. So this research explore $H \to Sh$ process with $S$ having the Higgs-like decay modes. Since the ATLAS data and the simulation of MC samples were used throughout this dissertation, we gave a short introduction on the LHC and the ATLAS detector in chapter 4. In chapter 5 we investigated the non-resonant and resonant Higgs boson pair production in the LHC by using the data collected by the ATLAS experiment. Lastly, the phenomenology of the $H \to Sh$ is studied and a comparison of this signal to the Run-I data is explored in chapter 6. The results of these studies are discussed in the next section.

## 7.2 Key results

Firstly, a search for the non-resonant ($pp \to hh$) and resonant ($pp \to X \to hh$) Higgs boson pair production is performed. We investigated the presence of the Higgs boson pair in $WW\gamma\gamma$ channel. The data used is p–p collision data collected by the ATLAS detector corresponds to luminosity of 36.1 fb$^{-1}$ at centre-of-mass energy of 13 TeV. No significant deviation is observed in the data. The expected (observed) upper limit at 95% CL for the $pp \to hh$ cross-section is 5.3 pb (7.6 pb). While for the resonance

production cross-section times its branching ratio the expected (observed) upper limit at 95% CL as function of the mass of the resonant range from 16.9 pb (37.5 pb) to 4.4 pb (6.1 pb) for the masses between 260 GeV-500 GeV.

Secondly, we elaborated on the phenomenology discussed in Refs. [1, 14, 2] by discussing various multilepton final states. This includes the production of SS and OS di-leptons and three leptons. Here we consider Higgs-like decays of $S$ as well as the leptonic decays via heavy neutrinos. Available data is compared against predictions from a simplified scenario. This includes the production of OS di-leptons with missing transverse energy in conjunction with jets and $b$-tagged jets, and the production of SS di-leptons and tri-leptons in association with $b$-tagged jets. The inclusion of the simplified BSM scenario, where $H$ decays only to $Sh$, significantly improves the description of the data compared to the SM-only hypothesis.

The available OS di-lepton invariant mass spectra are fitted to the spectra predicted from the direct production of $H \to Sh$ assuming $m_H = 270$ GeV. The mass of $m_S$ is scanned, where the best fit is obtained with $m_S = 150 \pm 5$ GeV. The hadronic jet activity in events with SS di-leptons and tri-leptons in association with $b$-tagged jets reported by CMS is studied in the context of the production of $H \to Sh$ in association with single and double top quarks. In both cases the BSM signal yields with $m_H = 270$ GeV and $m_S = 150$ GeV are fit by varying $\beta_g^2$, where $\beta_g = 0$ corresponds to the absence of a BSM signal. For the OS di-lepton invariant mass spectra, it is found that $\beta_g^2 = 1.22 \pm 0.38$, whereas in the multileptons in association with $b$-tagged jets, we find that $\beta_g^2 = 1.69 \pm 0.54$. These compare well with $\beta_g^2 = 1.38 \pm 0.22$ obtained from available measurements of various Higgs boson signal strengths, excluding the production of $tth$. This is compatible with previous studies on the BSM scenario we have considered and is an encouraging insight into potential BSM physics which may already be visible in the existing ATLAS and CMS data. A comprehensive study of these and other effects present in the data that are related to the model described here is beyond the scope of this research. The combination of $\beta_g^2$ values for different datasets discussed above yield $\beta_g^2 = 1.38 \pm 0.22$ which corresponds to $6.3\sigma$.

In addition, we point out to corners of the phase-space with leptons and hadronic jets that have not been explored at the LHC, where the simplified model considered here predicts anomalous production. It is suggested that the experiments explore the production of OS di-lepton with missing transverse energy in association with two or more hadronic jets and vetoing on $b$-tagged jets. This region of the phase-space is not explored in the measurements of production cross-section of the non-resonant $WW$ production, which to date are constrained to the measurement of the cross-section with a full jet veto and in association with exactly one jet. The measurement of the signal strength of $tth$ does not seem to capture the full extent of the discrepancy between the data and the SM. In the context of the model discussed here this would imply that an anomalously large rate of SS di-leptons and tri-leptons in association with at least three $b$-tagged jets is expected. So far the experiments have not reported results in this corner of the phase-space. It is important to study the possible connection between the elevated rate of SS di-leptons and tri-leptons with $1 \leq N_{b\text{-jet}} \leq 2$ observed so far with the rate in association $N_{b\text{-jet}} \geq 3$. It is also suggested that we explore the production of

OS di-leptons in association with $N_{b\text{-jet}} \geq 3$.

# A

# Higgs-like Scalar Boson Signal

Using the information provided in chapter 6 section 6.1 a scan is performed for the mass of the scalar boson $S$. We consider the range of the mass to be between $(130-160)$ GeV taking a step of 5 GeV. In this chapter, the di-lepton invariant mass distributions that have been discussed in Refs. [85, 86, 87, 88, 89] will be analysed in terms of the Higgs-like scalar boson signal explained in chapter 6.

## A.1 Analysis techniques

In this analysis, we use the di-lepton invariant mass that produced by the ATLAS and CMS collaboration in Refs. [85, 86, 87, 88, 89]. In these results, we consider the MCs to be the SM prediction and the signal that we generated to be the BSM signal.

The SM backgrounds are normalised to the data for the mass of the di-lepton $m_{\ell\ell} > 110$ GeV. Hence, the BSM signal is added to the normalised backgrounds and a fit for each signal is performed. RooFit [92] packages are used to re-fit (a binned likelihood fit) the data to the new SM backgrounds and the BSM signals. After fitting the data to the MC prediction, the event yield is calculated using $\chi^2$ defined bellow for $m_{\ell\ell} < 100$ GeV:

$$\chi^2 = \sum_i \frac{\left(N_i^{\text{Data}} - N_i^{\text{SM}} - N_i^{\text{BSM}}\right)^2}{\left(\Delta N_i^{\text{Data}}\right)^2 + \left(\Delta N_i^{\text{SM}}\right)^2}, \tag{A.1.1}$$

where $N_i^{Data}$, $N_i^{SM}$ and $N_i^{BSM}$ are the number of the events after the fit for bin number $i$ of the data, SM background and the BSM signal, respectively. $\Delta N_i^{Data}$ and $\Delta N_i^{SM}$ are the systematic uncertainty in the data and the theoretical model, respectively. The systematic in the data is estimated by the square-root of the bin $(i)$ content. For the MCs the systematic uncertainty of the measurement in Ref. [85] is taken to be 1.2% and 2% for the other six measurements, as it is difficult to estimate the systematic from the results directly.

## A.2 ATLAS, 20.2 fb$^{-1}$ with $e^{\pm}\mu^{\mp}$ and $N_{b-\text{jet}} \geq 1$

We follow same analysis produced as in Ref. [85] on the Higgs-like scalar boson signal. Events are required to have two OS leptons ($e$, or $\mu$) with at least one $b$-tagged jet. Electrons must have transverse momentum $p_{\text{T}} > 25$ GeV and pseudorapidity $|\eta| < 2.47$ excluding the transition region between $1.37 < |\eta| < 1.52$. Muons are required to have transverse momentum $p_{\text{T}} > 25$ GeV and pseudorapidity $|\eta| < 2.5$. Jets should have $p_{\text{T}} > 25$ GeV and $|\eta| < 2.5$. Events pass the selection criteria descried above are shown in Table A.1.

| | $m_S = 130$ GeV | $m_S = 135$ GeV | $m_S = 140$ GeV | $m_S = 145$ GeV | $m_S = 150$ GeV | $m_S = 155$ GeV | $m_S = 160$ GeV |
|---|---|---|---|---|---|---|---|
| All events | 2000000.00 | 2000000.00 | 2000000.00 | 2000000.00 | 2000000.00 | 2000000.00 | 2000000.00 |
| $e^{\pm}\mu^{\pm}$ events | 4389.00 | 5262.00 | 5980.00 | 6803.00 | 5370.00 | 5159.00 | 4603.00 |
| $N_{b-\text{jet}} \geq 1$ | 1542.00 | 1836.00 | 1920.00 | 2104.00 | 1989.00 | 1892.00 | 1746.00 |
| Efficiency | 0.000771 | 0.000918 | 0.00096 | 0.001052 | 0.0009945 | 0.000946 | 0.000873 |

**Table A.1:** *Cutflow of the events survived the cuts for the selection of two OS leptons (e or μ) and the efficiency with luminosity of 20.2 fb$^{-1}$; according to the ATLAS simulation.*

The kinematic distribution of the di-lepton invariant mass is shown in Figure A.1(a), in which peaks in the region where the data differ from the simulation in Ref. [85]. To see whether the invariant mass peaks around the mass of the $S$, $W$s or $Z$ boson we define the transverse mass (as shown in Figure A.1(b)) as,

$$m_{\text{T}}^{\ell\ell} = \sqrt{\left(E_{\text{T}}^{\ell\ell} + E_{\text{T}}^{\text{miss}}\right)^2 - \left|p_{\text{T}}^{\ell\ell} + E_{\text{T}}^{\text{miss}}\right|^2}, \tag{A.2.1}$$

where $E_{\text{T}}^{\ell\ell} = \sqrt{|p_{\text{T}}^{\ell\ell}|^2 + m_{\ell\ell}^2}$, $E_{\text{T}}^{\text{miss}}$ is the missing energy transverse, $p_{\text{T}}^{\ell\ell}$ and $m_{\text{T}}^{\ell\ell}$ are the transverse momentum and the invariant mass of the di-lepton system, respectively. The transverse momentum of the leading and the di-lepton system are also shown in Figures A.1(c) and A.1(d). The azimuthal angle of the di-lepton $\Delta\phi_{\ell\ell}$ is flat, as could be seen in Figure A.1(e).

| | $\chi^2$ | | $\chi^2/ndf$ | | p-value | | N. signal | Significance |
|---|---|---|---|---|---|---|---|---|
| | SM background | SM+BSM | SM Background | SM+BSM | SM Background | SM+BSM | | |
| $m_S = 130$ GeV | 18.122 | 6.256 | 3.624 | 1.564 | 0.003 | 0.181 | 400±95 | 0.912 |
| $m_S = 135$ GeV | 18.122 | 7.211 | 3.624 | 1.803 | 0.003 | 0.125 | 363±89 | 1.150 |
| $m_S = 140$ GeV | 18.122 | 6.817 | 3.624 | 1.704 | 0.003 | 0.146 | 391±95 | 1.054 |
| $m_S = 145$ GeV | 18.122 | 6.991 | 3.624 | 1.748 | 0.003 | 0.136 | 395±96 | 1.097 |
| $m_S = 150$ GeV | 18.122 | 6.014 | 3.624 | 1.503 | 0.003 | 0.198 | 397±93 | 0.848 |
| $m_S = 155$ GeV | 18.122 | 7.892 | 3.624 | 1.973 | 0.003 | 0.096 | 361±91 | 1.307 |
| $m_S = 160$ GeV | 18.122 | 6.102 | 3.624 | 1.526 | 0.003 | 0.197 | 389±92 | 0.872 |

**Table A.2:** $\chi^2$ *values, p-value, signal yield after the fitting and the significance for the SM background and the SM+BSM for events contain two OS leptons (e or μ). The BSM signal is Higgs-like S boson (pp → H → Sh); for the ATLAS data with luminosity of 20.2 fb$^{-1}$ [85].*

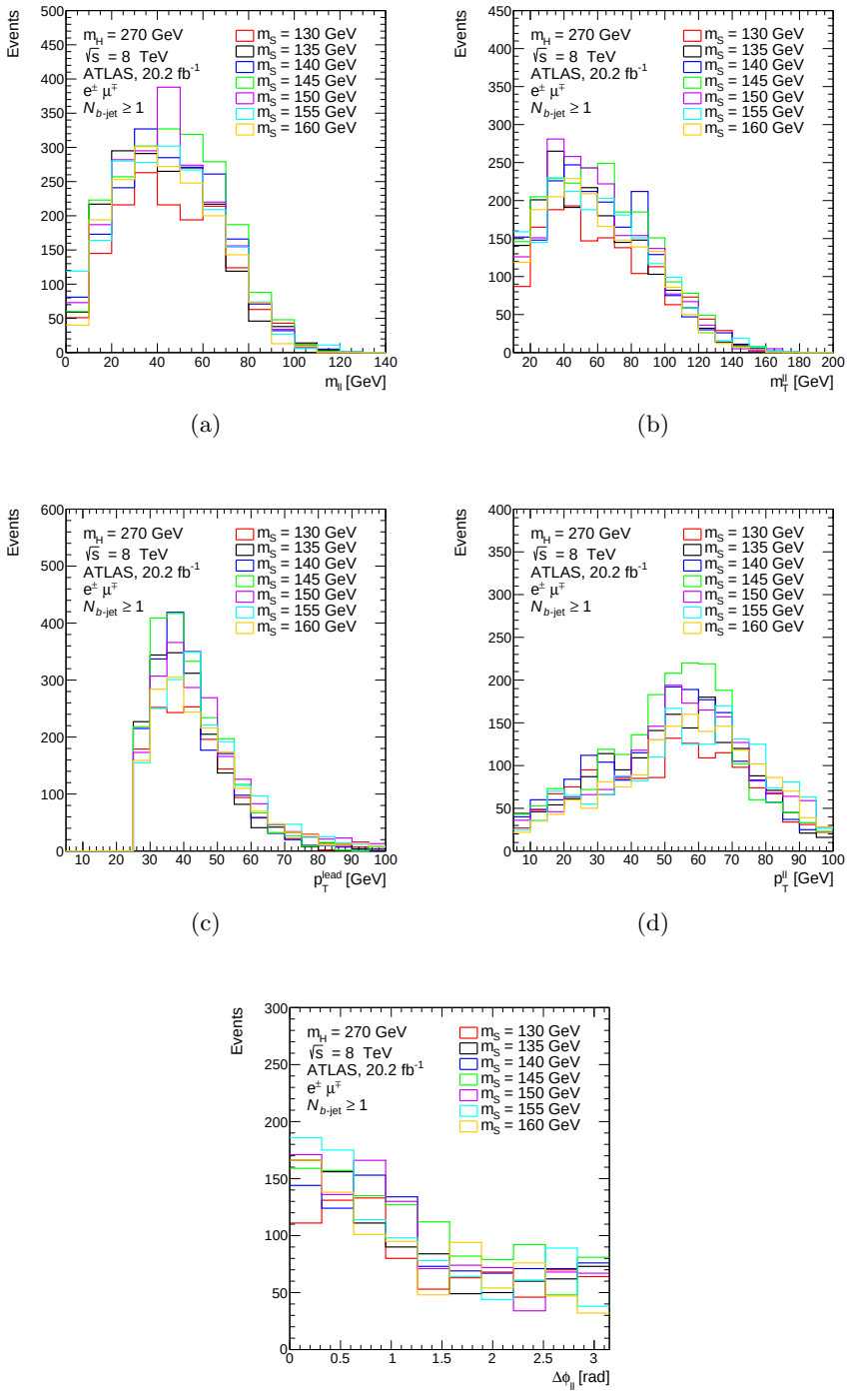


**Figure A.1:** *Kinematic distribution of (a) the di-lepton invariant mass, (b) the transverse mass of the di-lepton system, (c) the $p_T$ of the leading lepton, (d) the $p_T$ of the di-lepton system and (e) the azimuthal angle of two leptons; in events with an OS leptons ($e$ or $\mu$) and at least one b-tagged jet with the ATLAS detector simulation.*

## A.3 ATLAS, 20.3 fb$^{-1}$ with $e^+e^-/\mu^+\mu^-/e^\pm\mu^\mp$ and $N_{\text{jet}} = 0$

In this analysis, we use the event selections descried in Ref. [86]. In which, two OS and same-flavour ($ee$ or $\mu\mu$) or different-flavour ($e$ or $\mu$) leptons are selected. Electron must be within $|\eta| < 2.47$ excluding the region $1.37 < |\eta| < 1.52$. Muons should originated from the region in the ATLAS detector where $|\eta| < 2.4$. Jets are required to have $p_{\text{T}} > 25$ GeV and pseudorapidity $|\eta| < 4.5$.

In addition to the two leptons selection the leading and the sub-leading lepton must have $p_{\text{T}} > 25$ and $p_{\text{T}} > 20$ GeV, respectively. In order to remove the multi-jet background, in case of the different-flavour, the invariant mass of the di-lepton should be greater than 10 GeV and missing energy $E_{\text{T}}^{\text{miss}} > 45$ GeV; as shown in Table A.3. Similarly, for the same-flavour the di-lepton invariant mass must be above 15 GeV to remove the contributions that come from $J/\psi$ events and missing energy $E_{\text{T}}^{\text{miss}} > 45$ GeV; the cutflow of these events are presented in Table A.4. In these events, no jets are selected for both same-flavour and different-flavour.

The kinematic distributions of two OS and different-flavour leptons are shown in Figure. A.2 and for same-flavour leptons are shown in Figure A.3. Equation A.2.1 is used for the di-lepton invariant mass.

| | $m_S = 130$ GeV | $m_S = 135$ GeV | $m_S = 140$ GeV | $m_S = 145$ GeV | $m_S = 150$ GeV | $m_S = 155$ GeV | $m_S = 160$ GeV |
|---|---|---|---|---|---|---|---|
| All events | 2000000.00 | 2000000.00 | 2000000.00 | 2000000.00 | 2000000.00 | 2000000.00 | 2000000.00 |
| $e^\pm\mu^\pm$ | 10757.00 | 12382.00 | 13882.00 | 14812.00 | 12095.00 | 11338.00 | 10594.00 |
| $p_{\text{T}}^{\text{lead}}$ GeV | 8843.00 | 10338.00 | 11726.00 | 12669.00 | 10262.00 | 9627.00 | 8923.00 |
| $p_{\text{T}}^{\text{sub-lead}}$ GeV | 4902.00 | 5911.00 | 6992.00 | 7666.00 | 6061.00 | 5818.00 | 5258.00 |
| $m_{\ell\ell} > 10$ GeV | 4758.00 | 5727.00 | 6724.00 | 7426.00 | 5820.00 | 5575.00 | 5099.00 |
| $N_{b\text{-jet}}$ | 543.00 | 628.00 | 751.00 | 892.00 | 617.00 | 504.00 | 502.00 |
| $E_{\text{T}}^{\text{miss}}$ GeV | 411.00 | 489.00 | 592.00 | 729.00 | 493.00 | 398.00 | 383.00 |
| Efficiency | 0.0002055 | 0.0002445 | 0.000296 | 0.0003645 | 0.0002465 | 0.000199 | 0.0001915 |

**Table A.3:** *Cutflow of the events survived the cuts for the selection of two leptons (e or $\mu$) and the efficiency with luminosity of 20.3 fb$^{-1}$; according to the ATLAS simulation.*

| | $m_S = 130$ GeV | $m_S = 135$ GeV | $m_S = 140$ GeV | $m_S = 145$ GeV | $m_S = 150$ GeV | $m_S = 155$ GeV | $m_S = 160$ GeV |
|---|---|---|---|---|---|---|---|
| All events | 2000000.00 | 2000000.00 | 2000000.00 | 2000000.00 | 2000000.00 | 2000000.00 | 2000000.00 |
| $e^+e^-/\mu^+\mu^-$ | 15373.00 | 17587.00 | 20508.00 | 21784.00 | 18036.00 | 16219.00 | 15060.00 |
| $p_{\text{T}}^{\text{lead}} > 25$ GeV | 12677.00 | 14656.00 | 17218.00 | 18503.00 | 15208.00 | 13698.00 | 12581.00 |
| $p_{\text{T}}^{\text{sub-lead}} > 20$ GeV | 7814.00 | 9131.00 | 11144.00 | 12084.00 | 9735.00 | 8781.00 | 7906.00 |
| $m_{\ell\ell} > 15$ GeV | 7331.00 | 8512.00 | 10495.00 | 11417.00 | 9147.00 | 8210.00 | 7414.00 |
| $\lvert m_{\ell\ell} - m_z \rvert > 15$ GeV | 4985.00 | 5619.00 | 7012.00 | 7672.00 | 6125.00 | 5808.00 | 5203.00 |
| $N_{jet} = 0$ | 494.00 | 510.00 | 796.00 | 956.00 | 666.00 | 531.00 | 451.00 |
| $E_{\text{T}}^{\text{miss}} > 45$ GeV | 150.00 | 201.00 | 338.00 | 408.00 | 288.00 | 207.00 | 194.00 |
| Efficiency | 0.000075 | 0.0001005 | 0.000169 | 0.000204 | 0.000144 | 0.0001035 | 0.000097 |

**Table A.4:** *Cutflow of the events survived the cuts for the selection of two OS and same-flavour leptons (ee or $\mu\mu$) and the efficiency with luminosity of 20.3 fb$^{-1}$; according to ATLAS simulation.*

The data and SM background in Ref. [86] is compared to the BSM signal. And the results are shown in Table. A.5 for the different-flavour and Table. A.6 for the same-flavour.

| | $\chi^2$ | | $\chi^2/ndf$ | | p-value | | N. signal | Significance |
|---|---|---|---|---|---|---|---|---|
| | SM background | SM+BSM | SM Background | SM+BSM | SM Background | SM+BSM | | |
| $m_S = 130$ GeV | 14.665 | 14.615 | 1.629 | 1.827 | 0.101 | 0.067 | $30 \pm 47$ | 1.498 |
| $m_S = 135$ GeV | 14.665 | 14.250 | 1.629 | 1.781 | 0.101 | 0.075 | $49 \pm 47$ | 1.436 |
| $m_S = 140$ GeV | 14.665 | 14.023 | 1.629 | 1.753 | 0.101 | 0.081 | $52 \pm 45$ | 1.397 |
| $m_S = 145$ GeV | 14.665 | 14.388 | 1.629 | 1.798 | 0.101 | 0.072 | $41 \pm 47$ | 1.460 |
| $m_S = 150$ GeV | 14.665 | 14.239 | 1.629 | 1.780 | 0.101 | 0.076 | $48 \pm 46$ | 1.434 |
| $m_S = 155$ GeV | 14.665 | 14.521 | 1.629 | 1.815 | 0.101 | 0.069 | $34 \pm 48$ | 1.482 |
| $m_S = 160$ GeV | 14.665 | 13.802 | 1.629 | 1.725 | 0.101 | 0.087 | $58 \pm 45$ | 1.359 |

**Table A.5:** *$\chi^2$ values, p-value, signal yield after the fitting and the significance for the SM background and the SM+BSM for events contain two different-flavour and OS leptons (e or $\mu$). The BSM signal is Higgs-like S boson $pp \to H \to Sh$; for the ATLAS data with luminosity of 20.3 fb$^{-1}$ [86].*

| | $\chi^2$ | | $\chi^2/ndf$ | | p-value | | N. signal | Significance |
|---|---|---|---|---|---|---|---|---|
| | SM background | SM+BSM | SM Background | SM+BSM | SM Background | SM+BSM | | |
| $m_S = 130$ GeV | 18.313 | 11.566 | 3.052 | 2.313 | 0.005 | 0.041 | $86 \pm 21$ | 1.736 |
| $m_S = 135$ GeV | 18.313 | 9.861 | 3.052 | 1.972 | 0.005 | 0.079 | $94 \pm 20$ | 1.410 |
| $m_S = 140$ GeV | 18.313 | 10.974 | 3.052 | 2.195 | 0.005 | 0.052 | $81 \pm 20$ | 1.627 |
| $m_S = 145$ GeV | 18.313 | 10.875 | 3.052 | 2.175 | 0.005 | 0.054 | $88 \pm 20$ | 1.608 |
| $m_S = 150$ GeV | 18.313 | 11.005 | 3.052 | 2.201 | 0.005 | 0.051 | $82 \pm 20$ | 1.633 |
| $m_S = 155$ GeV | 18.313 | 11.829 | 3.052 | 2.366 | 0.005 | 0.037 | $81 \pm 20$ | 1.784 |
| $m_S = 160$ GeV | 18.313 | 12.292 | 3.052 | 2.458 | 0.005 | 0.031 | $81 \pm 21$ | 1.866 |

**Table A.6:** *$\chi^2$ values, p-values, signal yield after the fitting and the significance for the SM background and the SM+BSM for events contain two same-flavour and OS lepton ($ee/\mu\mu$) category. The BSM signal is Higgs-like S boson $pp \to H \to Sh$; for the ATLAS data with luminosity of 20.3 fb$^{-1}$.*

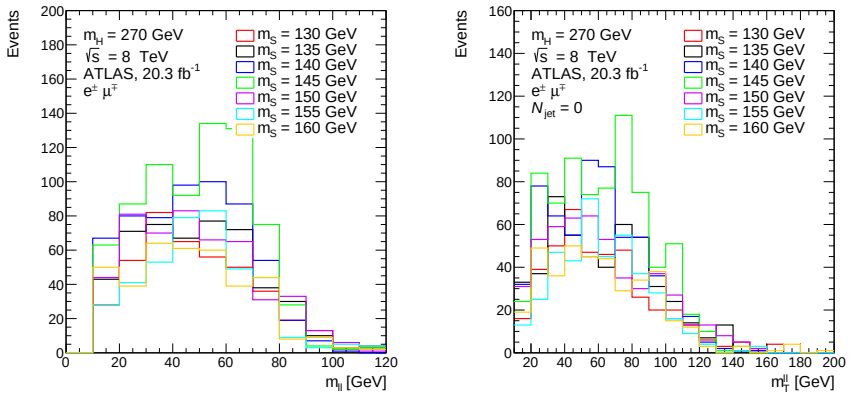


(a)




(b)

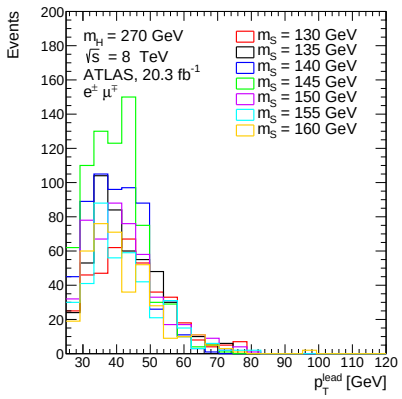


(c)

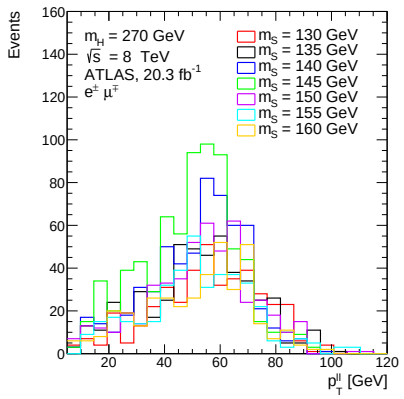


(d)

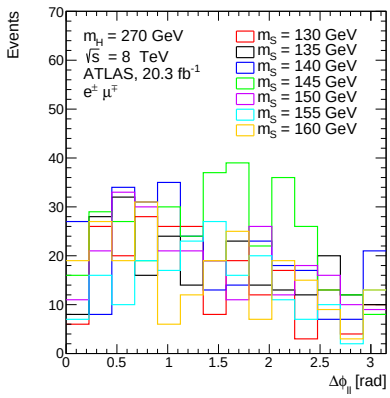


(e)

**Figure A.2:** *Kinematic distribution of (a) the di-lepton invariant mass, (b) the transverse mass of the di-lepton system, (c) the $p_T$ of the leading lepton, (d) the $p_T$ of the di-lepton system and (e) the azimuthal angle of two leptons; in events with an OS and different-flavour leptons (e or $\mu$) and zero jet with the ATLAS detector simulation.*

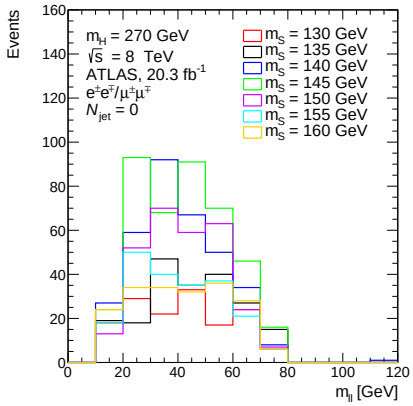


(a)

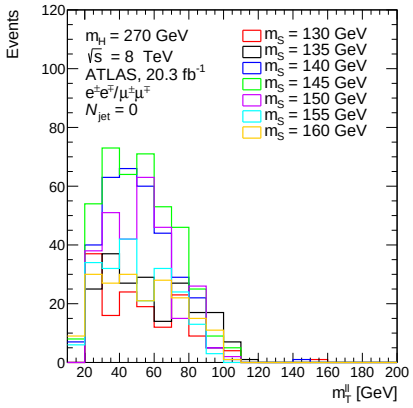


(b)

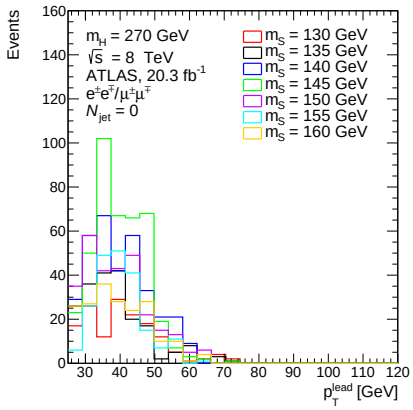


(c)

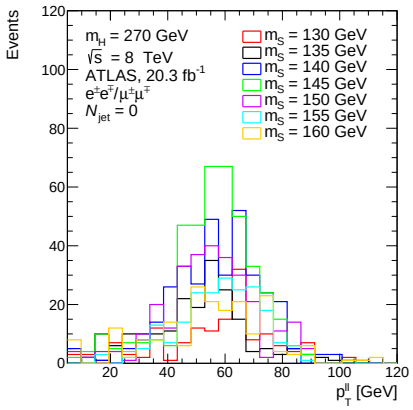


(d)

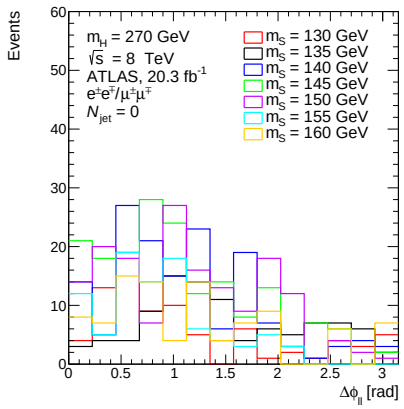


(e)

**Figure A.3:** *Kinematic distribution of (a) the di-lepton invariant mass, (b) the transverse mass of the di-lepton system, (c) the $p_T$ of the leading lepton, (d) the $p_T$ of the di-lepton system and (e) the azimuthal angle of two leptons; in events with an OS and same-flavour leptons ($ee$ or $\mu\mu$) and zero jet with the ATLAS detector simulation.*

## A.4 ATLAS, 20.3 fb$^{-1}$ with $e^{\pm}\mu^{\mp}$ and $N_{\text{jet}} = 1$

Table A.7 shows the events selected with the same even selections applied on Section A.3 in addition to exactly one jet. The kinematic distributions of the di-lepton invariant mass, transverse mass, $p_{\text{T}}$ of the leading and sub-leading lepton and the azimuthal angle between the di-lepton are shown in Figure A.4. The comparison of the data and SM prediction in Ref. [87] is compared to the BSM as shown in Table A.8.

| | $m_S = 130$ GeV | $m_S = 135$ GeV | $m_S = 140$ GeV | $m_S = 145$ GeV | $m_S = 150$ GeV | $m_S = 155$ GeV | $m_S = 160$ GeV |
|---|---|---|---|---|---|---|---|
| All events | 2000000.00 | 2000000.00 | 2000000.00 | 2000000.00 | 2000000.00 | 2000000.00 | 2000000.00 |
| $e^{\pm}\mu^{\pm}$ | 10757.00 | 12382.00 | 13882.00 | 14812.00 | 12095.00 | 11338.00 | 10594.00 |
| $p_{\text{T}}^{\text{lead}}$ GeV | 8843.00 | 10338.00 | 11726.00 | 12669.00 | 10262.00 | 9627.00 | 8923.00 |
| $p_{\text{T}}^{\text{sub-lead}}$ GeV | 4902.00 | 5911.00 | 6992.00 | 7666.00 | 6061.00 | 5818.00 | 5258.00 |
| $m_{\ell\ell} > 10$ GeV | 4758.00 | 5727.00 | 6724.00 | 7426.00 | 5820.00 | 5575.00 | 5099.00 |
| $N_{jet} = 1$ | 1100.00 | 1444.00 | 1735.00 | 1749.00 | 1577.00 | 1642.00 | 1388.00 |
| $E_{\text{T}}^{\text{miss}}$ GeV | 768.00 | 1051.00 | 1353.00 | 1402.00 | 1229.00 | 1264.00 | 1046.00 |
| Efficiency | 0.000384 | 0.0005255 | 0.0006765 | 0.000701 | 0.0006145 | 0.000632 | 0.000523 |

**Table A.7:** *Cutflow of the events survived the cuts for the selection of two OS leptons (e or $\mu$) plus exactly one jet and the efficiency with luminosity of 20.3 fb$^{-1}$; according to ATLAS simulation.*

| | $\chi^2$ | | $\chi^2/ndf$ | | p-value | | N. signal | Significance |
|---|---|---|---|---|---|---|---|---|
| | SM background | SM+BSM | SM Background | SM+BSM | SM Background | SM+BSM | | |
| $m_S = 130$ GeV | 12.965 | 12.931 | 1.441 | 1.616 | 0.164 | 0.114 | $13 \pm 35$ | 1.204 |
| $m_S = 135$ GeV | 12.965 | 12.764 | 1.441 | 1.596 | 0.164 | 0.120 | $23 \pm 37$ | 1.174 |
| $m_S = 140$ GeV | 12.965 | 12.800 | 1.441 | 1.600 | 0.164 | 0.119 | $22 \pm 37$ | 1.180 |
| $m_S = 145$ GeV | 12.965 | 12.925 | 1.441 | 1.616 | 0.164 | 0.114 | $16 \pm 37$ | 1.203 |
| $m_S = 150$ GeV | 12.965 | 12.803 | 1.441 | 1.600 | 0.164 | 0.119 | $20 \pm 36$ | 1.181 |
| $m_S = 155$ GeV | 12.965 | 12.805 | 1.441 | 1.601 | 0.164 | 0.119 | $21 \pm 36$ | 1.181 |
| $m_S = 160$ GeV | 12.965 | 12.913 | 1.441 | 1.614 | 0.164 | 0.115 | $16 \pm 36$ | 1.201 |

**Table A.8:** *$\chi^2$ values, p-value, signal yield after the fitting and the significance for the SM background and the SM+BSM for two OS leptons (e or $\mu$) plus exactly one jet. The BSM signal is Higgs-like S boson $pp \to H \to Sh$; for the ATLAS data with luminosity of 20.3 fb$^{-1}$ [87].*

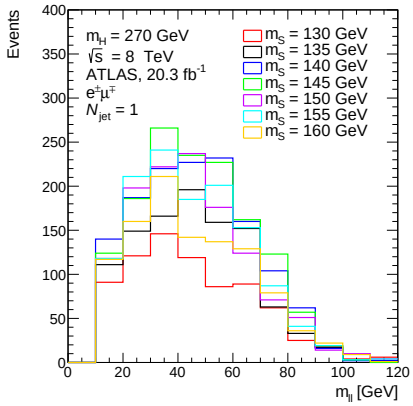


(a)

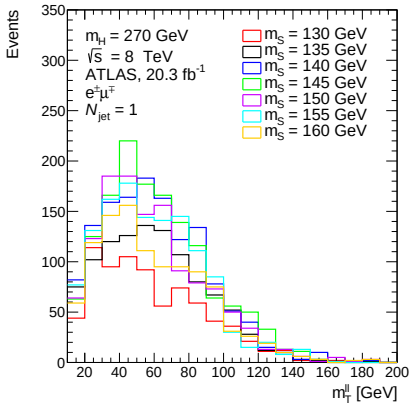


(b)

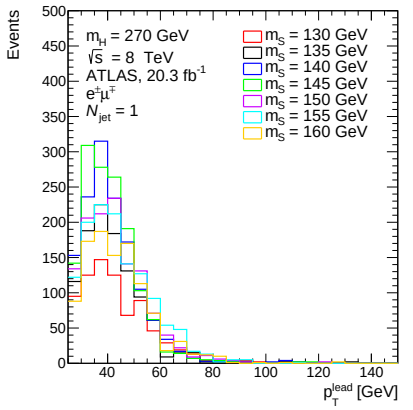


(c)

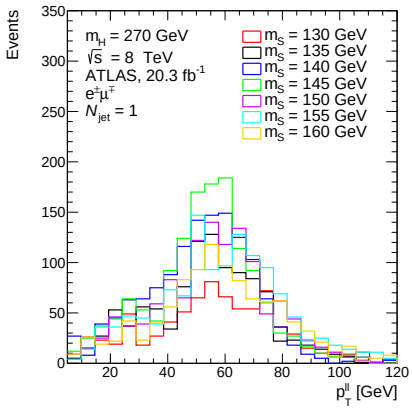


(d)

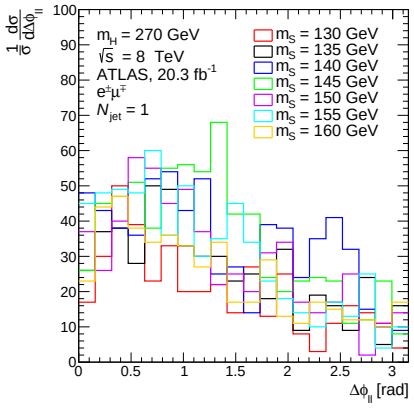


(e)

**Figure A.4:** *Kinematic distribution of (a) the di-lepton invariant mass, (b) the transverse mass of the di-lepton system, (c) the $p_T$ of the leading lepton, (d) the $p_T$ of the di-lepton system and (e) the azimuthal angle of two leptons; in events with an OS leptons ($e$ or $\mu$) and exactly one jet with the ATLAS detector simulation.*

## A.5 CMS, 19.4 fb$^{-1}$ with $e^+e^-/\mu^+\mu^-/e^\pm\mu^\mp$, $N_{\rm jet} = 1$ and $N_{\rm jet} = 0$

Following the analysis in Ref. [88], two OS leptons ($e^+e^-/\mu^+\mu^-/e^\pm\mu^\pm$) are selected. These leptons are considered from the leptonic decay of the $W^\pm$ boson ($W^+W^- \to \ell^+\nu\ell^-\bar{\nu}$), where $\ell$ could be ($e$ or $\mu$). Electrons are required to be within pseudorapidity $|\eta| < 2.5$ and muons within $|\eta| < 2.4$. Both leading and sub-leading leptons must have $p_{\rm T} > 20$ GeV.

Jets are required to have $p_{\rm T} > 30$ GeV and pseudorapidity $|\eta| < 2.7$. Events are categorised into two categories; zero jet (0-jet) category when no jets are selected and one jet (1-jet) category when it required exactly one jet in the events. For the 0-jet category, the di-lepton invariant mass is seated to be greater than 12 GeV. The missing transverse energy $E_{\rm T}^{\rm miss}$ is greater than 20 GeV for the two categories. The cutflows of the event selections for the 0-jet and 1-jet categories are shown in Tables A.9 and A.10.

The kinematic distribution of the di-lepton invariant mass $m_{\ell\ell}$, the transverse mass of the di-lepton system $m_{\rm T}^{\ell\ell}$, the $p_{\rm T}$ of the leading lepton, the $p_{\rm T}$ of the di-lepton system for the 0-jet and 1-jet categories are shown in Figures A.5 and A.6.

| | $m_S = 130$ GeV | $m_S = 135$ GeV | $m_S = 140$ GeV | $m_S = 145$ GeV | $m_S = 150$ GeV | $m_S = 155$ GeV | $m_S = 160$ GeV |
|---|---|---|---|---|---|---|---|
| All events | 2000000.00 | 2000000.00 | 2000000.00 | 2000000.00 | 2000000.00 | 2000000.00 | 2000000.00 |
| 2 lepton | 27495.00 | 31579.00 | 36133.00 | 38881.00 | 32061.00 | 29165.00 | 26975.00 |
| $p_{\rm T}^{\rm lead}$/sub-lead $> 20$ GeV | 13896.00 | 16282.00 | 19654.00 | 21583.00 | 17505.00 | 15938.00 | 14194.00 |
| $m_{\ell\ell} > 12$ GeV | 13303.00 | 15483.00 | 18753.00 | 20650.00 | 16690.00 | 15134.00 | 13605.00 |
| $e^+e^-/\mu^+\mu^-/e^\pm\mu^\mp$ | 7404.00 | 8587.00 | 10429.00 | 11594.00 | 9728.00 | 9134.00 | 8288.00 |
| $E_{\rm T}^{\rm miss} > 20$ GeV | 713.00 | 883.00 | 1182.00 | 1484.00 | 949.00 | 823.00 | 715.00 |
| $N_{jet} = 0$ | 600.00 | 749.00 | 1075.00 | 1359.00 | 849.00 | 704.00 | 631.00 |
| Efficiency | 0.0003 | 0.0003745 | 0.0005375 | 0.0006795 | 0.0004245 | 0.000352 | 0.0003155 |

**Table A.9:** *Cutflow of the events survived the cuts for the selection of two OS leptons ($e^+e^-/\mu^+\mu^-/e^\pm\mu^\pm$) with zero jet and the efficiency with luminosity of 19.4 fb$^{-1}$; according to CMS simulation.*

| | $m_S = 130$ GeV | $m_S = 135$ GeV | $m_S = 140$ GeV | $m_S = 145$ GeV | $m_S = 150$ GeV | $m_S = 155$ GeV | $m_S = 160$ GeV |
|---|---|---|---|---|---|---|---|
| All events | 2000000.00 | 2000000.00 | 2000000.00 | 2000000.00 | 2000000.00 | 2000000.00 | 2000000.00 |
| 2 lepton | 27495.00 | 31579.00 | 36133.00 | 38881.00 | 32061.00 | 29165.00 | 26975.00 |
| $p_{\rm T}^{lead}/sub-lead > 20$ GeV | 13896.00 | 16282.00 | 19654.00 | 21583.00 | 17505.00 | 15938.00 | 14194.00 |
| $m_{\ell\ell} > 12$ GeV | 13303.00 | 15483.00 | 18753.00 | 20650.00 | 16690.00 | 15134.00 | 13605.00 |
| $e^+e^-/\mu^+\mu^-/e^\pm\mu^\mp$ | 7404.00 | 8587.00 | 10429.00 | 11594.00 | 9728.00 | 9134.00 | 8288.00 |
| $E_{\rm T}^{\rm miss} > 20$ GeV | 1776.00 | 2091.00 | 2580.00 | 2666.00 | 2515.00 | 2357.00 | 2220.00 |
| $N_{jet} = 1$ | 1390.00 | 1709.00 | 2260.00 | 2342.00 | 2054.00 | 1888.00 | 1773.00 |
| Efficiency | 0.000695 | 0.0008545 | 0.00113 | 0.001171 | 0.001027 | 0.000944 | 0.0008865 |

**Table A.10:** *Cutflow of the events survived the cuts for the selection of two OS leptons ($e^+e^-/\mu^+\mu^-/e^\pm\mu^\pm$) with one jet and the efficiency with luminosity of 19.4 fb$^{-1}$; according to CMS simulation.*

The comparison of the BSM signal to the CMS data and the SM background [88] is shown in Tables A.11 and A.12.

| | $\chi^2$ | | $\chi^2/ndf$ | | p-value | | N. signal | Significance |
|---|---|---|---|---|---|---|---|---|
| | SM background | SM+BSM | SM Background | SM+BSM | SM Background | SM+BSM | | |
| $m_S = 130$ GeV | 18.220 | 13.837 | 1.656 | 1.384 | 0.077 | 0.181 | $158 \pm 60$ | 0.913 |
| $m_S = 135$ GeV | 18.220 | 14.327 | 1.656 | 1.433 | 0.077 | 0.159 | $145 \pm 58$ | 1.000 |
| $m_S = 140$ GeV | 18.220 | 15.343 | 1.656 | 1.534 | 0.077 | 0.120 | $124 \pm 56$ | 1.175 |
| $m_S = 145$ GeV | 18.220 | 15.388 | 1.656 | 1.539 | 0.077 | 0.119 | $125 \pm 57$ | 1.182 |
| $m_S = 150$ GeV | 18.220 | 14.907 | 1.656 | 1.491 | 0.077 | 0.136 | $136 \pm 58$ | 1.101 |
| $m_S = 155$ GeV | 18.220 | 15.439 | 1.656 | 1.544 | 0.077 | 0.117 | $122 \pm 56$ | 1.191 |
| $m_S = 160$ GeV | 18.220 | 16.343 | 1.634 | 1.618 | 0.077 | 0.090 | $107 \pm 55$ | 1.339 |

**Table A.11:** *$\chi^2$ values, p-value, signal yield after the fitting and the significance of the SM background and the SM+BSM for two OS leptons ($e^+e^-/\mu^+\mu^-/e^\pm\mu^\pm$) with zero jet selection. The BSM signal is Higgs-like $S$ boson $pp \to H \to Sh$; for the CMS data with luminosity of 19.4 fb$^{-1}$ [88].*

| | $\chi^2$ | | $\chi^2/ndf$ | | p-value | | N. signal | Significance |
|---|---|---|---|---|---|---|---|---|
| | SM background | SM+BSM | SM Background | SM+BSM | SM Background | SM+BSM | | |
| $m_S = 130$ GeV | 14.695 | 14.309 | 1.336 | 1.431 | 0.197 | 0.159 | $39 \pm 42$ | 0.997 |
| $m_S = 135$ GeV | 14.695 | 14.148 | 1.336 | 1.414 | 0.197 | 0.166 | $47 \pm 43$ | 0.969 |
| $m_S = 140$ GeV | 14.695 | 14.279 | 1.336 | 1.428 | 0.197 | 0.161 | $41 \pm 42$ | 0.992 |
| $m_S = 145$ GeV | 14.695 | 14.085 | 1.336 | 1.409 | 0.197 | 0.169 | $48 \pm 43$ | 0.958 |
| $m_S = 150$ GeV | 14.695 | 14.111 | 1.336 | 1.411 | 0.197 | 0.168 | $46 \pm 43$ | 0.962 |
| $m_S = 155$ GeV | 14.695 | 14.093 | 1.409 | 1.409 | 0.197 | 0.169 | $46 \pm 43$ | 0.959 |
| $m_S = 160$ GeV | 14.695 | 14.495 | 1.336 | 1.450 | 0.197 | 0.152 | $32 \pm 41$ | 1.030 |

**Table A.12:** *$\chi^2$ values, p-value, signal yield after the fitting and the significance of the SM background and the SM+BSM for two OS leptons ($e^+e^-/\mu^+\mu^-/e^\pm\mu^\pm$) with one jet selection. The BSM signal is Higgs-like $S$ boson $pp \to H \to Sh$; for the CMS data with luminosity of 19.4 fb$^{-1}$ [88].*

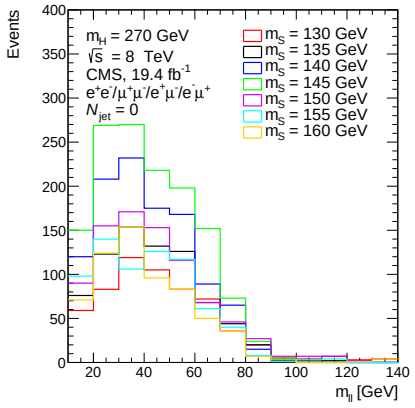


(a)

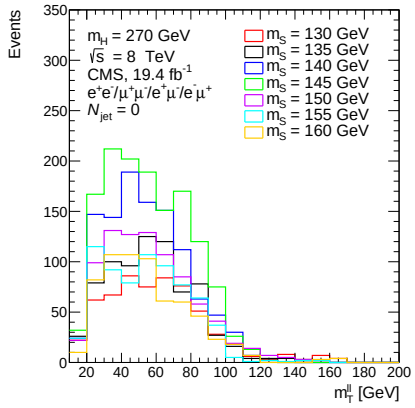


(b)

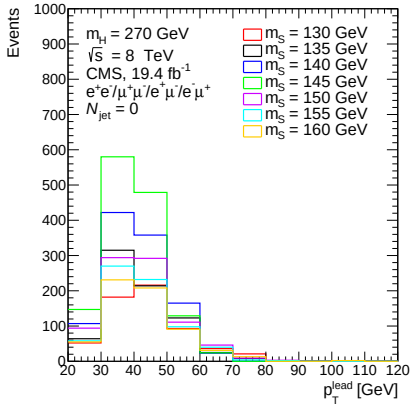


(c)

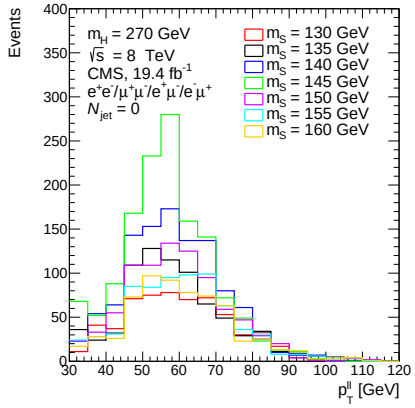


(d)

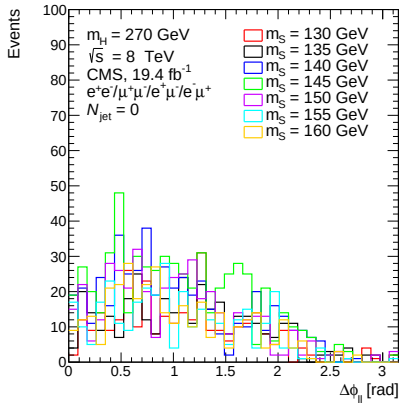


(e)

**Figure A.5:** *Kinematic distribution of (a) the di-lepton invariant mass, (b) the transverse mass of the di-lepton system, (c) the $p_T$ of the leading lepton, (d) the $p_T$ of the di-lepton system and (e) the azimuthal angle of two leptons; in events with an OS leptons ($e^+e^-/\mu^+\mu^-/e^\pm\mu^\pm$) and zero jet with the CMS detector simulation.*

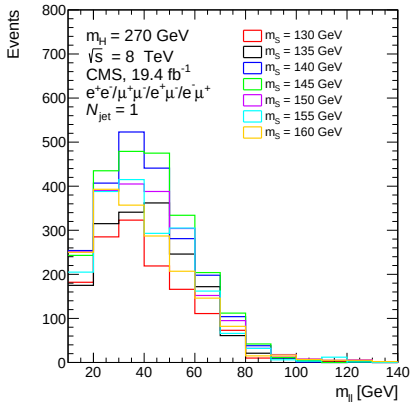


(a)

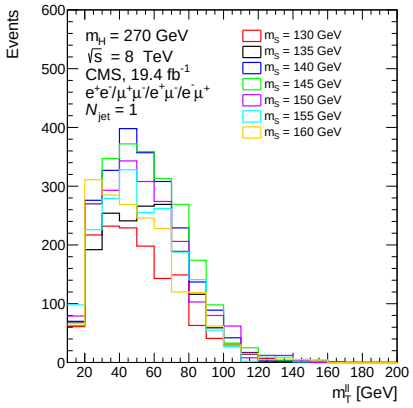


(b)

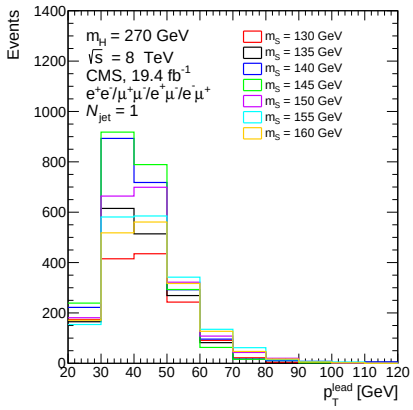


(c)

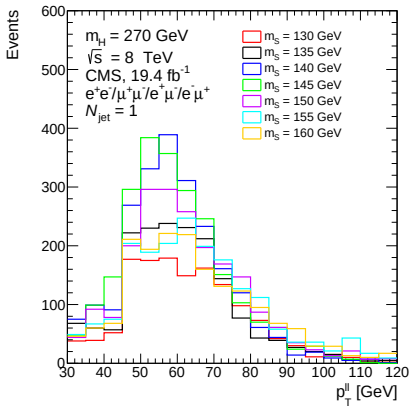


(d)

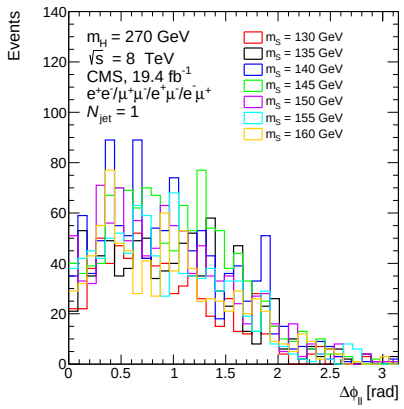


(e)

**Figure A.6:** *Kinematic distribution of (a) the di-lepton invariant mass, (b) the transverse mass of the di-lepton system, (c) the $p_T$ of the leading lepton, (d) the $p_T$ of the di-lepton system and (e) the azimuthal angle of two leptons; in events with an OS leptons ($e^+e^-/\mu^+\mu^-/e^\pm\mu^\pm$) and one jet with the CMS detector simulation.*

## A.6 CMS, 5.3 fb$^{-1}$ with $e^+e^-/\mu^+\mu^+/e^\pm\mu^\mp$, $N_{\rm jet} \geq 2$ and $N_{b-\rm jet} \geq 2$

Events with two OS leptons ($e$ or $\mu$) are selected, leptons should have $p_{\rm T} > 20$ GeV and $|\eta^e| < 2.5$ for the electron and $|\eta^\mu| < 2.1$ if it is muon, as described Ref. [89]. In addition, at least two jets and one $b$-tagged jet are selected, the jets must acquire $p_{\rm T} > 30$ GeV and $|\eta^{\rm jet}| < 2.5$. The di-lepton invariant mass should be greater than 10 GeV, the cutflow of these selections are shown in Table A.13.

| | $m_S = 130$ GeV | $m_S = 135$ GeV | $m_S = 140$ GeV | $m_S = 145$ GeV | $m_S = 150$ GeV | $m_S = 155$ GeV | $m_S = 160$ GeV |
|---|---|---|---|---|---|---|---|
| All events | 2000000.00 | 2000000.00 | 2000000.00 | 2000000.00 | 2000000.00 | 2000000.00 | 2000000.00 |
| $e^\pm\mu^\mp$ | 11003.00 | 12612.00 | 13977.00 | 15312.00 | 12670.00 | 11696.00 | 10888.00 |
| $p_{\rm T}^{lead} > 20$ GeV | 10172.00 | 11754.00 | 13104.00 | 14470.00 | 11841.00 | 10944.00 | 10141.00 |
| $p_{\rm T}^{sub-lead} > 20$ GeV | 5213.00 | 6230.00 | 7262.00 | 8182.00 | 6660.00 | 6248.00 | 5513.00 |
| $m_{\ell\ell} > 10$ GeV | 4597.00 | 5417.00 | 6272.00 | 7056.00 | 5733.00 | 5393.00 | 4840.00 |
| $N_{b\text{-jet}} \geq 1$ | 1697.00 | 1803.00 | 2053.00 | 2414.00 | 2197.00 | 1956.00 | 1867.00 |
| $N_{jet} \geq 2$ | 1387.00 | 1500.00 | 1672.00 | 2064.00 | 1690.00 | 1505.00 | 1444.00 |
| Efficiency | 0.0006935 | 0.00075 | 0.000836 | 0.001032 | 0.000845 | 0.0007525 | 0.000722 |

**Table A.13:** *Cutflow of the events survived the cuts for the selection of two OS leptons ($e$ or $\mu$), at least two jets and two b-tagged jets and the efficiency with luminosity of 5.3 fb$^{-1}$; according to CMS simulation.*

| | $\chi^2$ | | $\chi^2/ndf$ | | p-value | | N. signal | Significance |
|---|---|---|---|---|---|---|---|---|
| | SM background | SM+BSM | SM Background | SM+BSM | SM Background | SM+BSM | | |
| $m_S = 130$ GeV | 12.859 | 12.752 | 0.756 | 0.797 | 0.746 | 0.691 | $38 \pm 60$ | -0.498 |
| $m_S = 135$ GeV | 12.859 | 12.880 | 0.756 | 0.805 | 0.746 | 0.682 | $21 \pm 58$ | -0.472 |
| $m_S = 140$ GeV | 12.859 | 12.889 | 0.756 | 0.806 | 0.746 | 0.681 | $18 \pm 61$ | -0.470 |
| $m_S = 145$ GeV | 12.859 | 12.902 | 0.756 | 0.806 | 0.746 | 0.680 | $15 \pm 65$ | -0.467 |
| $m_S = 150$ GeV | 12.859 | 12.895 | 0.756 | 0.806 | 0.746 | 0.680 | $17 \pm 58$ | 1.089 |
| $m_S = 155$ GeV | 12.859 | 12.866 | 0.756 | 0.804 | 0.746 | 0.683 | $24 \pm 60$ | -0.475 |
| $m_S = 160$ GeV | 12.859 | 12.818 | 0.756 | 0.801 | 0.746 | 0.686 | $28 \pm 57$ | -0.485 |

**Table A.14:** *$\chi^2$ values, p-value, signal yield after the fitting and the significance of the SM background and the SM+BSM for ($e^\pm\mu^\mp$) with at least two jets and two b-tagged jets. The BSM signal is Higgs-like $S$ boson $pp \to H \to Sh$; for the CMS data with luminosity of 5.3 fb$^{-1}$ [89].*

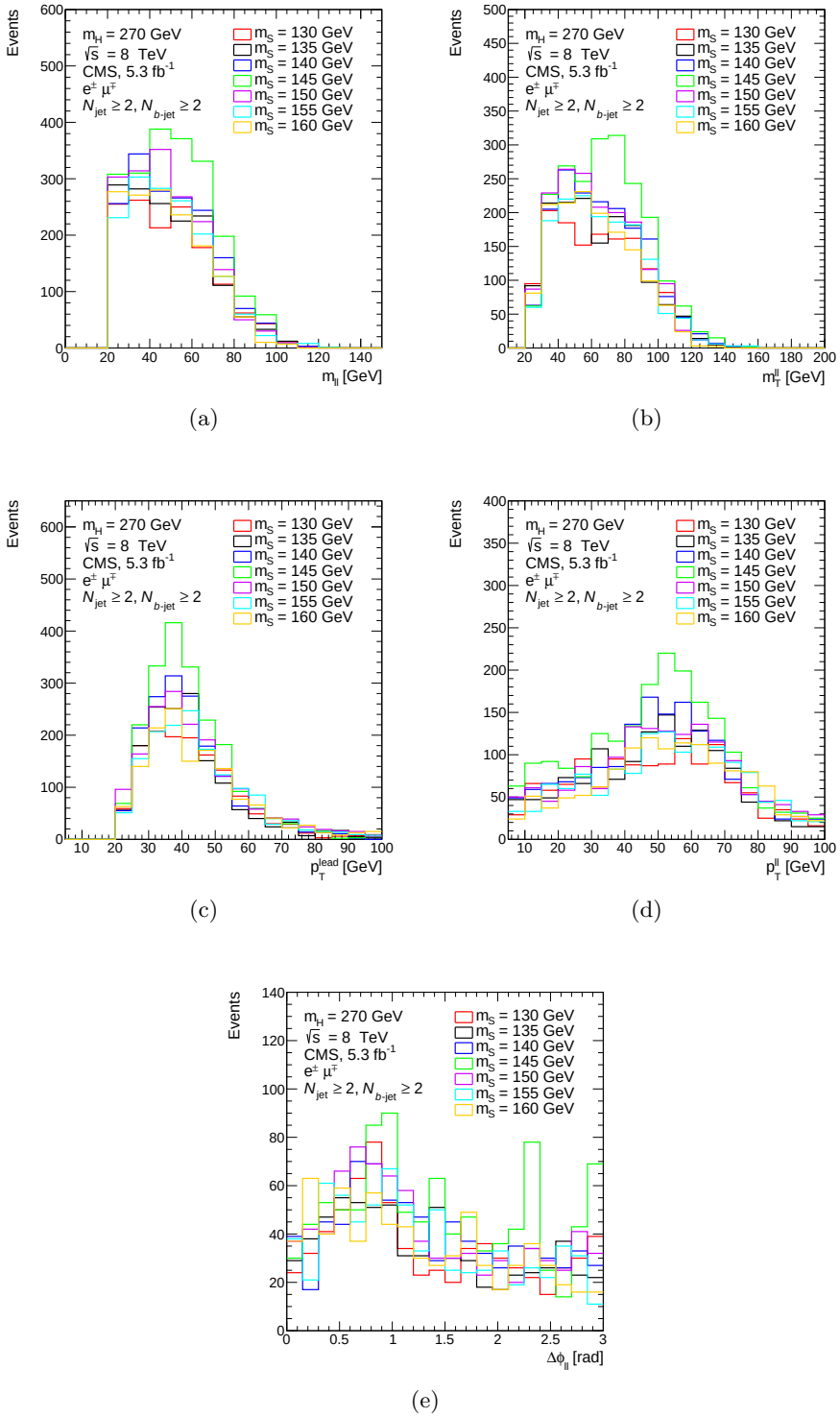


(a) (b)

(c) (d)

(e)

**Figure A.7:** *Kinematic distribution of (a) the di-lepton invariant mass, (b) the transverse mass of the di-lepton system, (c) the $p_T$ of the leading lepton, (d) the $p_T$ of the di-lepton system and (e) the azimuthal angle of two leptons; in events with an OS leptons ($e$ or $\mu$) and at least two jets and two b-tagged jets with the CMS simulation.*

## A.7 Method for extracting $\beta_g^2$

In order to get the $\beta_g^2$ value, we make use of the results presented in Tables A.2, A.5, A.6 and A.8 of the ATLAS data comparison and for CMS Table A.11, A.12 and A.14. First, we identify the point mass of the interest, for instance $m_S = 145$ GeV, then we apply the following: the expected number events ($\mu^{\text{exp}}$) is computed by the cross-section $\sigma$ of the production of the heavy boson $H$, the luminosity (lumi) of the measurement and the efficiency (eff) of the selection as:

$$\mu^{\text{exp}} = \text{eff} \times \sigma \times \text{lumi}, \tag{A.7.1}$$

$$\Delta\mu^{\text{exp}} = \frac{\beta_g^{*\,2}}{\Delta\beta_g^{*\,2}} \times \mu^{\text{exp}}, \tag{A.7.2}$$

where $\beta_g^{*\,2}$ and $\Delta\beta_g^{*\,2}$ are estimated cross-section from Higgs signal collected from the data up to date [19] $\beta_g^{*\,2} \pm \Delta\beta_g^{*\,2} = 1.38 \pm 0.32$. Since the mass of the $H$ is fixed ($m_H = 270$ GeV) the cross-section (4.04 pb) of the production as taken from Higgs cross-section working group [8] is scaled by the value of the extracted $\beta_g^{*\,2}$. $\beta_g'^{\,2}$, considered as a central value for each measurement, results from our analysis in Tables A.2, A.5, A.6, A.8, A.11, A.12 and A.14 is calculated by:

$$\beta_g'^{\,2} = \frac{\text{yield} \times \beta_g^{*\,2}}{\mu^{\text{exp}}}, \tag{A.7.3}$$

$$\Delta\beta_g'^{\,2} = \frac{\text{yield error}}{\text{yield}}, \tag{A.7.4}$$

For $m_S = 145$ GeV and $m_S = 135$ GeV the expected events, event yield $\beta_g'^{\,2}$ and $\Delta\chi^2$ are shown in Table A.15 Table A.16, respectively. Since we are dealing with samples of Gaussian nature but each measure has different standard deviation, by using weighted mean, following chapter 4 in Ref. [93], the combined $\beta_g^2$ can be written as:

$$\beta_g^2 = \sum_{i=1}^{N} \frac{\beta_{g_i}'^{\,2}}{\left(\Delta\beta_{g_i}'^{\,2}\right)^2}, \tag{A.7.5}$$

where $N$ runs on all the seven measurements from the ATLAS and CMS collaboration discussed above. The extracted $\beta_g'^{\,2}$s for each measurements are displayed in Table A.15 for $m_S = 145 \pm 5$ GeV and Table A.16 for $m_S = 135 \pm 5$ GeV. By using Equation A.7.5 the combined $\beta_g^2$ is found to be $\beta_g^2 = 1.35 \pm 0.32$ and $\beta_g^2 = 1.09 \pm 0.28$ for $m_S = 145$ GeV and $m_S = 135$ GeV, respectively.

| **Measurement** | **Reference** | **Expected events** | **Post-fit event yield** | $\beta_g^2$ | $\chi^2_{SM} - \chi^2_{SM+BSM}$ |
|---|---|---|---|---|---|
| ATLAS, 20.2 fb$^{-1}$<br>$e^{\pm}\mu^{\mp}$<br>$n_b \geq 1$ | [85] | $118 \pm 27$ | $395 \pm 96$ | $4.62 \pm 1.12$ | 11.13 |
| ATLAS, 20.3 fb$^{-1}$<br>$e^{\pm}\mu^{\mp}$<br>$N_{\text{jet}} = 0$ | [86] | $41 \pm 10$ | $41 \pm 47$ | $1.38 \pm 1.58$ | 0.28 |
| ATLAS, 20.3 fb$^{-1}$<br>$e^{+}e^{-},\ \mu^{+}\mu^{-}$<br>$N_{\text{jet}} = 0$ | [86] | $23 \pm 5$ | $88 \pm 20$ | $5.28 \pm 1.20$ | 7.44 |
| ATLAS, 20.3 fb$^{-1}$<br>$e^{\pm}\mu^{\mp}$<br>$N_{\text{jet}} = 1$ | [87] | $79 \pm 18$ | $16 \pm 37$ | $0.28 \pm 0.65$ | 0.04 |
| CMS, 19.4 fb$^{-1}$<br>$e^{+}e^{-},\ \mu^{+}\mu^{-},\ e^{\pm}\mu^{\mp}$<br>$N_{\text{jet}} = 0$ | [88] | $73 \pm 17$ | $125 \pm 56$ | $2.36 \pm 1.08$ | 2.82 |
| CMS, 19.4 fb$^{-1}$<br>$e^{+}e^{-},\ \mu^{+}\mu^{-},\ e^{\pm}\mu^{\mp}$<br>$N_{\text{jet}} = 1$ | [88] | $127 \pm 29$ | $48 \pm 43$ | $0.52 \pm 0.48$ | 0.61 |
| CMS, 5.3 fb$^{-1}$<br>$e^{+}e^{-},\ \mu^{+}\mu^{-},\ e^{\pm}\mu^{\mp}$<br>$N_{\text{jet}} \geq 2,\ n_b \geq 2$ | [89] | $30 \pm 7$ | $15 \pm 56$ | $0.69 \pm 2.58$ | $-0.04$ |

**Table A.15:** *Best fits to the di-lepton invariant mass spectra reported by ATLAS and CMS at a proton-proton centre of mass of $\sqrt{s} = 8$ TeV. The post-fit event yield reflects the number of BSM events required to fit the data (in excess of the SM prediction). The value of $\beta_g^2$ corresponding to the post-fit event yield is reported along with the test statistic $\chi^2_{SM} - \chi^2_{SM+BSM}$ in order to gauge the significance of the fit. The mass of the heavy scalar is fixed at $m_H = 270\,GeV$ and the mass of $S$ is allowed to vary, where the best fit is found for $m_S = 145$ GeV. For simplicity, it is assumed that $H$ decays exclusively into $Sh$.*

| Measurement | Reference | Expected events | Post-fit event yield | $\beta_g^2$ | $\chi^2_{SM} - \chi^2_{SM+BSM}$ |
|---|---|---|---|---|---|
| ATLAS, 20.2 fb$^{-1}$<br>$e^{\pm}\mu^{\mp}$<br>$n_b \geq 1$ | [85] | $103 \pm 24$ | $363 \pm 89$ | $4.86 \pm 1.19$ | 10.91 |
| ATLAS, 20.3 fb$^{-1}$<br>$e^{\pm}\mu^{\mp}$<br>$N_{\text{jet}} = 0$ | [86] | $28 \pm 6$ | $49 \pm 47$ | $2.42 \pm 2.32$ | 0.4 |
| ATLAS, 20.3 fb$^{-1}$<br>$e^{+}e^{-},\ \mu^{+}\mu^{-}$<br>$N_{\text{jet}} = 0$ | [86] | $11 \pm 3$ | $94 \pm 20$ | $11.79 \pm 2.51$ | 8.45 |
| ATLAS, 20.3 fb$^{-1}$<br>$e^{\pm}\mu^{\mp}$<br>$N_{\text{jet}} = 1$ | [87] | $59 \pm 14$ | $23 \pm 37$ | $0.54 \pm 0.34$ | 0.20 |
| CMS, 19.4 fb$^{-1}$<br>$e^{+}e^{-},\ \mu^{+}\mu^{-},\ e^{\pm}\mu^{\mp}$<br>$N_{\text{jet}} = 0$ | [88] | $41 \pm 9$ | $145 \pm 58$ | $4.88 \pm 1.95$ | 3.89 |
| CMS, 19.4 fb$^{-1}$<br>$e^{+}e^{-},\ \mu^{+}\mu^{-},\ e^{\pm}\mu^{\mp}$<br>$N_{\text{jet}} = 1$ | [88] | $92 \pm 21$ | $47 \pm 43$ | $0.71 \pm 0.65$ | 0.55 |
| CMS, 5.3 fb$^{-1}$<br>$e^{+}e^{-},\ \mu^{+}\mu^{-},\ e^{\pm}\mu^{\mp}$<br>$N_{\text{jet}} \geq 2,\ n_b \geq 2$ | [89] | $22 \pm 5$ | $21 \pm 58$ | $1.32 \pm 3.64$ | $-0.02$ |

**Table A.16:** *Best fits to the di-lepton invariant mass spectra reported by ATLAS and CMS at a proton-proton centre of mass of $\sqrt{s} = 8$ TeV. The post-fit event yield reflects the number of BSM events required to fit the data (in excess of the SM prediction). The value of $\beta_g^2$ corresponding to the post-fit event yield is reported along with the test statistic $\chi^2_{SM} - \chi^2_{SM+BSM}$ in order to gauge the significance of the fit. The mass of the heavy scalar is fixed at $m_H = 270\,GeV$ and the mass of $S$ is allowed to vary, where the best fit is found for $m_S = 135$ GeV. For simplicity, it is assumed that $H$ decays exclusively into $Sh$.*

# B

# Heavy Neutrino Signal with $m_{N_i} > m_S$

This appendix follow the same analysis procedure applied in appendix A. However, here we consider the mass of the heavy neutrino $N_i$ to be off-shell ($m_{N_i} = 1$ TeV).

## B.1 ATLAS, 20.2 fb$^{-1}$ with $e^{\pm}\mu^{\mp}$ and $N_{b-\text{jet}} \geq 1$

| | $m_S = 130$ GeV | $m_S = 135$ GeV | $m_S = 140$ GeV | $m_S = 145$ GeV | $m_S = 150$ GeV | $m_S = 155$ GeV | $m_S = 160$ GeV |
|---|---|---|---|---|---|---|---|
| All events | 500000.00 | 500000.00 | 500000.00 | 500000.00 | 500000.00 | 500000.00 | 500000.00 |
| $e^{\pm}\mu^{\mp}$ events | 23090.00 | 22597.00 | 22916.00 | 23376.00 | 25005.00 | 25416.00 | 25929.00 |
| $N_{b-\text{jet}} \geq 1$ | 541.00 | 513.00 | 573.00 | 571.00 | 568.00 | 617.00 | 669.00 |
| Efficiency | 0.001082 | 0.001026 | 0.001146 | 0.001142 | 0.001136 | 0.001234 | 0.001338 |

**Table B.1:** *Cutflow of the events survived the cuts for the selection of two leptons (e or $\mu$) and the efficiency with luminosity of 20.2 fb$^{-1}$. The BSM signal is the heavy neutrino model with $m_{N_i} > m_S$ according to the ATLAS simulation.*

| | $\chi^2$ | | $\chi^2/ndf$ | | p-value | | N. signal | Significance |
|---|---|---|---|---|---|---|---|---|
| | SM background | SM+BSM | SM Background | SM+BSM | SM Background | SM+BSM | | |
| $m_S = 130$ GeV | 18.122 | 6.268 | 3.624 | 1.567 | 0.003 | 0.180 | 421±99 | 0.915 |
| $m_S = 135$ GeV | 18.122 | 6.787 | 3.624 | 1.697 | 0.003 | 0.148 | 403±97 | 1.048 |
| $m_S = 140$ GeV | 18.122 | 5.911 | 3.624 | 1.478 | 0.003 | 0.206 | 430±100 | 0.821 |
| $m_S = 145$ GeV | 18.122 | 7.705 | 3.624 | 1.926 | 0.003 | 0.103 | 395±98 | 1.265 |
| $m_S = 150$ GeV | 18.122 | 5.876 | 3.624 | 1.469 | 0.003 | 0.209 | 477±111 | 0.81127 |
| $m_S = 155$ GeV | 18.122 | 4.825 | 3.624 | 1.206 | 0.003 | 0.306 | 535±121 | 0.508 |
| $m_S = 160$ GeV | 18.122 | 7.525 | 3.624 | 1.881 | 0.003 | 0.111 | 478±118 | 1.223 |

**Table B.2:** *$\chi^2$ values, p-value, signal yield after the fitting and the significance for the SM background and the SM+BSM. The BSM signal is the heavy neutrino model with $m_{N_i} > m_S$ ($pp \to H \to Sh$); for the ATLAS data with luminosity of 20.2 fb$^{-1}$ [85].*

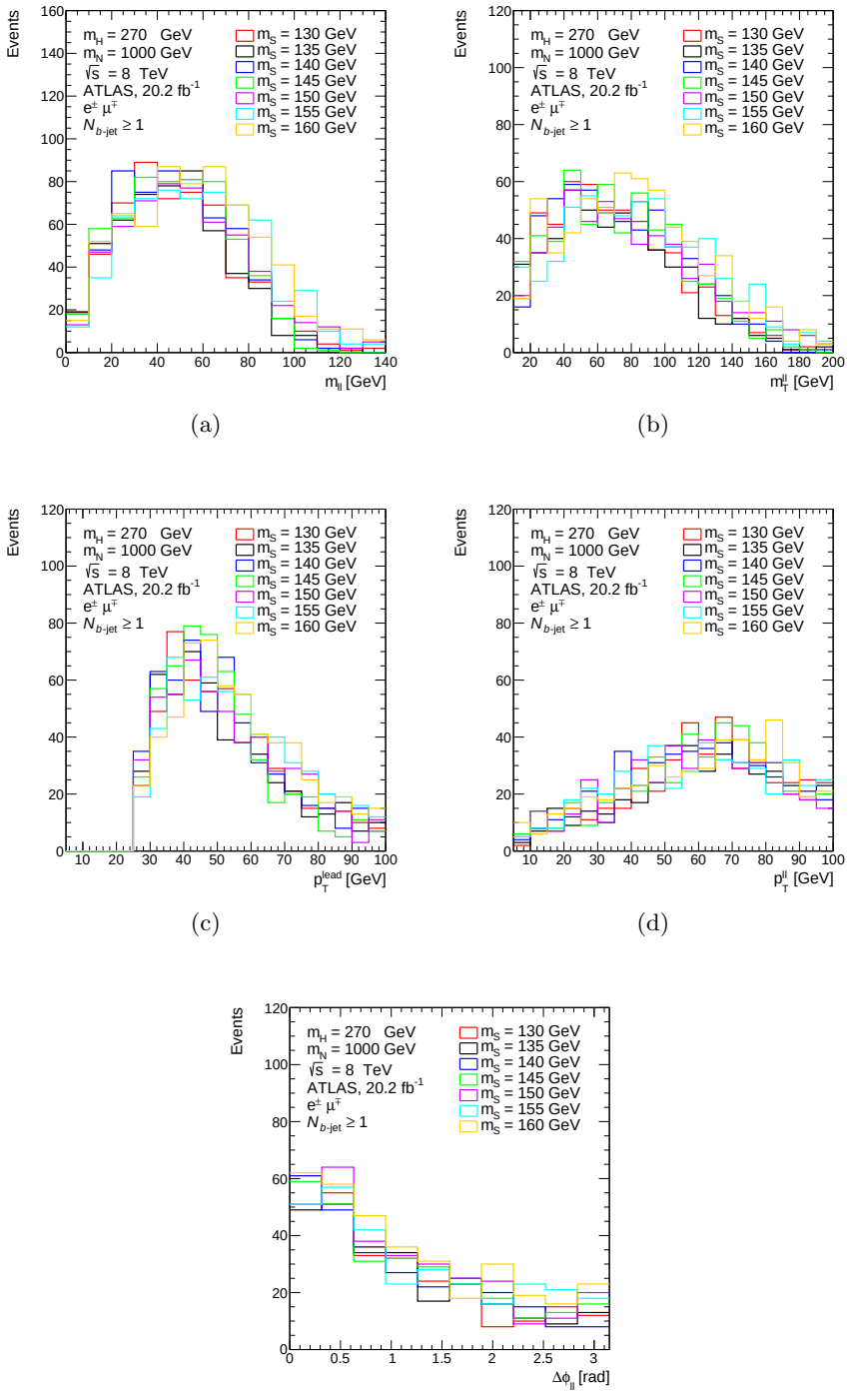


**Figure B.1:** *Kinematic distribution of (a) the di-lepton invariant mass, (b) the transverse mass of the di-lepton system, (c) the $p_T$ of the leading lepton, (d) the $p_T$ of the di-lepton system and (e) the azimuthal angle of two leptons; in events with an OS leptons ($e$ or $\mu$) and at least one b-tagged jet with the ATLAS detector simulation. The BSM signal is the heavy neutrino signal with $m_{N_i} > m_S$.*

## B.2 ATLAS, 20.3 fb$^{-1}$ with $e^+e^-/\mu^+\mu^-/e^\pm\mu^\mp$ and $N_{\rm jet} = 0$

| | $m_S = 130$ GeV | $m_S = 135$ GeV | $m_S = 140$ GeV | $m_S = 145$ GeV | $m_S = 150$ GeV | $m_S = 155$ GeV | $m_S = 160$ GeV |
|---|---|---|---|---|---|---|---|
| All events | 500000.00 | 500000.00 | 500000.00 | 500000.00 | 500000.00 | 500000.00 | 500000.00 |
| $e^\pm\mu^\pm$ | 44206.00 | 48808.00 | 42719.00 | 42443.00 | 42667.00 | 42203.00 | 41917.00 |
| $p_{\rm T}^{\rm lead} > 25$ GeV | 39486.00 | 41945.00 | 38511.00 | 38380.00 | 39204.00 | 39024.00 | 38898.00 |
| $p_{\rm T}^{\rm sub\text{-}lead} > 20$ GeV | 25284.00 | 25161.00 | 25326.00 | 25709.00 | 27258.00 | 27645.00 | 28120.00 |
| $m_{ll} > 10$ | 24573.00 | 24385.00 | 24582.00 | 24998.00 | 26589.00 | 26968.00 | 27491.00 |
| $N_{jet} = 0$ | 6997.00 | 7190.00 | 6784.00 | 6762.00 | 6744.00 | 6651.00 | 6469.00 |
| $E_{\rm T}^{\rm miss} > 20$ GeV | 6016.00 | 5972.00 | 5838.00 | 5875.00 | 5873.00 | 5869.00 | 5629.00 |
| Efficiency | 0.012032 | 0.011944 | 0.011676 | 0.01175 | 0.011746 | 0.011738 | 0.011258 |

**Table B.3:** *Cutflow of the events survived the cuts for the selection of two leptons (e or $\mu$) and the efficiency with luminosity of 20.3 fb$^{-1}$. The BSM signal is the heavy neutrino model with $m_{N_i} > m_S$ according to the ATLAS simulation.*

| | $m_S = 130$ GeV | $m_S = 135$ GeV | $m_S = 140$ GeV | $m_S = 145$ GeV | $m_S = 150$ GeV | $m_S = 155$ GeV | $m_S = 160$ GeV |
|---|---|---|---|---|---|---|---|
| All events | 500000.00 | 500000.00 | 500000.00 | 500000.00 | 500000.00 | 500000.00 | 500000.00 |
| $e^+e^-/\mu^+\mu^-$ | 61146.00 | 61305.00 | 60642.00 | 60745.00 | 61431.00 | 61127.00 | 61079.00 |
| $p_{\rm T}^{lead} > 25$ GeV | 54713.00 | 52977.00 | 54677.00 | 55353.00 | 56610.00 | 56750.00 | 56972.00 |
| $p_{\rm T}^{sub-lead} > 20$ GeV | 36150.00 | 33419.00 | 37240.00 | 38119.00 | 40412.00 | 41632.00 | 42144.00 |
| $m_{ll} > 15$ | 34112.00 | 31488.00 | 35250.00 | 36269.00 | 38541.00 | 39867.00 | 40287.00 |
| $\lvert m_{ll} - m_z\rvert > 15$ | 24916.00 | 23438.00 | 25648.00 | 26186.00 | 26538.00 | 27021.00 | 26665.00 |
| $N_{jet} = 0$ | 7433.00 | 6955.00 | 7443.00 | 7447.00 | 7158.00 | 7051.00 | 6930.00 |
| $E_{\rm T}^{\rm miss} > 45$ GeV | 3603.00 | 2464.00 | 3500.00 | 3448.00 | 3544.00 | 3612.00 | 3570.00 |
| Efficiency | 0.007206 | 0.004928 | 0.007 | 0.006896 | 0.007088 | 0.007224 | 0.00714 |

**Table B.4:** *Cutflow of the events survived the cuts for the selection of two OS and same-flavour leptons (ee or $\mu\mu$) and the efficiency with luminosity of 20.3 fb$^{-1}$. The BSM signal is the heavy neutrino model with $m_{N_i} > m_S$ according to the ATLAS simulation.*

| | $\chi^2$ | | $\chi^2/ndf$ | | | | N. signal | Significance |
|---|---|---|---|---|---|---|---|---|
| | SM background | SM+BSM | SM Background | SM+BSM | SM Background | SM+BSM | | |
| $m_S = 130$ GeV | 14.665 | 14.080 | 1.629 | 1.760 | 0.101 | 0.080 | 61±52 | 1.407 |
| $m_S = 135$ GeV | 14.665 | 14.243 | 1.629 | 1.780 | 0.101 | 0.076 | 51±50 | 1.435 |
| $m_S = 140$ GeV | 14.665 | 14.115 | 1.629 | 1.764 | 0.101 | 0.079 | 56±51 | 1.413 |
| $m_S = 145$ GeV | 14.665 | 14.114 | 1.629 | 1.764 | 0.101 | 0.079 | 57±51 | 1.413 |
| $m_S = 150$ GeV | 14.665 | 13.935 | 1.629 | 1.742 | 0.101 | 0.083 | 72±55 | 1.382 |
| $m_S = 155$ GeV | 14.665 | 13.992 | 1.629 | 1.749 | 0.101 | 0.082 | 74±56 | 1.392 |
| $m_S = 160$ GeV | 14.665 | 13.729 | 1.629 | 1.716 | 0.101 | 0.089 | 88±58 | 1.346 |

**Table B.5:** *$\chi^2$ values, p-value, yield signal after the fitting and the significance for the SM background and the SM+BSM of ($e\mu$) events. The BSM signal is the heavy neutrino model with $m_{N_i} > m_S$ ($pp \to H \to Sh$); for the ATLAS data with luminosity of 20.3 fb$^{-1}$ [86].*

| | $\chi^2$ | | $\chi^2/ndf$ | | p-value | | N. signal | Significance |
|---|---|---|---|---|---|---|---|---|
| | SM background | SM+BSM | SM Background | SM+BSM | SM Background | SM+BSM | | |
| $m_S = 130$ GeV | 18.313 | 10.818 | 3.052 | 2.164 | 0.005 | 0.055 | 93±21 | 1.597 |
| $m_S = 135$ GeV | 18.313 | 10.591 | 3.052 | 2.118 | 0.005 | 0.060 | 94±21 | 1.554 |
| $m_S = 140$ GeV | 18.313 | 10.587 | 3.052 | 2.117 | 0.005 | 0.060 | 94±21 | 1.553 |
| $m_S = 145$ GeV | 18.313 | 10.418 | 3.052 | 2.084 | 0.005 | 0.064 | 95±21 | 1.520 |
| $m_S = 150$ GeV | 18.313 | 10.230 | 3.052 | 2.046 | 0.005 | 0.069 | 102±22 | 1.483 |
| $m_S = 155$ GeV | 18.313 | 10.245 | 3.052 | 2.049 | 0.005 | 0.069 | 104±22 | 1.486 |
| $m_S = 160$ GeV | 18.313 | 10.220 | 3.052 | 2.044 | 0.005 | 0.069 | 108±23 | 1.481 |

**Table B.6:** *$\chi^2$ value, p-value, yield signal after the fitting and the significance for the SM background and the SM+BSM of $(ee/\mu\mu)$ events.The BSM signal is the heavy neutrino model with $m_{N_i} > m_S$ ($pp \to H \to Sh$); for the ATLAS data with luminosity of 20.2 fb$^{-1}$ [86].*

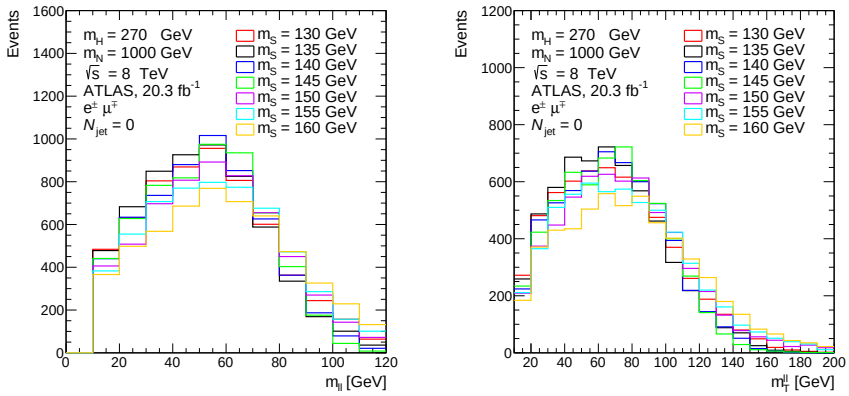


(a) (b)

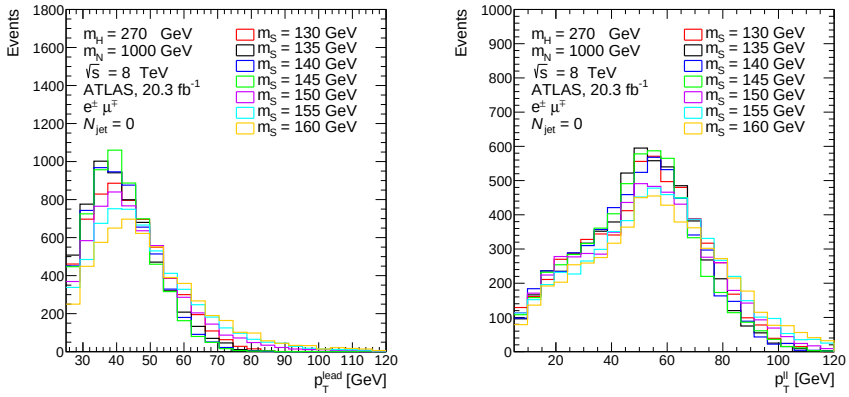


(c) (d)

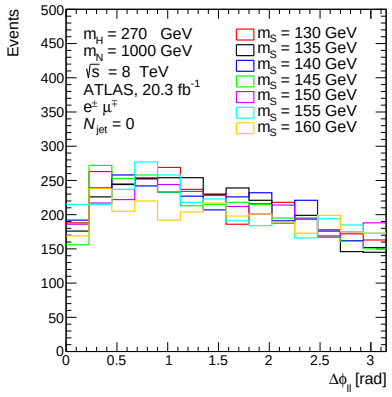


(e)

**Figure B.2:** *Kinematic distribution of (a) the di-lepton invariant mass, (b) the transverse mass of the di-lepton system, (c) the $p_T$ of the leading lepton, (d) the $p_T$ of the di-lepton system and (e) the azimuthal angle of two leptons; in events with an OS and different-flavour leptons (e or $\mu$) and zero jet with the ATLAS detector simulation. The BSM signal is the heavy neutrino signal with $m_{N_i} > m_S$.*

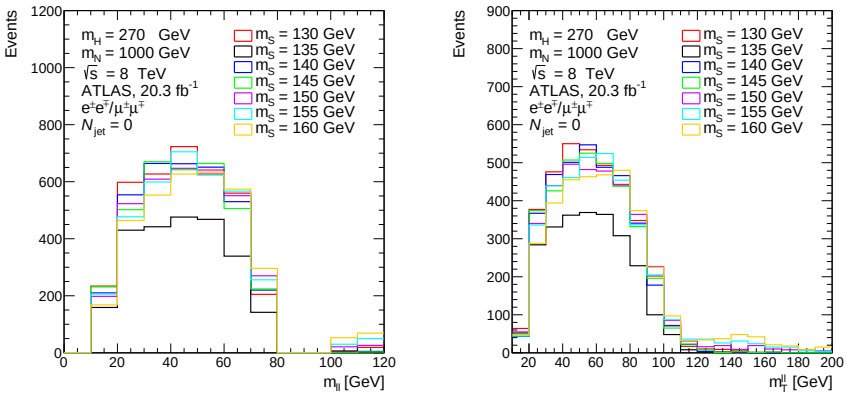


(a) (b)

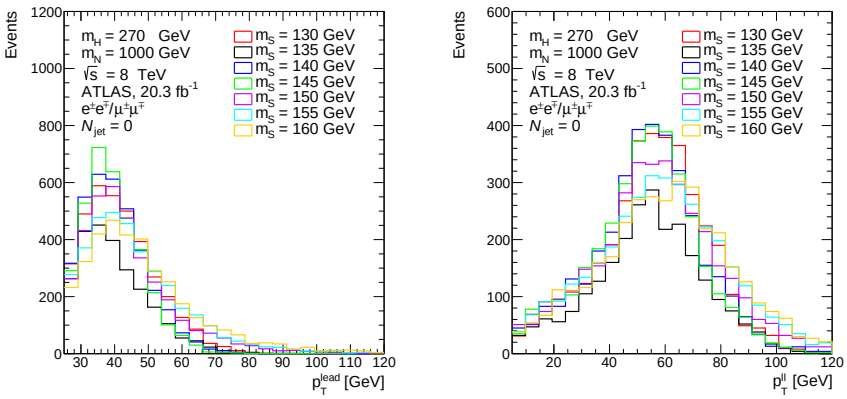


(c) (d)

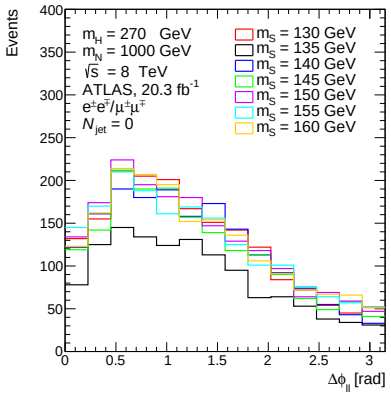


(e)

**Figure B.3:** *Kinematic distribution of (a) the di-lepton invariant mass, (b) the transverse mass of the di-lepton system, (c) the $p_T$ of the leading lepton, (d) the $p_T$ of the di-lepton system and (e) the azimuthal angle of two leptons; in events with an OS and same-flavour leptons (ee or $\mu\mu$) and zero jet with the ATLAS detector simulation. The BSM signal is the heavy neutrino signal with $m_{N_i} > m_S$.*

## B.3 ATLAS, 20.3 fb$^{-1}$ with $e^{\pm}\mu^{\mp}$ and $N_{\rm jet} = 1$

| | $m_S = 130$ GeV | $m_S = 135$ GeV | $m_S = 140$ GeV | $m_S = 145$ GeV | $m_S = 150$ GeV | $m_S = 155$ GeV | $m_S = 160$ GeV |
|---|---|---|---|---|---|---|---|
| All events | 500000.00 | 500000.00 | 500000.00 | 500000.00 | 500000.00 | 500000.00 | 500000.00 |
| $e^{\pm}\mu^{\pm}$ | 44206.00 | 48808.00 | 42719.00 | 42443.00 | 42667.00 | 42203.00 | 41917.00 |
| $p_{\rm T}^{\rm lead} > 25$ GeV | 39486.00 | 41945.00 | 38511.00 | 38380.00 | 39204.00 | 39024.00 | 38898.00 |
| $p_{\rm T}^{\rm sub\text{-}lead} > 25$ GeV | 25284.00 | 25161.00 | 25326.00 | 25709.00 | 27258.00 | 27645.00 | 28120.00 |
| $m_{ll} > 10$ | 24573.00 | 24385.00 | 24582.00 | 24998.00 | 26589.00 | 26968.00 | 27491.00 |
| $N_{jet} = 1$ | 8841.00 | 8604.00 | 8867.00 | 8974.00 | 9512.00 | 9502.00 | 9883.00 |
| $E_{\rm T}^{\rm miss} > 20$ GeV | 7785.00 | 7143.00 | 7795.00 | 7873.00 | 8340.00 | 8382.00 | 8742.00 |
| Efficiency | 0.01557 | 0.014286 | 0.01559 | 0.015746 | 0.01668 | 0.016764 | 0.017484 |

**Table B.7:** *Cutflow of the events survived the cuts for the selection of two leptons (e or $\mu$) plus exactly one jet and the efficiency with luminosity of 20.3 fb$^{-1}$. The BSM signal is the heavy neutrino model with $m_{N_i} > m_S$ according to ATLAS simulation.*

| | $\chi^2$ | | $\chi^2/ndf$ | | p-value | | N. signal | Significance |
|---|---|---|---|---|---|---|---|---|
| | SM background | SM+BSM | SM Background | SM+BSM | SM Background | SM+BSM | | |
| $m_S = 130$ GeV | 12.965 | 12.959 | 1.441 | 1.620 | 0.164 | 0.113 | 15±42 | 1.209 |
| $m_S = 135$ GeV | 12.965 | 12.943 | 1.441 | 1.618 | 0.164 | 0.114 | 16±40 | 1.206 |
| $m_S = 140$ GeV | 12.965 | 12.949 | 1.441 | 1.619 | 0.164 | 0.114 | 16±41 | 1.208 |
| $m_S = 145$ GeV | 12.965 | 12.961 | 1.441 | 1.620 | 0.164 | 0.113 | 15±41 | 1.210 |
| $m_S = 150$ GeV | 12.965 | 12.999 | 1.441 | 1.625 | 0.164 | 0.112 | 10±49 | 1.216 |
| $m_S = 155$ GeV | 12.965 | 12.998 | 1.441 | 1.625 | 0.164 | 0.112 | 6±82 | 1.216 |
| $m_S = 160$ GeV | 12.965 | 13.003 | 1.441 | 1.625 | 0.164 | 0.112 | 7±76 | 1.217 |

**Table B.8:** *$\chi^2$ values, p-value, yield signal after the fitting and the significance for the SM background and the SM+BSM for ($e^{\pm}\mu^{\mp}$) with 1jet. The BSM signal is the heavy neutrino model with $m_{N_i} > m_S$ ($pp \to H \to Sh$); for the ATLAS data with luminosity of 20.3 fb$^{-1}$.*

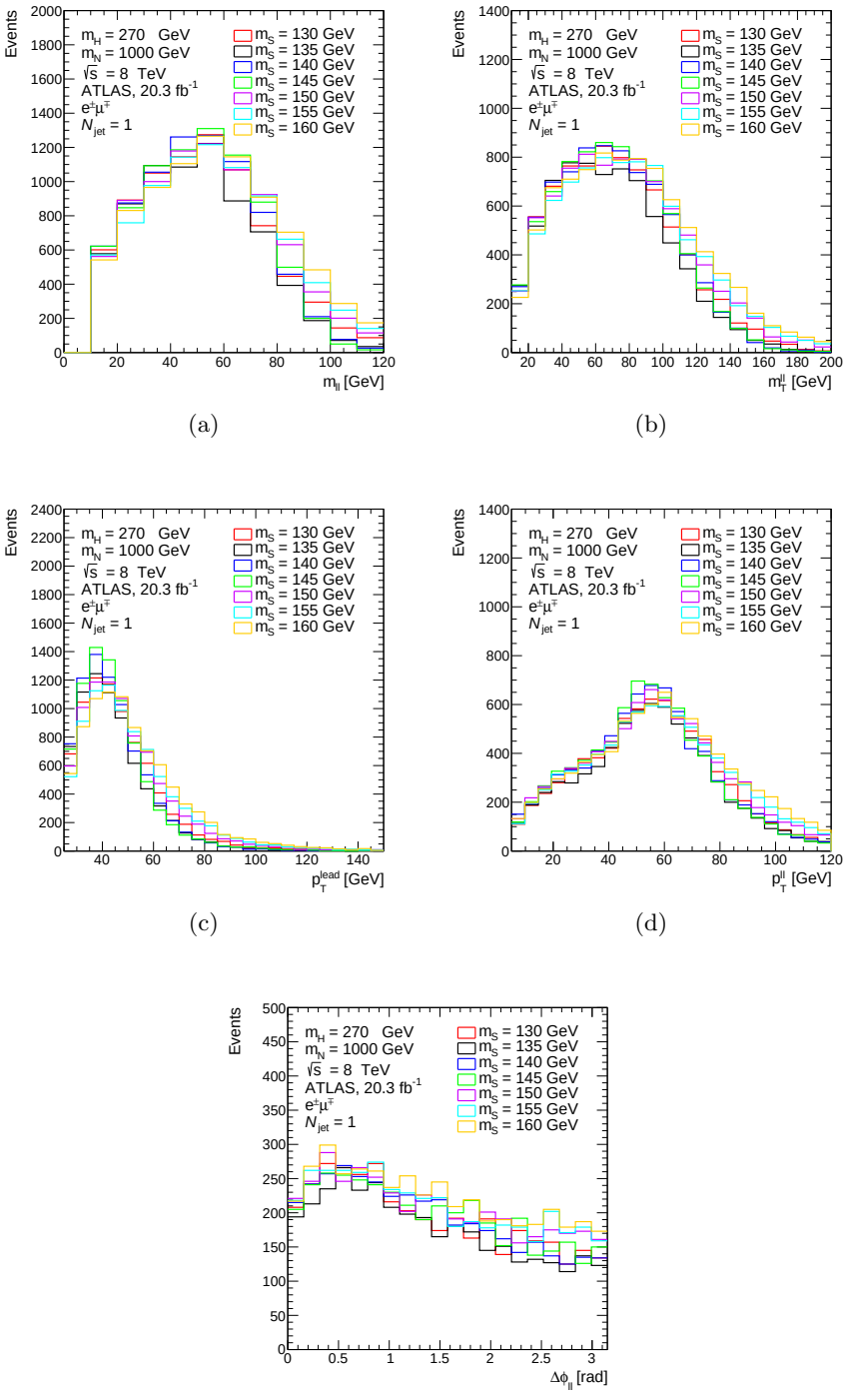


**Figure B.4:** *Kinematic distribution of (a) the di-lepton invariant mass, (b) the transverse mass of the di-lepton system, (c) the $p_T$ of the leading lepton, (d) the $p_T$ of the di-lepton system and (e) the azimuthal angle of two leptons; in events with an OS leptons ($e$ or $\mu$) and exactly one jet with the ATLAS detector simulation. The BSM signal is the heavy neutrino signal with $m_{N_i} > m_S$.*

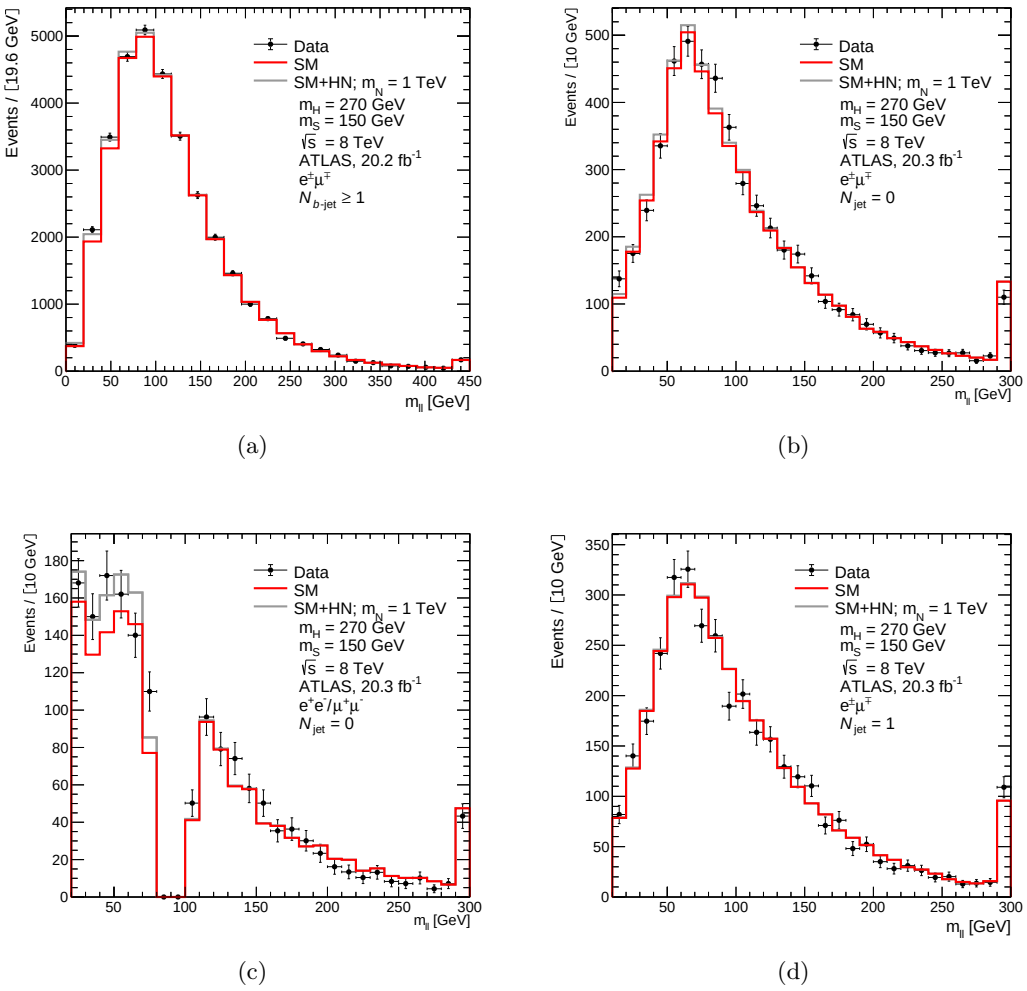


**Figure B.5:** *Distributions of the ATLAS data and SM background compared to the BSM signal (HN model with $m_{N_i} > m_S$) for the di-lepton invariant mass. In (a) events are required to have two opposite-charge leptons ($e$, $\mu$) with at least one b-tagged jet [85]. For (b) events are required to have two opposite-charge leptons with different-flavour ($e\mu$) and (c) with same-flavour ($ee/\mu\mu$), where both analysis require zero jets [86]. In case of (d) events are required to have two opposite-charge leptons ($e$, $\mu$) with exactly one jet. The data used here is from pp collision collected by the ATLAS experiment at $\sqrt{s} = 8$ TeV with luminosity of 20.3 fb$^{-1}$ for (b), (c) and (d), and 20.2 fb$^{-1}$ for (a).*

## B.4 CMS, 19.4 fb$^{-1}$ with $e^+e^-/\mu^+\mu^-/e^\pm\mu^\mp$, $N_{\rm jet}=1$ and $N_{\rm jet}=0$

| | $m_S=130$ GeV | $m_S=135$ GeV | $m_S=140$ GeV | $m_S=145$ GeV | $m_S=150$ GeV | $m_S=155$ GeV | $m_S=160$ GeV |
|---|---|---|---|---|---|---|---|
| All events | 500000.00 | 500000.00 | 500000.00 | 500000.00 | 500000.00 | 500000.00 | 500000.00 |
| 2 lepton | 102649.00 | 112413.00 | 100253.00 | 99096.00 | 100225.00 | 99390.00 | 99099.00 |
| $p_{\rm T}^{\rm lead}$/sub-lead $>20$ GeV | 62005.00 | 62093.00 | 62541.00 | 62961.00 | 66655.00 | 67919.00 | 68888.00 |
| $m_{ll}>12$ GeV | 59592.00 | 59461.00 | 60163.00 | 60753.00 | 64505.00 | 65782.00 | 66857.00 |
| $e^+e^-/\mu^+\mu^-/e^\pm\mu^\pm$ | 38900.00 | 38550.00 | 38575.00 | 38724.00 | 41560.00 | 42673.00 | 43197.00 |
| $E_{\rm T}^{\rm miss}>20$ GeV | 9654.00 | 10661.00 | 9346.00 | 9314.00 | 9383.00 | 9103.00 | 8921.00 |
| $N_{jet}=0$ | 8675.00 | 9203.00 | 8393.00 | 8414.00 | 8437.00 | 8217.00 | 8048.00 |
| Efficiency | 0.01735 | 0.018406 | 0.016786 | 0.016828 | 0.016874 | 0.016434 | 0.016096 |

**Table B.9:** *Cutflow of the events survived the cuts for the selection of two OS leptons ($e^+e^-/\mu^+\mu^-/e^\pm\mu^\pm$) with zero jet and the efficiency with luminosity of 19.4 fb$^{-1}$. The BSM signal is the heavy neutrino model with $m_{N_i}>m_S$ according to CMS simulation.*

| | $m_S=130$ GeV | $m_S=135$ GeV | $m_S=140$ GeV | $m_S=145$ GeV | $m_S=150$ GeV | $m_S=155$ GeV | $m_S=160$ GeV |
|---|---|---|---|---|---|---|---|
| All events | 500000.00 | 500000.00 | 500000.00 | 500000.00 | 500000.00 | 500000.00 | 500000.00 |
| 2 lepton | 102649.00 | 112413.00 | 100253.00 | 99096.00 | 100225.00 | 99390.00 | 99099.00 |
| $p_{\rm T}^{\rm lead}$/sub-lead $>20$ GeV | 62005.00 | 62093.00 | 62541.00 | 62961.00 | 66655.00 | 67919.00 | 68888.00 |
| $m_{ll}>12$ GeV | 59592.00 | 59461.00 | 60163.00 | 60753.00 | 64505.00 | 65782.00 | 66857.00 |
| $e^+e^-/\mu^+\mu^-/e^\pm\mu^\mp$ | 38900.00 | 38550.00 | 38575.00 | 38724.00 | 41560.00 | 42673.00 | 43197.00 |
| $E_{\rm T}^{\rm miss}>20$ GeV | 14180.00 | 13904.00 | 14337.00 | 14319.00 | 15029.00 | 15454.00 | 15541.00 |
| $N_{jet}=1$ | 12576.00 | 11564.00 | 12719.00 | 12639.00 | 13346.00 | 13728.00 | 13733.00 |
| Efficiency | 0.025152 | 0.023128 | 0.025438 | 0.025278 | 0.026692 | 0.027456 | 0.027466 |

**Table B.10:** *Cutflow of the events survived the cuts for the selection of two OS leptons ($e^+e^-/\mu^+\mu^-/e^\pm\mu^\pm$) with one jet and the efficiency with luminosity of 19.4 fb$^{-1}$. The BSM signal is the heavy neutrino model with $m_{N_i}>m_S$ according to CMS simulation.*

| | $\chi^2$ | | $\chi^2/ndf$ | | p-value | | N. signal | Significance |
|---|---|---|---|---|---|---|---|---|
| | SM background | SM+BSM | SM Background | SM+BSM | SM Background | SM+BSM | | |
| $m_S=130$ GeV | 18.220 | 14.163 | 1.656 | 1.416 | 0.077 | 0.166 | 155±61 | 0.971 |
| $m_S=135$ GeV | 18.220 | 14.024 | 1.656 | 1.402 | 0.077 | 0.172 | 153±59 | 0.947 |
| $m_S=140$ GeV | 18.220 | 13.785 | 1.656 | 1.374 | 0.077 | 0.183 | 158±60 | 0.904 |
| $m_S=145$ GeV | 18.220 | 14.076 | 1.656 | 1.408 | 0.077 | 0.170 | 154±60 | 0.956 |
| $m_S=150$ GeV | 18.220 | 13.753 | 1.656 | 1.375 | 0.077 | 0.185 | 171±64 | 0.898 |
| $m_S=155$ GeV | 18.220 | 13.778 | 1.656 | 1.378 | 0.077 | 0.183 | 175±66 | 0.903 |
| $m_S=160$ GeV | 18.220 | 13.619 | 1.656 | 1.362 | 0.077 | 0.191 | 182±68 | 0.874 |

**Table B.11:** *$\chi^2$ values, p-value, signal yield after the fitting and the significance of the SM background and the SM+BSM for two OS leptons ($e^+e^-/\mu^+\mu^-/e^\pm\mu^\pm$) with zero jet selection. The BSM signal is the heavy neutrino model with $m_{N_i}>m_S$ ($pp\to H\to Sh$); for the CMS data with luminosity of 19.4 fb$^{-1}$ [88].*

| | $\chi^2$ | | $\chi^2/ndf$ | | p-value | | N. signal | Significance |
|---|---|---|---|---|---|---|---|---|
| | SM background | SM+BSM | SM Background | SM+BSM | SM Background | SM+BSM | | |
| $m_S = 130$ GeV | 14.695 | 13.435 | 1.336 | 1.344 | 0.197 | 0.200 | 70±47 | 0.840 |
| $m_S = 135$ GeV | 14.695 | 13.609 | 1.336 | 1.361 | 0.197 | 0.192 | 64±45 | 0.872 |
| $m_S = 140$ GeV | 14.695 | 13.377 | 1.336 | 1.338 | 0.197 | 0.203 | 70±46 | 0.830 |
| $m_S = 145$ GeV | 14.695 | 13.189 | 1.336 | 1.319 | 0.197 | 0.213 | 75±46 | 0.795 |
| $m_S = 150$ GeV | 14.695 | 12.861 | 1.336 | 1.286 | 0.197 | 0.232 | 88±49 | 0.734 |
| $m_S = 155$ GeV | 14.695 | 12.832 | 1.336 | 1.283 | 0.197 | 0.233 | 91±51 | 0.728 |
| $m_S = 160$ GeV | 14.695 | 12.510 | 1.336 | 1.251 | 0.197 | 0.252 | 101±52 | 0.667 |

**Table B.12:** *$\chi^2$ values, p-value, signal yield after the fitting and the significance of the SM background and the SM+BSM for two OS leptons ($e^+e^-/\mu^+\mu^-/e^\pm\mu^\pm$) with one jet selection. The BSM signal is the heavy neutrino model with $m_{N_i} > m_S$ ($pp \to H \to Sh$); for the CMS data with luminosity of 19.4 fb$^{-1}$ [88].*

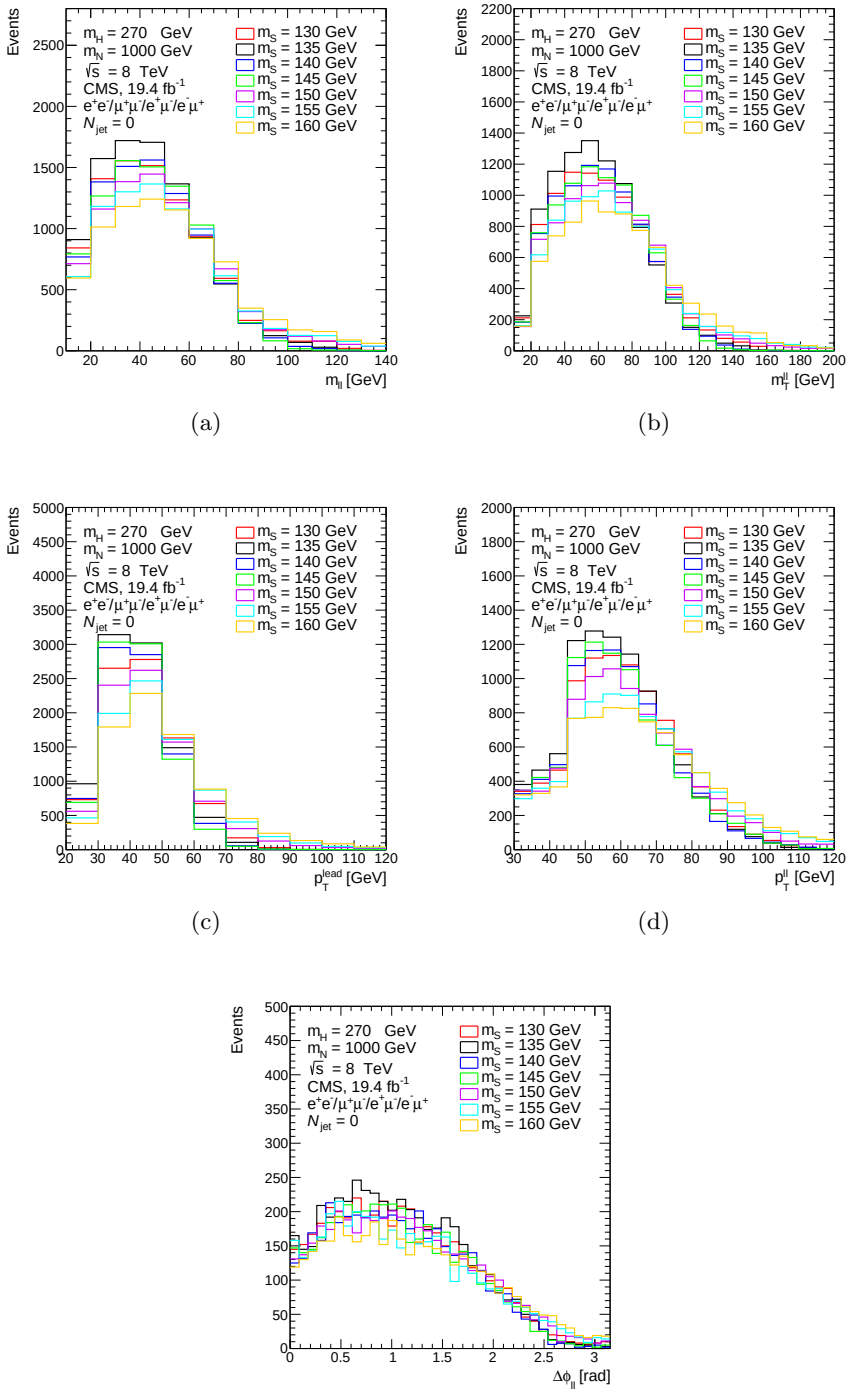


(a) (b)

(c) (d)

(e)

**Figure B.6:** *Kinematic distribution of (a) the di-lepton invariant mass, (b) the transverse mass of the di-lepton system, (c) the $p_T$ of the leading lepton, (d) the $p_T$ of the di-lepton system and (e) the azimuthal angle of two leptons; in events with an OS leptons ($e^+e^-/\mu^+\mu^-/e^\pm\mu^\pm$) and zero jet with the CMS detector simulation. The BSM signal is the heavy neutrino signal with $m_{N_i} > m_S$.*

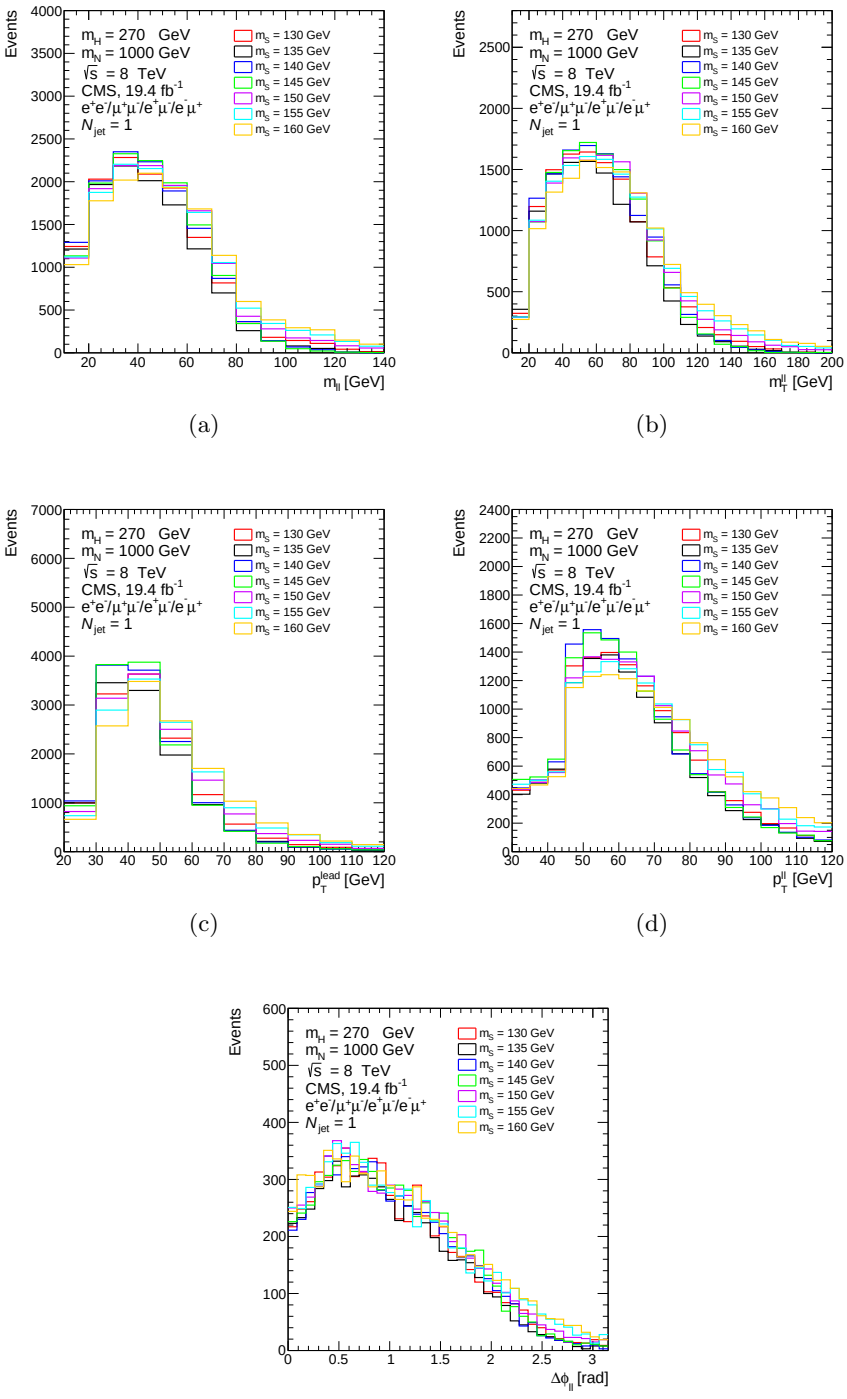


**Figure B.7:** *Kinematic distribution of (a) the di-lepton invariant mass, (b) the transverse mass of the di-lepton system, (c) the $p_T$ of the leading lepton, (d) the $p_T$ of the di-lepton system and (e) the azimuthal angle of two leptons; in events with an OS leptons ($e^+e^-/\mu^+\mu^-/e^\pm\mu^\pm$) and one jet with the CMS detector simulation. The BSM signal is the heavy neutrino signal with $m_{N_i} > m_S$.*

## B.5 CMS, 5.3 fb$^{-1}$ with $e^+e^-/\mu^+\mu^+/e^\pm\mu^\mp$, $N_{\text{jet}} \geq 2$ and $N_{b-\text{jet}} \geq 2$

| | $m_S = 130$ GeV | $m_S = 135$ GeV | $m_S = 140$ GeV | $m_S = 145$ GeV | $m_S = 150$ GeV | $m_S = 155$ GeV | $m_S = 160$ GeV |
|---|---|---|---|---|---|---|---|
| All events | 500000.00 | 500000.00 | 500000.00 | 500000.00 | 500000.00 | 500000.00 | 500000.00 |
| $e^\pm\mu^\mp$ | 44911.00 | 50040.00 | 43457.00 | 42947.00 | 43098.00 | 42937.00 | 42412.00 |
| $p_{\text{T}}^{\text{lead}} > 20$ GeV | 43164.00 | 47322.00 | 41919.00 | 41522.00 | 41860.00 | 41844.00 | 41358.00 |
| $p_{\text{T}}^{\text{sub-lead}} > 20$ GeV | 26483.00 | 27070.00 | 26448.00 | 26655.00 | 28108.00 | 28742.00 | 29073.00 |
| $m_{ll} > 10$ | 23655.00 | 23921.00 | 23504.00 | 23997.00 | 25416.00 | 26045.00 | 26627.00 |
| $N_{b-\text{jet}} \geq 1$ | 915.00 | 826.00 | 890.00 | 958.00 | 1017.00 | 1092.00 | 1144.00 |
| $N_{jet} \geq 2$ | 619.00 | 528.00 | 616.00 | 649.00 | 736.00 | 767.00 | 824.00 |
| Efficiency | 0.001238 | 0.001056 | 0.001232 | 0.001298 | 0.001472 | 0.001534 | 0.001648 |

**Table B.13:** *Cutflow of the events survived the cuts for the selection of two OS leptons ($e$ or $\mu$), at least two jets and two b-tagged jets and the efficiency with luminosity of 5.3 fb$^{-1}$. The BSM signal is the heavy neutrino model with $m_{N_i} > m_S$ according to CMS simulation.*

| | $\chi^2$ | | $\chi^2/ndf$ | | p-value | | N. signal | Significance |
|---|---|---|---|---|---|---|---|---|
| | SM background | SM+BSM | SM Background | SM+BSM | SM Background | SM+BSM | | |
| $m_S = 130$ GeV | 12.859 | 12.906 | 0.756 | 0.807 | 0.746 | 0.680 | 12±82 | -0.467 |
| $m_S = 135$ GeV | 12.859 | 12.891 | 0.756 | 0.806 | 0.746 | 0.681 | 10±90 | -0.470 |
| $m_S = 140$ GeV | 12.859 | 12.892 | 0.756 | 0.806 | 0.746 | 0.681 | 21±64 | -0.469 |
| $m_S = 145$ GeV | 12.859 | 12.883 | 0.756 | 0.805 | 0.746 | 0.681 | 23±64 | -0.471 |
| $m_S = 150$ GeV | 12.859 | 12.781 | 0.756 | 0.799 | 0.746 | 0.689 | 39±70 | -0.492 |
| $m_S = 155$ GeV | 12.859 | 12.921 | 0.756 | 0.808 | 0.746 | 0.678 | 24±71 | -0.463 |
| $m_S = 160$ GeV | 12.859 | 12.969 | 0.756 | 0.675 | 0.746 | 0.675 | 36±75 | -0.454 |

**Table B.14:** *$\chi^2$ values, p-value, signal yield after the fitting and the significance of the SM background and the SM+BSM for ($e^\pm\mu^\mp$) with at least two jets and two b-tagged jets. The BSM signal is the heavy neutrino model with $m_{N_i} > m_S$ ($pp \to H \to Sh$); for the CMS data with luminosity of 5.3 fb$^{-1}$ [89].*

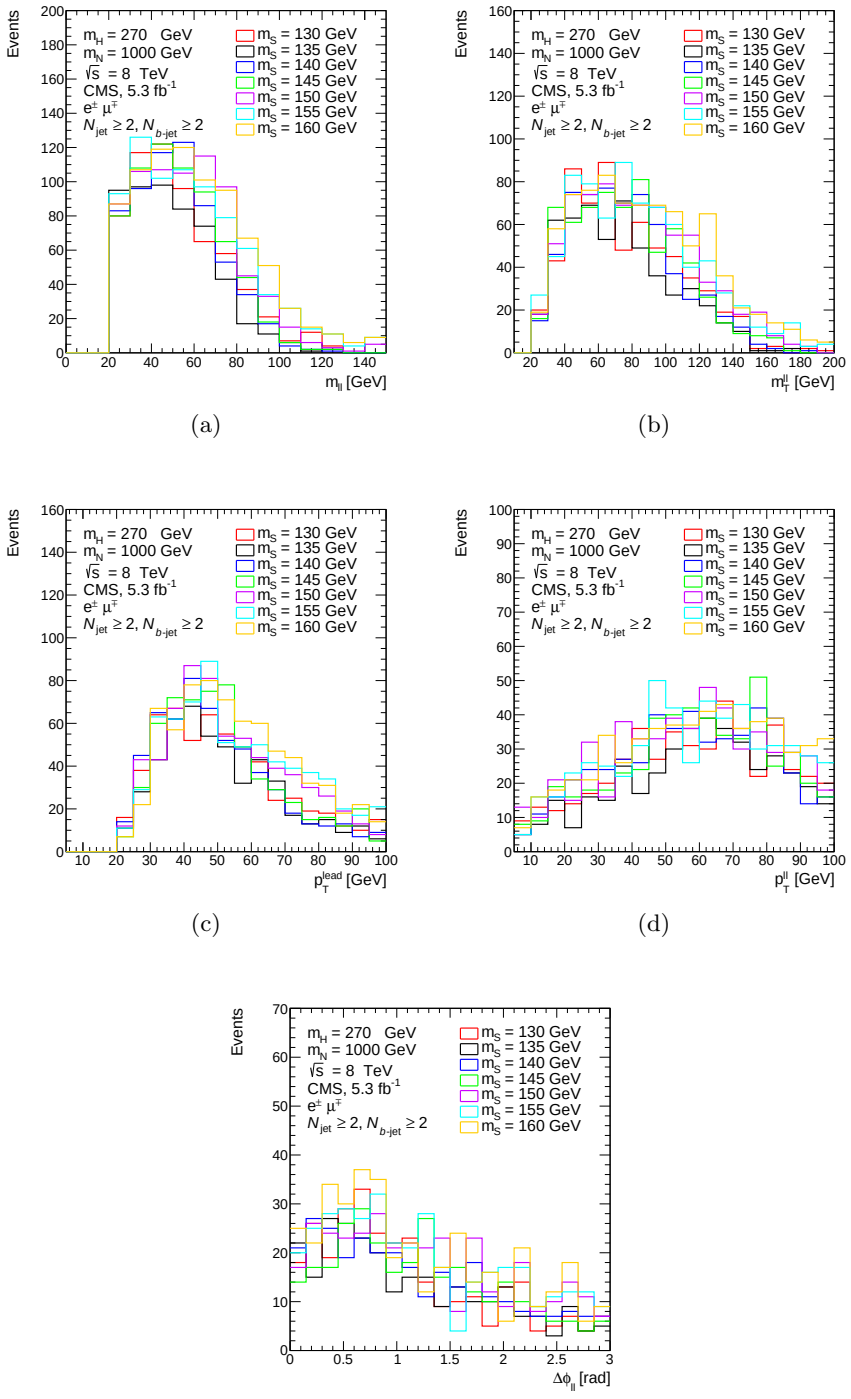


(a) (b)

(c) (d)

(e)

**Figure B.8:** *Kinematic distribution of (a) the di-lepton invariant mass, (b) the transverse mass of the di-lepton system, (c) the $p_T$ of the leading lepton, (d) the $p_T$ of the di-lepton system and (e) the azimuthal angle of two leptons; in events with an OS leptons ($e$ or $\mu$) and at least two jets and two b-tagged jets with the CMS simulation. The BSM signal is the heavy neutrino signal with $m_{N_i} > m_S$.*

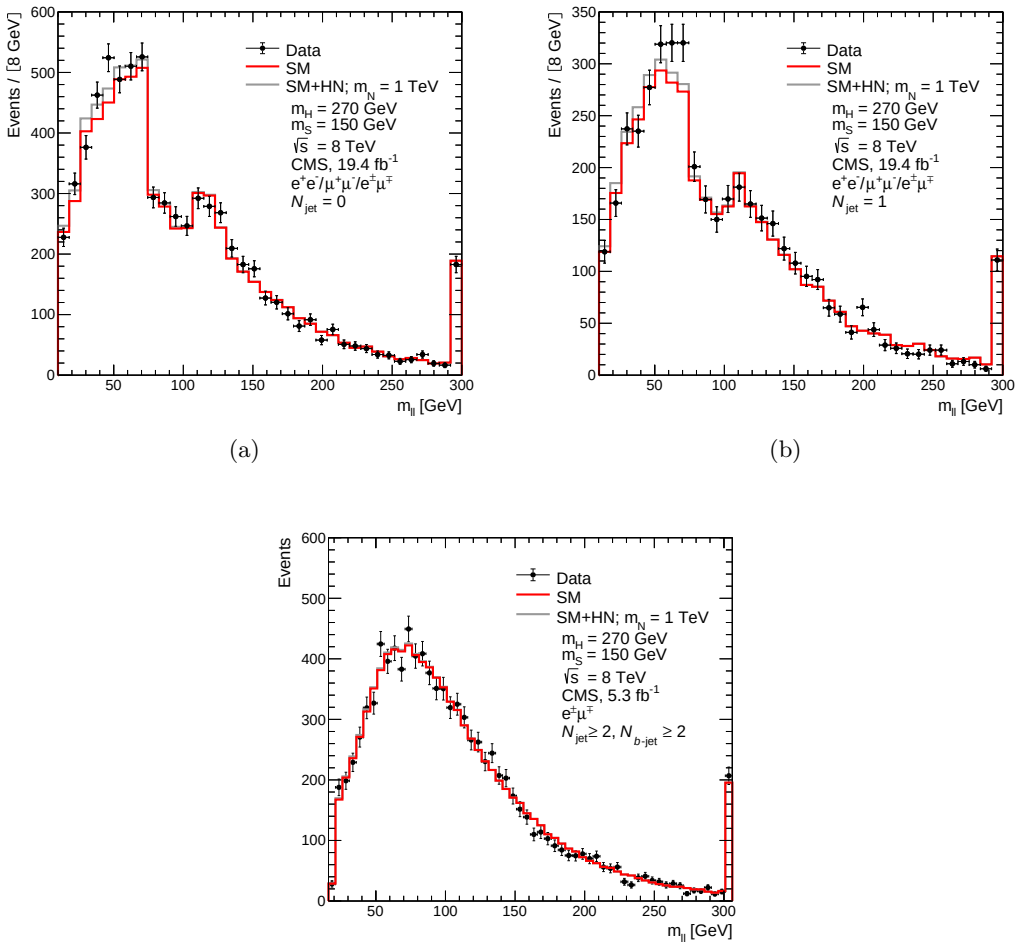


**Figure B.9:** *Distributions of the CMS data and SM background compared to the BSM signal (HN model with $m_{N_i} > m_S$) for the di-lepton invariant mass ($m_{ll}$). Events are required to have two opposite-charge leptons with (a) zero-jet, (b) one-jet [88] and (c) $e\mu$ channel [89] with at least two jets and one b-tagged jet. The data used here, are from the measurement of the $W^+W^-$ and $t\bar{t}$ production cross-section in pp collision at $\sqrt{s} = 8$ TeV with luminosity of 19.4 fb$^{-1}$ and 5.3 fb$^{-1}$ for top and bottom plots, respectively.*

# C

# Heavy Neutrino Signal with $m_{N_i} < m_S$

This appendix follow the same analysis procedure applied in appendix A. But here we use the mass of the heavy neutrino $N_i$ to be on-shell ($m_{N_i} = 100$ GeV).

## C.1 ATLAS, 20.2 fb$^{-1}$ with $e^{\pm}\mu^{\mp}$ and $N_{b-\text{jet}} \geq 1$

| | $m_S = 130$ GeV | $m_S = 135$ GeV | $m_S = 140$ GeV | $m_S = 145$ GeV | $m_S = 150$ GeV | $m_S = 155$ GeV | $m_S = 160$ GeV |
|---|---|---|---|---|---|---|---|
| All events | 500000.00 | 500000.00 | 500000.00 | 500000.00 | 500000.00 | 500000.00 | 500000.00 |
| $e^{\pm}\mu^{\pm}$ events | 21149.00 | 20921.00 | 20751.00 | 20598.00 | 20813.00 | 21438.00 | 22108.00 |
| $N_{b\text{-jet}} \geq 1$ | 506.00 | 509.00 | 532.00 | 539.00 | 502.00 | 531.00 | 517.00 |
| Efficiency | 0.001012 | 0.001018 | 0.001064 | 0.001078 | 0.001004 | 0.001062 | 0.001034 |

**Table C.1:** *Cutflow of the events survived the cuts for the selection of two leptons (e or $\mu$) and the efficiency with luminosity of 20.2 fb$^{-1}$. The BSM signal is the heavy neutrino model with $m_{N_i} < m_S$ according to the ATLAS simulation.*

| | $\chi^2$ | | $\chi^2/ndf$ | | p-value | | N. signal | Significance |
|---|---|---|---|---|---|---|---|---|
| | SM background | SM+BSM | SM Background | SM+BSM | SM Background | SM+BSM | | |
| $m_S = 130$ GeV | 18.122 | 7.300 | 3.624 | 1.825 | 0.003 | 0.121 | 381±93 | 1.171 |
| $m_S = 135$ GeV | 18.122 | 6.032 | 3.624 | 1.508 | 0.003 | 0.197 | 403±94 | 0.853 |
| $m_S = 140$ GeV | 18.122 | 7.349 | 3.624 | 1.837 | 0.003 | 0.119 | 374±91 | 1.182 |
| $m_S = 145$ GeV | 18.122 | 6.965 | 3.624 | 1.741 | 0.003 | 0.138 | 377±91 | 1.090 |
| $m_S = 150$ GeV | 18.122 | 7.462 | 3.624 | 1.866 | 0.003 | 0.113 | 360±88 | 1.209 |
| $m_S = 155$ GeV | 18.122 | 8.775 | 3.624 | 2.194 | 0.003 | 0.067 | 356±93 | 1.499 |
| $m_S = 160$ GeV | 18.122 | 7.940 | 3.624 | 1.985 | 0.003 | 0.094 | 368±92 | 1.318 |

**Table C.2:** *$\chi^2$ values, p-value, signal yield after the fitting and the significance for the SM background and the SM+BSM. The BSM signal is the heavy neutrino model with $m_{N_i} < m_S$ ($pp \to H \to Sh$); for the ATLAS data with luminosity of 20.2 fb$^{-1}$ [85].*

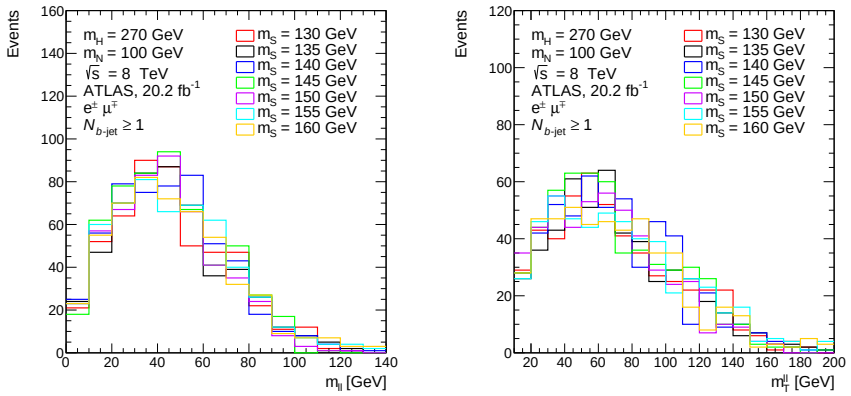


(a) (b)

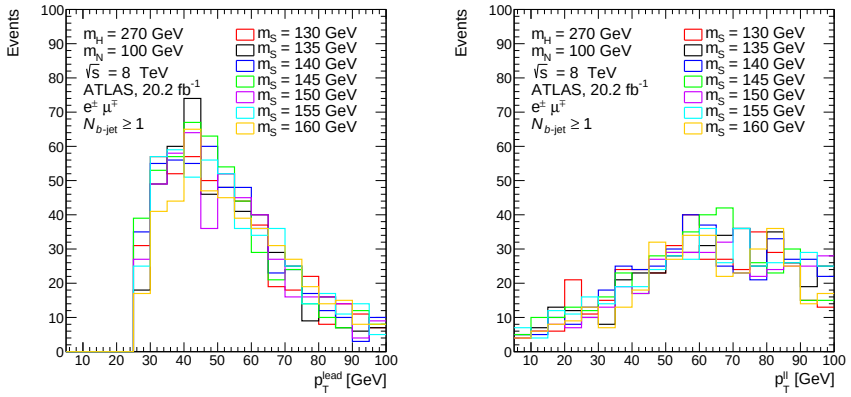


(c) (d)

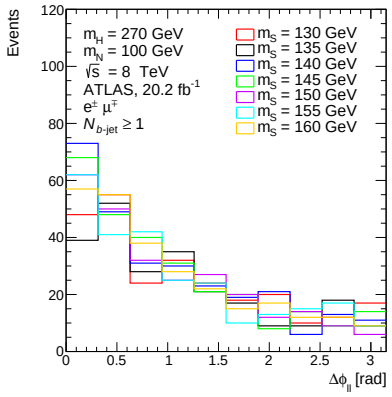


(e)

**Figure C.1:** *Kinematic distribution of (a) the di-lepton invariant mass, (b) the transverse mass of the di-lepton system, (c) the $p_T$ of the leading lepton, (d) the $p_T$ of the di-lepton system and (e) the azimuthal angle of two leptons; in events with an OS leptons ($e$ or $\mu$) and at least one b-tagged jet with the ATLAS detector simulation. The BSM signal is the heavy neutrino signal with $m_{N_i} < m_S$.*

## C.2 ATLAS, 20.3 fb$^{-1}$ with $e^+e^-/\mu^+\mu^-/e^\pm\mu^\mp$ and $N_{\text{jet}} = 0$

| | $m_S = 130$ GeV | $m_S = 135$ GeV | $m_S = 140$ GeV | $m_S = 145$ GeV | $m_S = 150$ GeV | $m_S = 155$ GeV | $m_S = 160$ GeV |
|---|---|---|---|---|---|---|---|
| All events | 500000.00 | 500000.00 | 500000.00 | 500000.00 | 500000.00 | 500000.00 | 500000.00 |
| $e^\pm\mu^\pm$ | 45598.00 | 45629.00 | 45544.00 | 45469.00 | 45447.00 | 45946.00 | 45701.00 |
| $p_{\text{T}}^{\text{lead}}$ GeV | 39785.00 | 39879.00 | 39814.00 | 39688.00 | 39752.00 | 40437.00 | 40569.00 |
| $p_{\text{T}}^{\text{sub-lead}}$ GeV | 23003.00 | 22813.00 | 22629.00 | 22477.00 | 22808.00 | 23322.00 | 23962.00 |
| $m_{\ell\ell} > 10$ GeV | 22231.00 | 22063.00 | 21824.00 | 21674.00 | 22037.00 | 22480.00 | 23187.00 |
| $N_{\text{jet}} = 0$ | 6318.00 | 6475.00 | 6356.00 | 6232.00 | 6521.00 | 6323.00 | 6398.00 |
| $E_{\text{T}}^{\text{miss}}$ GeV | 5458.00 | 5567.00 | 5465.00 | 5344.00 | 5620.00 | 5462.00 | 5549.00 |
| Efficiency | 0.010916 | 0.011134 | 0.01093 | 0.010688 | 0.01124 | 0.010924 | 0.011098 |

**Table C.3:** *Cutflow of the events survived the cuts for the selection of two leptons (e or $\mu$) and the efficiency with luminosity of 20.3 fb$^{-1}$. The BSM signal is the heavy neutrino model with $m_{N_i} < m_S$ according to the ATLAS simulation.*

| | $m_S = 130$ GeV | $m_S = 135$ GeV | $m_S = 140$ GeV | $m_S = 145$ GeV | $m_S = 150$ GeV | $m_S = 155$ GeV | $m_S = 160$ GeV |
|---|---|---|---|---|---|---|---|
| All events | 500000.00 | 500000.00 | 500000.00 | 500000.00 | 500000.00 | 500000.00 | 500000.00 |
| $e^+e^-/\mu^+\mu^-$ | 61044.00 | 60400.00 | 60019.00 | 59689.00 | 60080.00 | 60106.00 | 60743.00 |
| $p_{\text{T}}^{lead} > 25$ GeV | 53185.00 | 52639.00 | 52237.00 | 52063.00 | 52387.00 | 52701.00 | 53600.00 |
| $p_{\text{T}}^{\text{sub-lead}} > 20$ GeV | 31381.00 | 30771.00 | 30115.00 | 29990.00 | 30465.00 | 31088.00 | 32582.00 |
| $m_{\ell\ell} > 15$ GeV | 29217.00 | 28619.00 | 27958.00 | 27816.00 | 28281.00 | 28782.00 | 30213.00 |
| $\lvert m_{\ell\ell} - m_z \rvert > 15$ GeV | 22962.00 | 22635.00 | 22413.00 | 22301.00 | 22656.00 | 22945.00 | 24019.00 |
| $N_{\text{jet}} = 0$ | 6750.00 | 6641.00 | 6648.00 | 6707.00 | 6756.00 | 6602.00 | 6703.00 |
| $E_{\text{T}}^{\text{miss}} > 45$ GeV | 3327.00 | 3290.00 | 3240.00 | 3162.00 | 3333.00 | 3212.00 | 3282.00 |
| Efficiency | 0.006654 | 0.00658 | 0.00648 | 0.006324 | 0.006666 | 0.006424 | 0.006564 |

**Table C.4:** *Cutflow of the events survived the cuts for the selection of two OS and same-flavour leptons (ee or $\mu\mu$) and the efficiency with luminosity of 20.3 fb$^{-1}$. The BSM signal is the heavy neutrino model with $m_{N_i} < m_S$ according to the ATLAS simulation.*

| | $\chi^2$ | | $\chi^2/ndf$ | | p-value | | N. signal | Significance |
|---|---|---|---|---|---|---|---|---|
| | SM background | SM+BSM | SM Background | SM+BSM | SM Background | SM+BSM | | |
| $m_S = 130$ GeV | 14.665 | 13.867 | 1.629 | 1.735 | 0.101 | 0.085 | 65±50 | 1.372 |
| $m_S = 135$ GeV | 14.665 | 13.893 | 1.629 | 1.737 | 0.101 | 0.085 | 65±50 | 1.375 |
| $m_S = 140$ GeV | 14.665 | 14.011 | 1.629 | 1.751 | 0.101 | 0.081 | 60±49 | 1.395 |
| $m_S = 145$ GeV | 14.665 | 14.018 | 1.629 | 1.752 | 0.101 | 0.081 | 58±49 | 1.396 |
| $m_S = 150$ GeV | 14.665 | 13.893 | 1.629 | 1.737 | 0.101 | 0.085 | 62±49 | 1.375 |
| $m_S = 155$ GeV | 14.665 | 13.994 | 1.629 | 1.749 | 0.101 | 0.082 | 62±50 | 1.392 |
| $m_S = 160$ GeV | 14.665 | 13.900 | 1.629 | 1.738 | 0.101 | 0.084 | 66±49 | 1.278 |

**Table C.5:** *$\chi^2$ values, p-value, yield signal after the fitting and the significance for the SM background and the SM+BSM of ($e\mu$) events. The BSM signal is the heavy neutrino model with $m_{N_i} < m_S$ ($pp \to H \to Sh$); for the ATLAS data with luminosity of 20.3 fb$^{-1}$ [86].*

| | $\chi^2$ | | $\chi^2/ndf$ | | p-value | | N. signal | Significance |
|---|---|---|---|---|---|---|---|---|
| | SM background | SM+BSM | SM Background | SM+BSM | SM Background | SM+BSM | | |
| $m_S = 130$ GeV | 18.313 | 10.378 | 3.052 | 2.076 | 0.005 | 0.065 | 96±21 | 1.512 |
| $m_S = 135$ GeV | 18.313 | 10.306 | 3.052 | 2.061 | 0.005 | 0.067 | 95±21 | 1.498 |
| $m_S = 140$ GeV | 18.313 | 10.714 | 3.052 | 2.143 | 0.005 | 0.057 | 92±21 | 1.577 |
| $m_S = 145$ GeV | 18.313 | 10.512 | 3.052 | 2.102 | 0.005 | 0.062 | 92±21 | 1.538 |
| $m_S = 150$ GeV | 18.313 | 10.438 | 3.052 | 2.088 | 0.005 | 0.064 | 94±21 | 1.524 |
| $m_S = 155$ GeV | 18.313 | 10.151 | 3.052 | 2.030 | 0.005 | 0.071 | 97±21 | 1.468 |
| $m_S = 160$ GeV | 18.313 | 10.223 | 3.052 | 2.045 | 0.005 | 0.069 | 100±22 | 1.482 |

**Table C.6:** *$\chi^2$ value, p-value, yield signal after the fitting and the significance for the SM background and the SM+BSM of $(ee/\mu\mu)$ events.The BSM signal is the heavy neutrino model with $m_{N_i} < m_S$ ($pp \to H \to Sh$); for the ATLAS data with luminosity of 20.2 fb$^{-1}$ [86].*

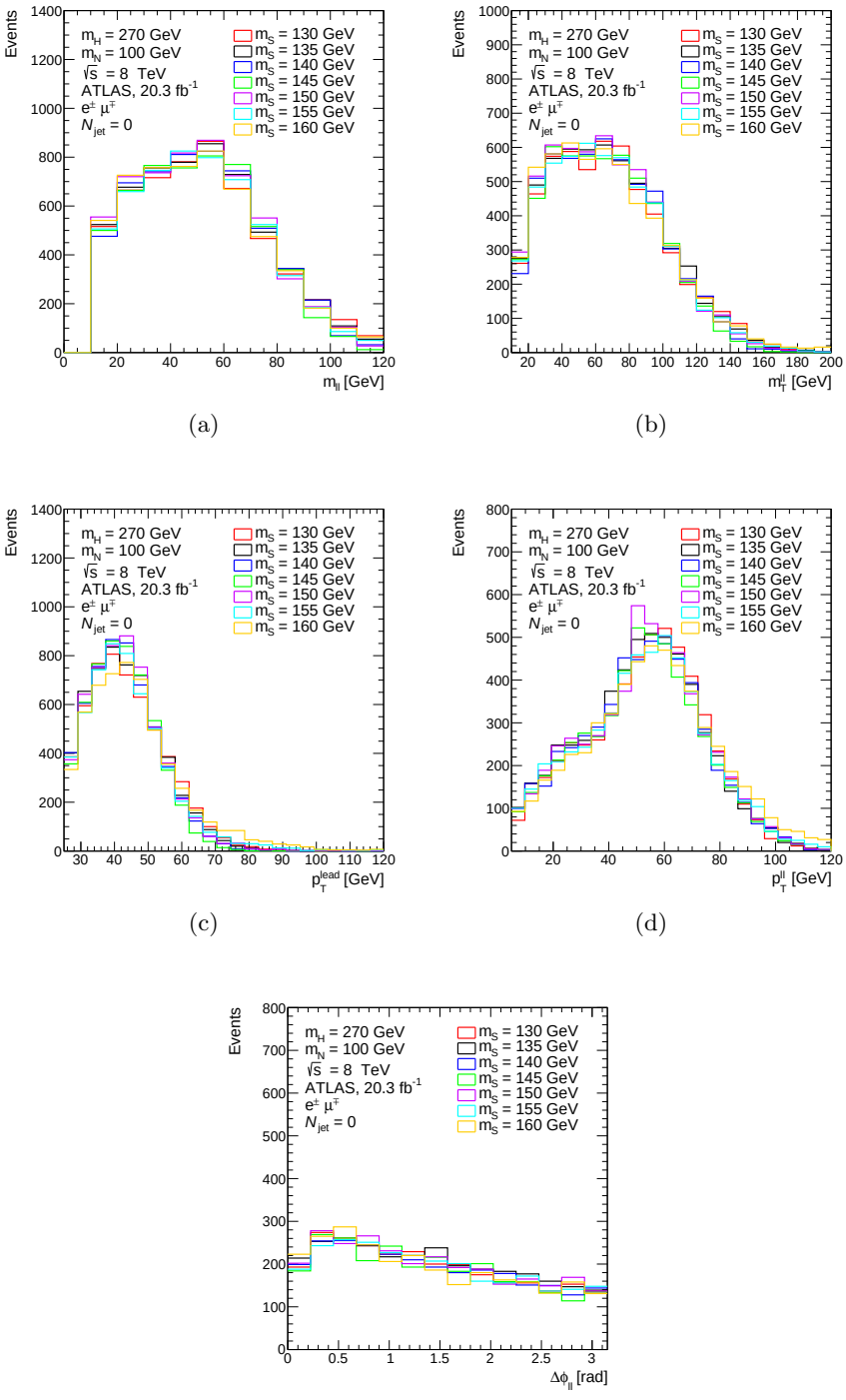


**Figure C.2:** *Kinematic distribution of (a) the di-lepton invariant mass, (b) the transverse mass of the di-lepton system, (c) the $p_T$ of the leading lepton, (d) the $p_T$ of the di-lepton system and (e) the azimuthal angle of two leptons; in events with an OS and different-flavour leptons (e or $\mu$) and zero jet with the ATLAS detector simulation. The BSM signal is the heavy neutrino signal with $m_{N_i} < m_S$.*

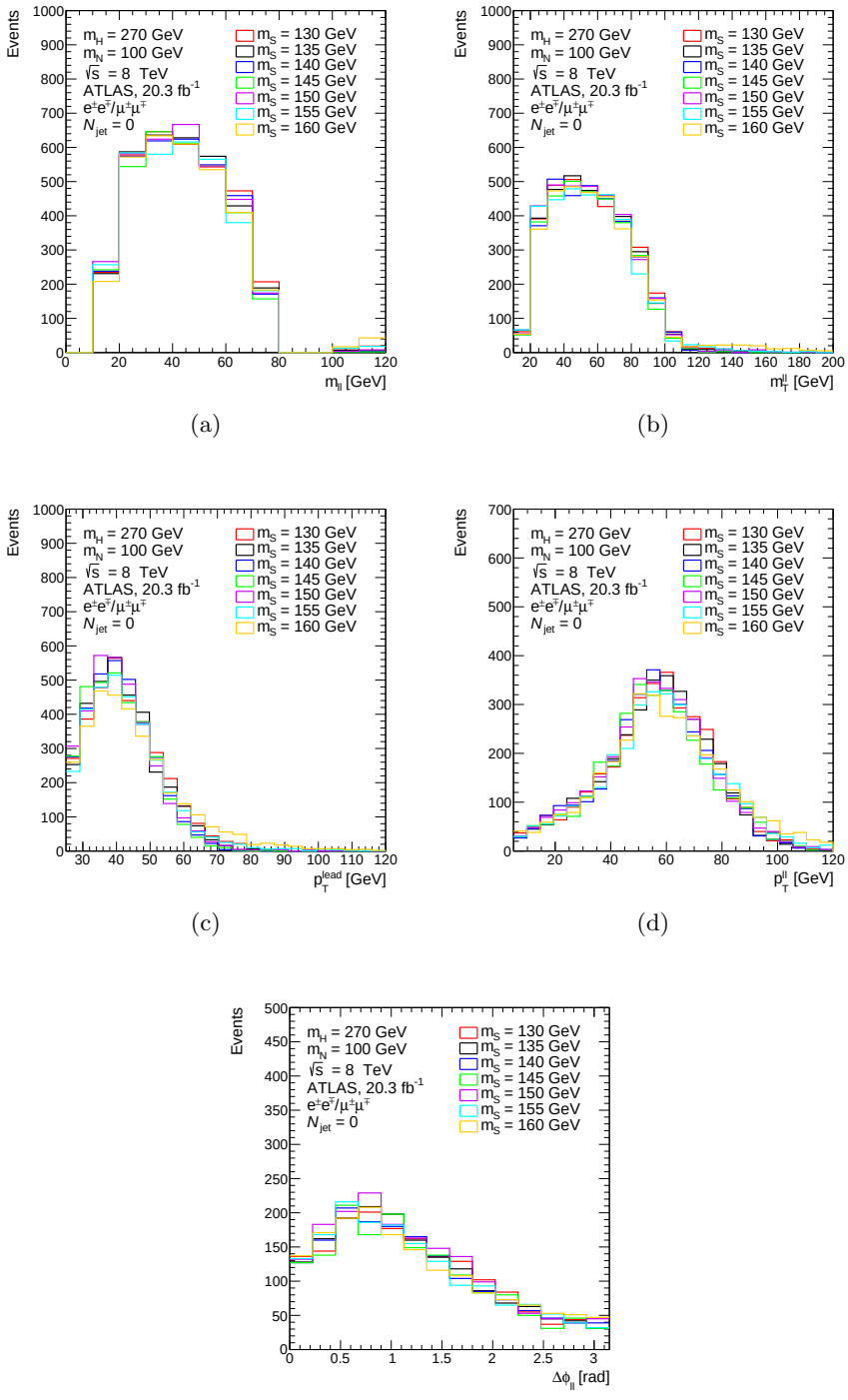


(a) (b)

(c) (d)

(e)

**Figure C.3:** *Kinematic distribution of (a) the di-lepton invariant mass, (b) the transverse mass of the di-lepton system, (c) the $p_T$ of the leading lepton, (d) the $p_T$ of the di-lepton system and (e) the azimuthal angle of two leptons; in events with an OS and same-flavour leptons (ee or $\mu\mu$) and zero jet with the ATLAS detector simulation. The BSM signal is the heavy neutrino signal with $m_{N_i} < m_S$.*

## C.3 ATLAS, 20.3 fb$^{-1}$ with $e^{\pm}\mu^{\mp}$ and $N_{\text{jet}} = 1$

| | $m_S = 130$ GeV | $m_S = 135$ GeV | $m_S = 140$ GeV | $m_S = 145$ GeV | $m_S = 150$ GeV | $m_S = 155$ GeV | $m_S = 160$ GeV |
|---|---|---|---|---|---|---|---|
| All events | 500000.00 | 500000.00 | 500000.00 | 500000.00 | 500000.00 | 500000.00 | 500000.00 |
| $e^{\pm}\mu^{\pm}$ | 45598.00 | 45629.00 | 45544.00 | 45469.00 | 45447.00 | 45946.00 | 45701.00 |
| $p_{\text{T}}^{\text{lead}} > 25$ GeV | 39785.00 | 39879.00 | 39814.00 | 39688.00 | 39752.00 | 40437.00 | 40569.00 |
| $p_{\text{T}}^{\text{sub-lead}} > 20$ GeV | 23003.00 | 22813.00 | 22629.00 | 22477.00 | 22808.00 | 23322.00 | 23962.00 |
| $m_{\ell\ell} > 10$ GeV | 22231.00 | 22063.00 | 21824.00 | 21674.00 | 22037.00 | 22480.00 | 23187.00 |
| $N_{\text{jet}} = 1$ | 7859.00 | 7807.00 | 7810.00 | 7709.00 | 7703.00 | 8020.00 | 8184.00 |
| $E_{\text{T}}^{\text{miss}} > 20$ GeV | 6928.00 | 6825.00 | 6847.00 | 6741.00 | 6738.00 | 7041.00 | 7203.00 |
| Efficiency | 0.013856 | 0.01365 | 0.013694 | 0.013482 | 0.013476 | 0.014082 | 0.014406 |

**Table C.7:** *Cutflow of the events survived the cuts for the selection of two leptons (e or $\mu$) plus exactly one jet and the efficiency with luminosity of 20.3 fb$^{-1}$. The BSM signal is the heavy neutrino model with $m_{N_i} < m_S$ according to ATLAS simulation.*

| | $\chi^2$ | | $\chi^2/ndf$ | | p-value | | N. signal | Significance |
|---|---|---|---|---|---|---|---|---|
| | SM background | SM+BSM | SM Background | SM+BSM | SM Background | SM+BSM | | |
| $m_S = 130$ GeV | 12.965 | 12.915 | 1.441 | 1.614 | 0.164 | 0.115 | 16±39 | 1.201 |
| $m_S = 135$ GeV | 12.965 | 12.915 | 1.441 | 1.614 | 0.164 | 0.115 | 17±39 | 1.201 |
| $m_S = 140$ GeV | 12.965 | 12.913 | 1.441 | 1.614 | 0.164 | 0.115 | 17±39 | 1.201 |
| $m_S = 145$ GeV | 12.965 | 12.917 | 1.441 | 1.615 | 0.164 | 0.115 | 17±38 | 1.202 |
| $m_S = 150$ GeV | 12.965 | 12.908 | 1.441 | 1.614 | 0.164 | 0.115 | 17±39 | 1.200 |
| $m_S = 155$ GeV | 12.965 | 12.932 | 1.441 | 1.616 | 0.164 | 0.114 | 16±39 | 1.204 |
| $m_S = 160$ GeV | 12.965 | 12.934 | 1.441 | 1.617 | 0.164 | 0.114 | 17±40 | 1.205 |

**Table C.8:** *$\chi^2$ values, p-value, signal yield after the fitting and the significance for the SM background and the SM+BSM for events contain two OS leptons ($e^{\pm}\mu^{\mp}$) plus one jet. The BSM signal is the heavy neutrino model with $m_{N_i} < m_S$ ($pp \to H \to Sh$); for the ATLAS data with luminosity of 20.3 fb$^{-1}$.*

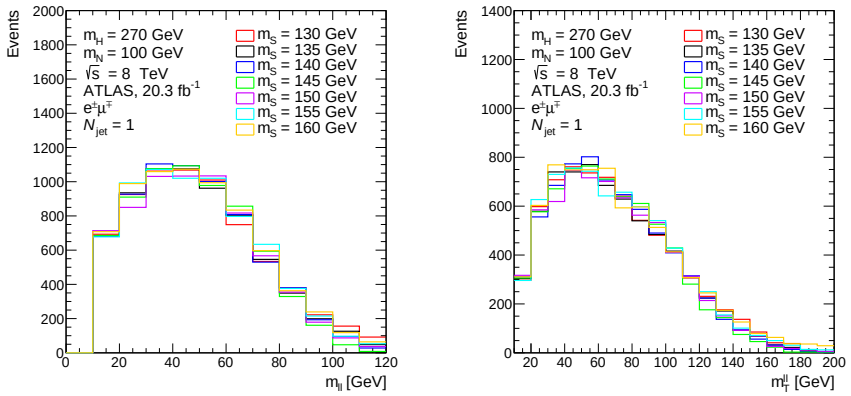


(a) (b)

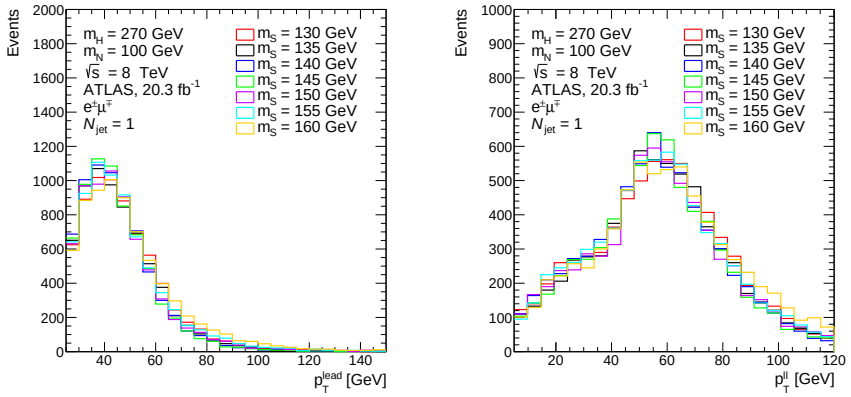


(c) (d)

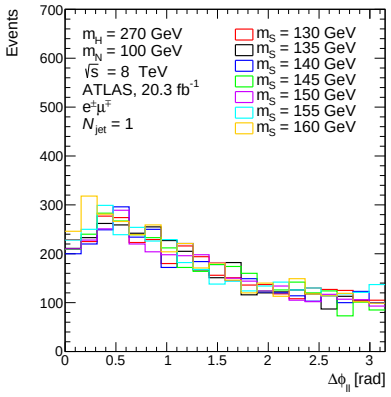


(e)

**Figure C.4:** *Kinematic distribution of (a) the di-lepton invariant mass, (b) the transverse mass of the di-lepton system, (c) the $p_T$ of the leading lepton, (d) the $p_T$ of the di-lepton system and (e) the azimuthal angle of two leptons; in events with an OS leptons ($e$ or $\mu$) and exactly one jet with the ATLAS detector simulation. The BSM signal is the heavy neutrino signal with $m_{N_i} < m_S$.*

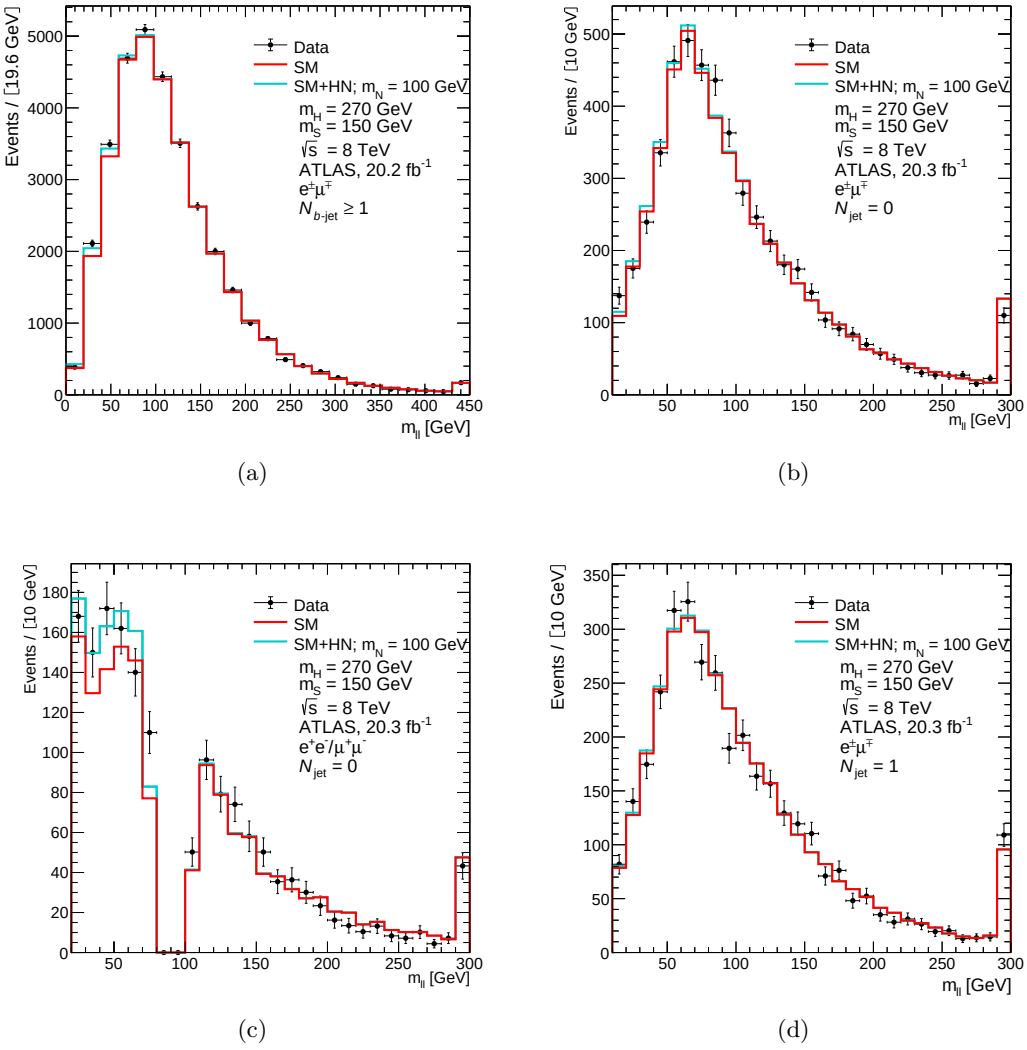


**Figure C.5:** *Distributions of the ATLAS data and SM background compared to the BSM signal (HN model with $m_{N_i} < m_S$) for the di-lepton invariant mass. In (a) events are required to have two opposite-charge leptons ($e$, $\mu$) with at least one b-tagged jet [85]. For (b) events are required to have two opposite-charge leptons with different-flavour ($e\mu$) and (c) with same-flavour ($ee/\mu\mu$), where both analysis require zero jets [86]. In case of (d) events are required to have two opposite-charge leptons ($e$, $\mu$) with exactly one jet. The data used here is from pp collision collected by the ATLAS experiment at $\sqrt{s} = 8$ TeV with luminosity of 20.2 fb$^{-1}$ for (b), (c) and (d), and 20.3 fb$^{-1}$ for (a).*

## C.4 CMS, 19.4 fb$^{-1}$ with $e^+e^-/\mu^+\mu^-/e^\pm\mu^\mp$, $N_{\rm jet}=1$ and $N_{\rm jet}=0$

| | $m_S=130$ GeV | $m_S=135$ GeV | $m_S=140$ GeV | $m_S=145$ GeV | $m_S=150$ GeV | $m_S=155$ GeV | $m_S=160$ GeV |
|---|---|---|---|---|---|---|---|
| All events | 500000.00 | 500000.00 | 500000.00 | 500000.00 | 500000.00 | 500000.00 | 500000.00 |
| 2 lepton | 103501.00 | 102958.00 | 101523.00 | 102232.00 | 102726.00 | 102512.00 | 103268.00 |
| $p_{\rm T}^{\rm lead}$/sub-lead $>20$ GeV | 54681.00 | 53787.00 | 52708.00 | 52787.00 | 53979.00 | 54477.00 | 56637.00 |
| $m_{\ell\ell}>12$ GeV | 52129.00 | 51232.00 | 50193.00 | 50173.00 | 51375.00 | 51815.00 | 53936.00 |
| $e^+e^-/\mu^+\mu^-/e^\pm\mu^\mp$ | 36092.00 | 35624.00 | 34882.00 | 34914.00 | 35927.00 | 36674.00 | 38470.00 |
| $E_{\rm T}^{\rm miss}>20$ GeV | 9160.00 | 9133.00 | 9050.00 | 9146.00 | 9247.00 | 9227.00 | 9562.00 |
| $N_{\rm jet}=0$ | 8272.00 | 8225.00 | 8113.00 | 8178.00 | 8293.00 | 8226.00 | 8525.00 |
| Efficiency | 0.016544 | 0.01645 | 0.016226 | 0.016356 | 0.016586 | 0.016452 | 0.01705 |

**Table C.9:** *Cutflow of the events survived the cuts for the selection of two OS leptons ($e^+e^-/\mu^+\mu^-/e^\pm\mu^\pm$) with zero jet and the efficiency with luminosity of 19.4 fb$^{-1}$. The BSM signal is the heavy neutrino model with $m_{N_i}<m_S$ according to CMS simulation.*

| | $m_S=130$ GeV | $m_S=135$ GeV | $m_S=140$ GeV | $m_S=145$ GeV | $m_S=150$ GeV | $m_S=155$ GeV | $m_S=160$ GeV |
|---|---|---|---|---|---|---|---|
| All events | 500000.00 | 500000.00 | 500000.00 | 500000.00 | 500000.00 | 500000.00 | 500000.00 |
| 2 lepton | 103501.00 | 102958.00 | 101523.00 | 102232.00 | 102726.00 | 102512.00 | 103268.00 |
| $p_{\rm T}^{\rm lead}$/sub-lead $>20$ GeV | 54681.00 | 53787.00 | 52708.00 | 52787.00 | 53979.00 | 54477.00 | 56637.00 |
| $m_{\ell\ell}>12$ GeV | 52129.00 | 51232.00 | 50193.00 | 50173.00 | 51375.00 | 51815.00 | 53936.00 |
| $e^+e^-/\mu^+\mu^-/e^\pm\mu^\mp$ | 36092.00 | 35624.00 | 34882.00 | 34914.00 | 35927.00 | 36674.00 | 38470.00 |
| $E_{\rm T}^{\rm miss}>20$ GeV | 13106.00 | 13037.00 | 12627.00 | 12644.00 | 12957.00 | 13115.00 | 13964.00 |
| $N_{\rm jet}=1$ | 11652.00 | 11523.00 | 11206.00 | 11189.00 | 11443.00 | 11586.00 | 12371.00 |
| Efficiency | 0.023304 | 0.023046 | 0.022412 | 0.022378 | 0.022886 | 0.023172 | 0.024742 |

**Table C.10:** *Cutflow of the events survived the cuts for the selection of two OS leptons ($e^+e^-/\mu^+\mu^-/e^\pm\mu^\pm$) with one jet and the efficiency with luminosity of 19.4 fb$^{-1}$. The BSM signal is the heavy neutrino model with $m_{N_i}<m_S$ according to CMS simulation.*

| | $\chi^2$ | | $\chi^2/ndf$ | | p-value | | N. signal | Significance |
|---|---|---|---|---|---|---|---|---|
| | SM background | SM+BSM | SM Background | SM+BSM | SM Background | SM+BSM | | |
| $m_S=130$ GeV | 18.220 | 14.881 | 1.656 | 1.488 | 0.077 | 0.136 | 142±60 | 1.096 |
| $m_S=135$ GeV | 18.220 | 14.385 | 1.656 | 1.439 | 0.077 | 0.156 | 149±60 | 1.010 |
| $m_S=140$ GeV | 18.220 | 14.643 | 1.656 | 1.464 | 0.077 | 0.146 | 144±60 | 1.055 |
| $m_S=145$ GeV | 18.220 | 14.548 | 1.656 | 1.455 | 0.077 | 0.149 | 144±59 | 1.039 |
| $m_S=150$ GeV | 18.220 | 14.357 | 1.656 | 1.436 | 0.077 | 0.157 | 148±60 | 1.005 |
| $m_S=155$ GeV | 18.220 | 14.650 | 1.656 | 1.465 | 0.077 | 0.145 | 146±60 | 1.057 |
| $m_S=160$ GeV | 18.220 | 14.531 | 1.656 | 1.453 | 0.077 | 0.150 | 153±61 | 1.036 |

**Table C.11:** *$\chi^2$ values, p-value, signal yield after the fitting and the significance of the SM background and the SM+BSM for two OS leptons ($e^+e^-/\mu^+\mu^-/e^\pm\mu^\pm$) with zero jet selection. The BSM signal is the heavy neutrino model with $m_{N_i}<m_S$ ($pp\to H\to Sh$); for the CMS data with luminosity of 19.4 fb$^{-1}$ [88].*

| | $\chi^2$ | | $\chi^2/ndf$ | | p-value | | N. signal | Significance |
|---|---|---|---|---|---|---|---|---|
| | SM background | SM+BSM | SM Background | SM+BSM | SM Background | SM+BSM | | |
| $m_S = 130$ GeV | 14.695 | 14.033 | 1.336 | 1.403 | 0.197 | 0.171 | 52±45 | 0.948 |
| $m_S = 135$ GeV | 14.695 | 14.096 | 1.336 | 1.410 | 0.197 | 0.169 | 49±44 | 0.960 |
| $m_S = 140$ GeV | 14.695 | 14.059 | 1.336 | 1.406 | 0.197 | 0.170 | 50±44 | 0.953 |
| $m_S = 145$ GeV | 14.695 | 14.018 | 1.336 | 1.402 | 0.197 | 0.172 | 51±44 | 0.946 |
| $m_S = 150$ GeV | 14.695 | 14.094 | 1.336 | 1.409 | 0.197 | 0.169 | 50±44 | 0.959 |
| $m_S = 155$ GeV | 14.695 | 14.017 | 1.336 | 1.402 | 0.197 | 0.172 | 53±45 | 0.945 |
| $m_S = 160$ GeV | 14.695 | 14.089 | 1.336 | 1.409 | 0.197 | 0.169 | 52±45 | 0.958 |

**Table C.12:** *$\chi^2$ values, p-value, signal yield after the fitting and the significance of the SM background and the SM+BSM for two OS leptons ($e^+e^-/\mu^+\mu^-/e^\pm\mu^\pm$) with one jet selection. The BSM signal is the heavy neutrino model with $m_{N_i} < m_S$ ($pp \to H \to Sh$); for the CMS data with luminosity of 19.4 fb$^{-1}$ [88].*

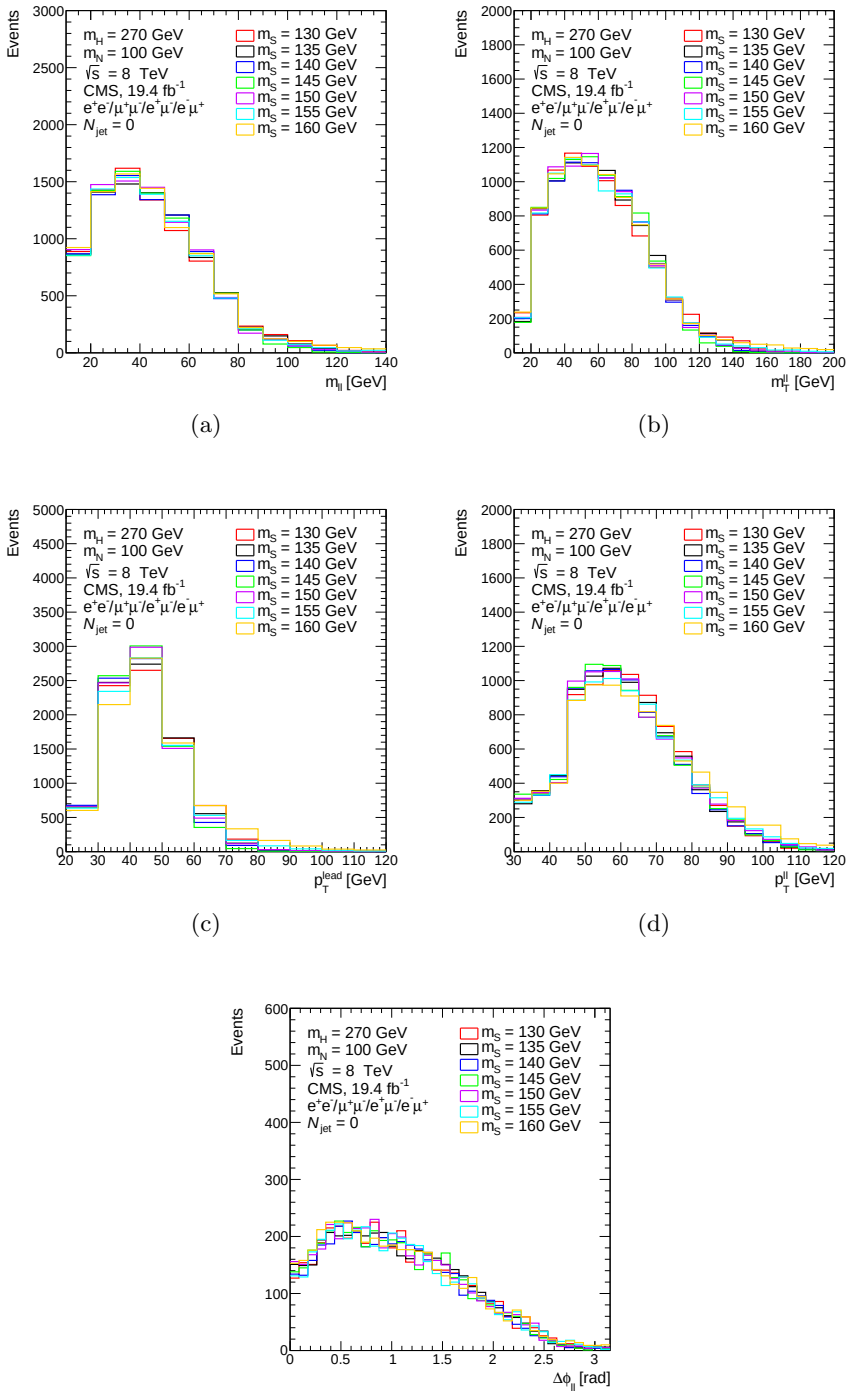


(a) (b)

(c) (d)

(e)

**Figure C.6:** *Kinematic distribution of (a) the di-lepton invariant mass, (b) the transverse mass of the di-lepton system, (c) the $p_T$ of the leading lepton, (d) the $p_T$ of the di-lepton system and (e) the azimuthal angle of two leptons; in events with an OS leptons ($e^+e^-/\mu^+\mu^-/e^\pm\mu^\pm$) and zero jet with the CMS detector simulation. The BSM signal is the heavy neutrino signal with $m_{N_i} < m_S$.*

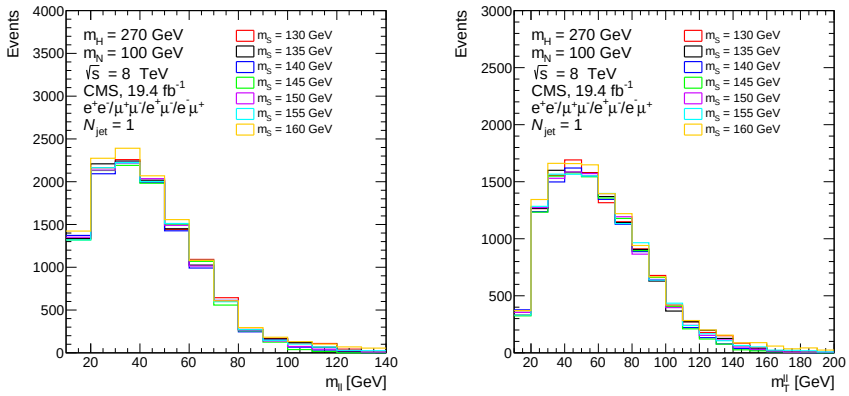


(a)




(b)

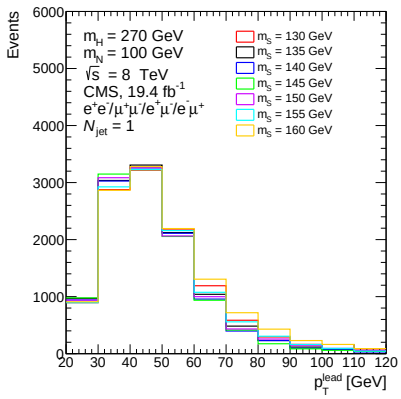


(c)

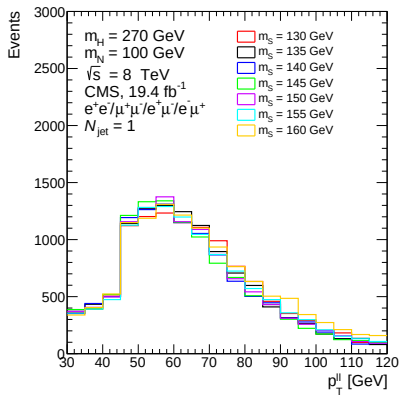


(d)

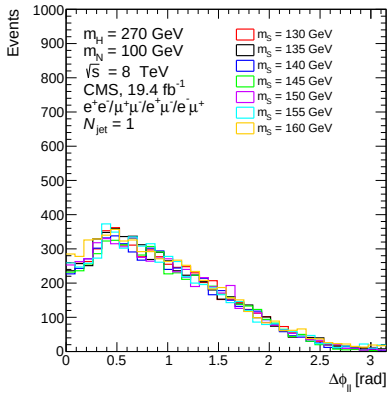


(e)

**Figure C.7:** *Kinematic distribution of (a) the di-lepton invariant mass, (b) the transverse mass of the di-lepton system, (c) the $p_T$ of the leading lepton, (d) the $p_T$ of the di-lepton system and (e) the azimuthal angle of two leptons; in events with an OS leptons ($e^+e^-/\mu^+\mu^-/e^\pm\mu^\pm$) and one jet with the CMS detector simulation. The BSM signal is the heavy neutrino signal with $m_{N_i} < m_S$.*

## C.5 CMS, 5.3 fb$^{-1}$ with $e^+e^-/\mu^+\mu^+/e^\pm\mu^\mp$, $N_{\text{jet}} \geq 2$ and $N_{b-\text{jet}} \geq 2$

| | $m_S = 130$ GeV | $m_S = 135$ GeV | $m_S = 140$ GeV | $m_S = 145$ GeV | $m_S = 150$ GeV | $m_S = 155$ GeV | $m_S = 160$ GeV |
|---|---|---|---|---|---|---|---|
| All events | 500000.00 | 500000.00 | 500000.00 | 500000.00 | 500000.00 | 500000.00 | 500000.00 |
| $e^\pm\mu^\mp$ | 46266.00 | 46162.00 | 45561.00 | 45963.00 | 46152.00 | 45909.00 | 46354.00 |
| $p_{\text{T}}^{\text{lead}} > 20$ GeV | 43944.00 | 43845.00 | 43244.00 | 43759.00 | 43878.00 | 43735.00 | 44351.00 |
| $p_{\text{T}}^{\text{sub-lead}} > 20$ GeV | 24296.00 | 23950.00 | 23390.00 | 23483.00 | 24162.00 | 24273.00 | 25258.00 |
| $m_{\ell\ell} > 10$ GeV | 21192.00 | 20791.00 | 20255.00 | 20377.00 | 20928.00 | 21093.00 | 21925.00 |
| $N_{b\text{-jet}} \geq 1$ | 845.00 | 812.00 | 781.00 | 772.00 | 836.00 | 913.00 | 915.00 |
| $N_{\text{jet}} \geq 2$ | 584.00 | 559.00 | 537.00 | 528.00 | 576.00 | 640.00 | 626.00 |
| Efficiency | 0.001168 | 0.001118 | 0.001074 | 0.001056 | 0.001152 | 0.00128 | 0.001252 |

**Table C.13:** *Cutflow of the events survived the cuts for the selection of two OS leptons ($e$ or $\mu$), at least two jets and two b-tagged jets and the efficiency with luminosity of 5.3 fb$^{-1}$. The BSM signal is the heavy neutrino model with $m_{N_i} < m_S$ according to CMS simulation.*

| | $\chi^2$ | | $\chi^2/ndf$ | | p-value | | N. signal | Significance |
|---|---|---|---|---|---|---|---|---|
| | SM background | SM+BSM | SM Background | SM+BSM | SM Background | SM+BSM | | |
| $m_S = 130$ GeV | 12.859 | 12.890 | 0.756 | 0.806 | 0.746 | 0.681 | 18±61 | -0.470 |
| $m_S = 135$ GeV | 12.859 | 12.865 | 0.756 | 0.804 | 0.746 | 0.683 | 25±60 | -0.475 |
| $m_S = 140$ GeV | 12.859 | 12.901 | 0.756 | 0.806 | 0.746 | 0.680 | 11±84 | -0.468 |
| $m_S = 145$ GeV | 12.859 | 12.830 | 0.756 | 0.802 | 0.746 | 0.685 | 27±57 | -0.482 |
| $m_S = 150$ GeV | 12.859 | 12.898 | 0.756 | 0.806 | 0.746 | 0.680 | 19±60 | -0.468 |
| $m_S = 155$ GeV | 12.859 | 12.782 | 0.756 | 0.799 | 0.746 | 0.689 | 31±58 | -0.492 |
| $m_S = 160$ GeV | 12.859 | 12.836 | 0.756 | 0.802 | 0.746 | 0.685 | 31±61 | -0.481 |

**Table C.14:** *$\chi^2$ values, p-value, signal yield after the fitting and the significance of the SM background and the SM+BSM for ($e^\pm\mu^\mp$) with at least two jets and two b-tagged jets. The BSM signal is the heavy neutrino model with $m_{N_i} < m_S$ ($pp \to H \to Sh$); for the CMS data with luminosity of 5.3 fb$^{-1}$ [89].*

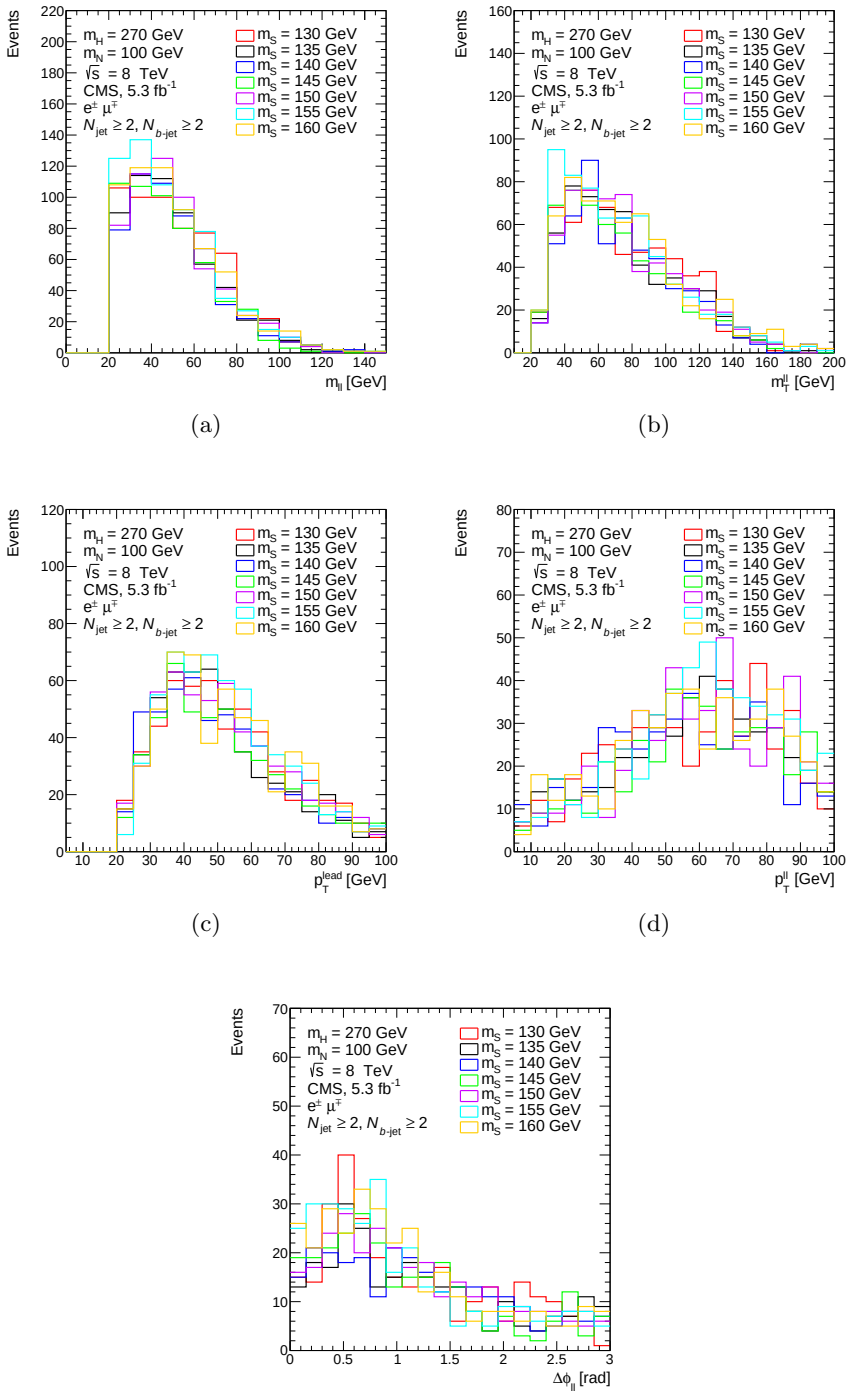


**Figure C.8:** *Kinematic distribution of (a) the di-lepton invariant mass, (b) the transverse mass of the di-lepton system, (c) the $p_T$ of the leading lepton, (c) the $p_T$ of the di-lepton system and (e) the azimuthal angle of two leptons; in events with an OS leptons ($e$ or $\mu$) and at least two jets and two b-tagged jets with the CMS simulation. The BSM signal is the heavy neutrino signal with $m_{N_i} < m_S$.*

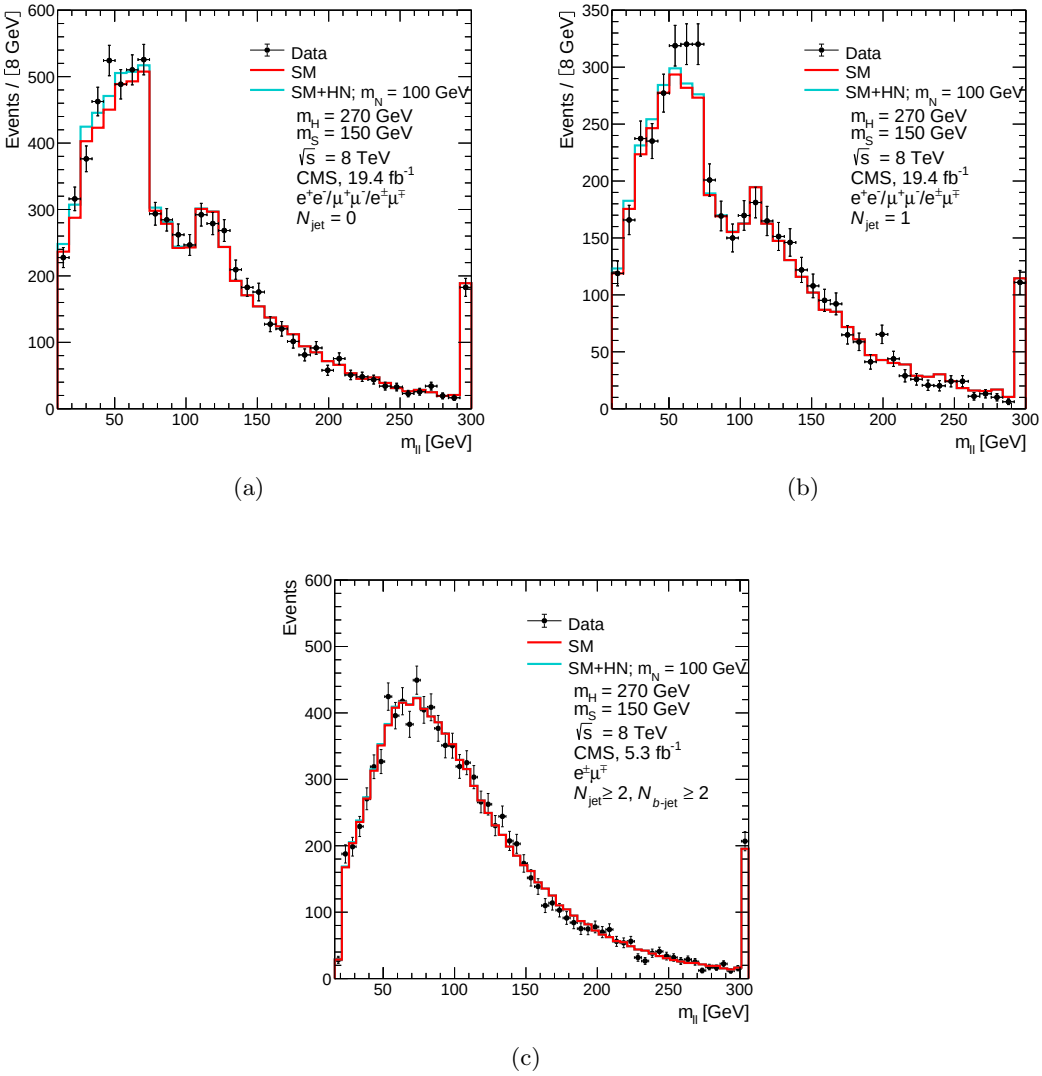


**Figure C.9:** *Distributions of the CMS data and SM background compared to the BSM signal (HN model with $m_{N_i} < m_S$) for the di-lepton invariant mass ($m_{ll}$). Events are required to have two opposite-charge leptons with (a) zero-jet (b) one-jet [88] and (c) $e\mu$ channel [89] with at least two jets and one b-tagged jet. The data used here, are from the measurement of the $W^+W^-$ and $t\bar{t}$ production cross-section in pp collision at $\sqrt{s} = 8$ TeV with luminosity of 19.4 fb$^{-1}$ and 5.3 fb$^{-1}$ for top and bottom plots, respectively.*

# References


[1] S. von Buddenbrock, N. Chakrabarty, A. S. Cornell, D. Kar, M. Kumar, T. Mandal, B. Mellado, B. Mukhopadhyaya, and R. G. Reed, "The compatibility of LHC Run 1 data with a heavy scalar of mass around 270 GeV," 2015. arXiv:1506.00612.

[2] S. von Buddenbrock, N. Chakrabarty, A. S. Cornell, D. Kar, M. Kumar, T. Mandal, B. Mellado, B. Mukhopadhyaya, R. G. Reed, and X. Ruan, "Phenomenological signatures of additional scalar bosons at the LHC," *Eur. Phys. J.*, vol. C76, no. 10, p. 580, 2016.

[3] F. Englert and R. Brout, "Broken Symmetry and the Mass of Gauge Vector Mesons," *Phys. Rev. Lett.*, vol. 13, pp. 321–323, 1964.

[4] P. W. Higgs, "Broken symmetries, massless particles and gauge fields," *Phys. Lett.*, vol. 12, pp. 132–133, 1964.

[5] ATLAS Collaboration, "Observation of a new particle in the search for the Standard Model Higgs boson with the ATLAS detector at the LHC," *Phys. Lett.*, vol. B716, pp. 1–29, 2012.

[6] CMS Collaboration, "Observation of a new boson at a mass of 125 GeV with the CMS experiment at the LHC," *Phys. Lett.*, vol. B716, pp. 30–61, 2012.

[7] G. C. Branco, P. M. Ferreira, L. Lavoura, M. N. Rebelo, M. Sher, and J. P. Silva, "Theory and phenomenology of two-Higgs-doublet models," *Phys. Rept.*, vol. 516, pp. 1–102, 2012.

[8] LHC Higgs Cross Section HH Sub-group, "Current recommendations for di-Higgs cross-sections." https://twiki.cern.ch/twiki/bin/view/LHCPhysics/LHCHXSWGHH.

[9] G. Aad *et al.*, "Searches for Higgs boson pair production in the $hh \to bb\tau\tau, \gamma\gamma WW^*, \gamma\gamma bb, bbbb$ channels with the ATLAS detector," *Phys. Rev.*, vol. D92, p. 092004, 2015.

[10] A. Atre, T. Han, S. Pascoli, and B. Zhang, "The Search for Heavy Majorana Neutrinos," *JHEP*, vol. 05, p. 030, 2009.

[11] C. Degrande, O. Mattelaer, R. Ruiz, and J. Turner, "Fully-Automated Precision Predictions for Heavy Neutrino Production Mechanisms at Hadron Colliders," *Phys. Rev.*, vol. D94, no. 5, p. 053002, 2016.

[12] D. Alva, T. Han, and R. Ruiz, "Heavy Majorana neutrinos from $W\gamma$ fusion at hadron colliders," *JHEP*, vol. 02, p. 072, 2015.

[13] T. Golling *et al.*, "Physics at a 100 TeV pp collider: beyond the Standard Model phenomena," *CERN Yellow Report*, no. 3, pp. 441–634, 2017.

[14] M. Kumar, S. von Buddenbrock, N. Chakrabarty, A. S. Cornell, D. Kar, T. Mandal, B. Mellado, B. Mukhopadhyaya, and R. Reed, "The impact of additional scalar bosons at the LHC," in *Workshop on High Energy Particle Physics (HEPPW2016) Johannesburg, South Africa, February 8-10, 2016*, 2016.

[15] S. Mthembu and M. Kumar, "The production of the heavy scalar H in association with top and anti-top quarks," 2017. arXiv:1702.08772.

[16] S. von Buddenbrock, "Exploring LHC Run 1 and 2 data using the Madala hypothesis," *J. Phys. Conf. Ser.*, vol. 878, no. 1, p. 012030, 2017.

[17] Y. Fang, M. Kumar, B. Mellado, Y. Zhang, and M. Zhu, "Impact of additional bosons on the exploration of the Higgs boson at the LHC," 2017. arXiv:1706.06659.

[18] S. von Buddenbrock, A. S. Cornell, M. Kumar, and B. Mellado, "The Madala hypothesis with Run 1 and 2 data at the LHC," *J. Phys. Conf. Ser.*, vol. 889, no. 1, p. 012020, 2017.

[19] B. Mellado, "The production of additional bosons and the impact on the Large Hadron Collider, Talk given at HDAYS2017, Santander, Spain." http://hdays.csic.es/HDays17/, 2017.

[20] S. L. Glashow, J. Iliopoulos, and L. Maiani, "Weak Interactions with Lepton-Hadron Symmetry," *Phys. Rev.*, vol. D2, pp. 1285–1292, 1970.

[21] D. Griffiths, *"Introduction to elementary particles"*. John Wiley & Sons, 2008.

[22] D. Dominguez, "Standard Model. Le modéle standard." https://cds.cern.ch/record/2002395, Mar 2015.

[23] A. Romanino, "The Standard model of particle physics," in *Physics of elementary particles and astrophysics. Proceedings, International Baikal Summer School, Bolshie Koty, Russia, July 23-30, 2009*, 2009.

[24] S. L. Glashow, "Partial Symmetries of Weak Interactions," *Nucl. Phys.*, vol. 22, pp. 579–588, 1961.

[25] A. Salam and J. C. Ward, "Electromagnetic and weak interactions," *Phys. Lett.*, vol. 13, pp. 168–171, 1964.

[26] P. W. Higgs, "Broken Symmetries and the Masses of Gauge Bosons," *Phys. Rev. Lett.*, vol. 13, pp. 508–509, 1964.

[27] P. W. Higgs, "Spontaneous Symmetry Breakdown without Massless Bosons," *Phys. Rev.*, vol. 145, pp. 1156–1163, 1966.

[28] D. McMahon, *"Quantum Field Theory Demystified"*. McGraw-Hill, 2008.

[29] R. Foot and R. R. Volkas, "Natural electroweak symmetry breaking in generalised mirror matter models," *Phys. Lett.*, vol. B645, pp. 75–81, 2007.

[30] S. M. Bilenky, "Neutrino in Standard Model and beyond," *Phys. Part. Nucl.*, vol. 46, no. 4, pp. 475–496, 2015.

[31] S. Weinberg, "A model of leptons," *Phys. Rev. Lett.*, vol. 19, no. 21, p. 1264, 1967.

[32] J. Alcaraz *et al.*, "A Combination of preliminary electroweak measurements and constraints on the standard model," 2006. CERN-PH-EP-2006-042, LEPEWWG-2006-01, ALEPH-2006-001-PHYSICS-2006-001, DELPHI-2006-014-PHYS-948, L3-NOTE-2833, OPAL-PR-419.

[33] T. Hambye and K. Riesselmann, "Matching conditions and Higgs mass upper bounds revisited," *Phys. Rev.*, vol. D55, pp. 7255–7262, 1997.

[34] P. Langacker, "Grand Unified Theories and Proton Decay," *Phys. Rept.*, vol. 72, p. 185, 1981.

[35] I. F. Ginzburg and M. Krawczyk, "Symmetries of two Higgs doublet model and CP violation," *Phys. Rev.*, vol. D72, p. 115013, 2005.

[36] I. F. Ginzburg, "Necessity of mixed kinetic term in the description of general system with identical scalar fields," *Phys. Lett.*, vol. B682, pp. 61–66, 2009.

[37] N. G. Deshpande and E. Ma, "Pattern of Symmetry Breaking with Two Higgs Doublets," *Phys. Rev.*, vol. D18, p. 2574, 1978.

[38] R. D. Peccei and H. R. Quinn, "CP Conservation in the Presence of Instantons," *Phys. Rev. Lett.*, vol. 38, pp. 1440–1443, 1977.

[39] S. Antusch and O. Fischer, "Non-unitarity of the leptonic mixing matrix: Present bounds and future sensitivities," *JHEP*, vol. 10, p. 094, 2014.

[40] A. De Gouva and A. Kobach, "Global Constraints on a Heavy Neutrino," *Phys. Rev.*, vol. D93, no. 3, p. 033005, 2016.

[41] B. Holzer and R. Alemany-Fernandez, "A Journey to the Heart of the LHC," *Springer International Publishing*, pp. 27–56, 2015.

[42] European Organisation for Nuclear Research, "ALICE: A Large Ion Collider Experiment." https://cds.cern.ch/record/1997265, Feb 2012.

[43] European Organisation for Nuclear Research, "ATLAS: The largest volume particle detector ever built." https://cds.cern.ch/record/1997264, Feb 2012.

[44] European Organisation for Nuclear Research, "CMS: The Compact Muon Solenoid." https://cds.cern.ch/record/1997263, Feb 2012.

[45] European Organisation for Nuclear Research, "LHCb: The Large Hadron Collider beauty experiment." https://cds.cern.ch/record/1997262, Feb 2012.

[46] European Organisation for Nuclear Research, "Experiments." https://cds.cern.ch/record/1997374, Jul 2012.

[47] European Organisation for Nuclear Research, "The Super Proton Synchrotron." https://cds.cern.ch/record/1997188, Jan 2012.

[48] F. Marcastel, "CERN's Accelerator Complex. La chane des acclrateurs du CERN," Oct 2013. General Photo.

[49] European Organisation for Nuclear Research, "Linear accelerator 2." https://cds.cern.ch/record/1997427, Sep 2012.

[50] European Organisation for Nuclear Research, "The Proton Synchrotron Booster." https://cds.cern.ch/record/1997372, Jul 2012.

[51] European Organisation for Nuclear Research, "The Proton Synchrotron." https://cds.cern.ch/record/1997189, Jan 2012.

[52] ATLAS Collaboration, "The ATLAS Experiment at the CERN Large Hadron Collider," *Journal of Instrumentation*, vol. 3, no. 08, p. S08003, 2008.

[53] ATLAS Collaboration, "ATLAS inner detector: Technical design report. Vol. 1," 1997. CERN-LHCC-97-16, ATLAS-TDR-4.

[54] ATLAS Collaboration, "Search for Higgs boson pair production in the final state of $\gamma\gamma WW^*(\rightarrow l\nu jj)$ using 36.1 fb$^{-1}$ of pp collision data recorded at $\sqrt{s}$= 13 TeV with the ATLAS detector," Tech. Rep. ATL-COM-PHYS-2017-1006, CERN, Geneva, Jul 2017.

[55] A. Fadol, B. Mellado, and X. Ruan, "Search for a heavy boson in $WW\gamma\gamma$ channel at the Large Hadron Collider in pp at $\sqrt{s} = 13$ TeV and integrated luminosity of 36.5 fb$^{-1}$ with the ATLAS detector," *J. Phys. Conf. Ser.*, vol. 889, no. 1, p. 012001, 2017.

[56] J. Alwall, M. Herquet, F. Maltoni, O. Mattelaer, and T. Stelzer, "MadGraph 5 : Going Beyond," *JHEP*, vol. 06, p. 128, 2011.

[57] S. Frixione and B. R. Webber, "Matching NLO QCD computations and parton shower simulations," *JHEP*, vol. 06, p. 029, 2002.

[58] S. Gieseke, C. Rohr, and A. Siodmok, "Colour reconnections in Herwig++," *Eur. Phys. J.*, vol. C72, p. 2225, 2012.

[59] P. M. Nadolsky, H.-L. Lai, Q.-H. Cao, J. Huston, J. Pumplin, D. Stump, W.-K. Tung, and C. P. Yuan, "Implications of CTEQ global analysis for collider observables," *Phys. Rev.*, vol. D78, p. 013004, 2008.

[60] K. Hamilton, P. Nason, E. Re, and G. Zanderighi, "NNLOPS simulation of Higgs boson production," *JHEP*, vol. 10, p. 222, 2013.

[61] E. Bagnaschi, G. Degrassi, P. Slavich, and A. Vicini, "Higgs production via gluon fusion in the POWHEG approach in the SM and in the MSSM," *JHEP*, vol. 1202, p. 088, 2012.

[62] S. Alioli, P. Nason, C. Oleari, and E. Re, "A general framework for implementing NLO calculations in shower Monte Carlo programs: the POWHEG BOX," *JHEP*, vol. 1006, p. 043, 2010.

[63] O. Brein, A. Djouadi, and R. Harlander, "NNLO QCD corrections to the Higgs-strahlung processes at hadron colliders," *Phys. Lett. B*, vol. 579, pp. 149–156, 2004.

[64] M. L. Ciccolini, S. Dittmaier, and M. Kramer, "Electroweak radiative corrections to associated WH and ZH production at hadron colliders," *Phys. Rev. D*, vol. 68, p. 073003, 2003.

[65] CERN Report4 2016, "SM Higgs production cross sections at $\sqrt{s} = 13$ TeV." https://twiki.cern.ch/twiki/bin/view/LHCPhysics/CERNYellowReportPageAt13TeV.

[66] ATLAS Collaboration, "Electron and photon energy calibration with the ATLAS detector using data collected in 2015 at $\sqrt{s} = 13$ TeV," Tech. Rep. ATL-PHYS-PUB-2016-015, CERN, Geneva, Aug 2016.

[67] M. Aaboud *et al.*, "Measurement of the photon identification efficiencies with the ATLAS detector using LHC Run-1 data," *Eur. Phys. J.*, vol. C76, no. 12, p. 666, 2016.

[68] ATLAS collaboration, "Electron efficiency measurements with the ATLAS detector using the 2015 LHC proton-proton collision data," 2016. ATLAS-CONF-2016-024.

[69] G. Aad *et al.*, "Muon reconstruction performance of the ATLAS detector in proton–proton collision data at $\sqrt{s}$ =13 TeV," *Eur. Phys. J.*, vol. C76, no. 5, p. 292, 2016.

[70] M. Cacciari, G. P. Salam, and G. Soyez, "The Anti-k(t) jet clustering algorithm," *JHEP*, vol. 04, p. 063, 2008.

[71] G. Aad *et al.*, "Performance of $b$-Jet Identification in the ATLAS Experiment," *JINST*, vol. 11, no. 04, p. P04008, 2016.

[72] ATLAS Collaboration, "Electron and photon energy calibration with the ATLAS detector using data collected in 2015 at $\sqrt{s} = 13$ TeV," Tech. Rep. ATL-PHYS-PUB-2015-022, CERN, Geneva, Jul 2015.

[73] M. Aaboud *et al.*, "Search for resonances in diphoton events at $\sqrt{s}$=13 TeV with the ATLAS detector," *JHEP*, vol. 09, p. 001, 2016.

[74] M. Aaboud *et al.*, "Luminosity determination in pp collisions at $\sqrt{s} = 8$ TeV using the ATLAS detector at the LHC," *Eur. Phys. J.*, vol. C76, no. 12, p. 653, 2016.

[75] G. Aad *et al.*, "Performance of the ATLAS Trigger System in 2010," *Eur. Phys. J.*, vol. C72, p. 1849, 2012.

[76] G. Cowan, K. Cranmer, E. Gross, and O. Vitells, "Asymptotic formulae for likelihood-based tests of new physics," *Eur. Phys. J.*, vol. C71, p. 1554, 2011. [Erratum: Eur. Phys. J.C73,2501(2013)].

[77] A. L. Read, "Presentation of search results: The CL(s) technique," *J. Phys.*, vol. G28, pp. 2693–2704, 2002.

[78] S. von Buddenbrock, A. S. Cornell, A. Fadol, M. Kumar, B. Mellado, and X. Ruan, "Multi-lepton signatures of additional scalar bosons beyond the Standard Model at the LHC," 2017. arXiv:1711.07874.

[79] A. Alloul, B. Fuks, and V. Sanz, "Phenomenology of the Higgs Effective Lagrangian via FEYNRULES," *JHEP*, vol. 04, p. 110, 2014.

[80] J. Alwall, R. Frederix, S. Frixione, V. Hirschi, F. Maltoni, O. Mattelaer, H. S. Shao, T. Stelzer, P. Torrielli, and M. Zaro, "The automated computation of tree-level and next-to-leading order differential cross sections, and their matching to parton shower simulations," *JHEP*, vol. 07, p. 079, 2014.

[81] T. Sjöstrand, S. Ask, J. R. Christiansen, R. Corke, N. Desai, P. Ilten, S. Mrenna, S. Prestel, C. O. Rasmussen, and P. Z. Skands, "An Introduction to PYTHIA 8.2," *Comput. Phys. Commun.*, vol. 191, pp. 159–177, 2015.

[82] R. D. Ball *et al.*, "Parton distributions with LHC data," *Nucl. Phys.*, vol. B867, pp. 244–289, 2013.

[83] J. De Favereau, C. Delaere, P. Demin, A. Giammanco, V. Lematre, A. Mertens, and M. Selvaggi, "DELPHES 3, A modular framework for fast simulation of a generic collider experiment," *JHEP*, vol. 02, p. 057, 2014.

[84] M. Cacciari, G. P. Salam, and G. Soyez, "FastJet User Manual," *Eur. Phys. J.*, vol. C72, p. 1896, 2012.

[85] ATLAS collaboration, "Measurement of lepton differential distributions and the top quark mass in $t\bar{t}$ production in $pp$ collisions at $\sqrt{s} = 8$ TeV with the ATLAS detector," 2017. ATLAS-CONF-2017-044.

[86] G. Aad *et al.*, "Measurement of total and differential $W^+W^-$ production cross sections in proton-proton collisions at $\sqrt{s} = 8$ TeV with the ATLAS detector and limits on anomalous triple-gauge-boson couplings," *JHEP*, vol. 09, p. 029, 2016.

[87] M. Aaboud *et al.*, "Measurement of $W^+W^-$ production in association with one jet in proton–proton collisions at $\sqrt{s} = 8$ TeV with the ATLAS detector," *Phys. Lett.*, vol. B763, pp. 114–133, 2016.

[88] V. Khachatryan *et al.*, "Measurement of the $\mathrm{W^+W^-}$ cross section in pp collisions at $\sqrt{s} = 8$ TeV and limits on anomalous gauge couplings," *Eur. Phys. J.*, vol. C76, no. 7, p. 401, 2016.

[89] S. Chatrchyan *et al.*, "Measurement of the $t\bar{t}$ production cross section in the dilepton channel in pp collisions at $\sqrt{s} = 8$ TeV," *JHEP*, vol. 02, p. 024, 2014. [Erratum: JHEP02,102(2014)].

[90] CMS Collaboration, "Search for production of a Higgs boson and a single top quark in multilepton final states in proton collisions at $\sqrt{s} = 13$ TeV," 2017. CMS-PAS-HIG-17-005.

[91] ATLAS Collaboration, "Evidence for the associated production of the Higgs boson and a top quark pair with the ATLAS detector," 2017. ATLAS-CONF-2017-77.

[92] W. Verkerke and D. P. Kirkby, "The RooFit toolkit for data modeling," *eConf*, vol. C0303241, p. MOLT007, 2003.

[93] W. R. Leo, *"Techniques for nuclear and particle physics experiments: a how-to approach"*. Springer Science & Business Media, 2012.